COMMONWEALTH OF PENNSYLVANIA
DEPARTMENT OF TRANSPORTATION

PENNDOT RESEARCH

PREDICTION OF MOVEMENT AND STRESSES IN CURVED AND SKEWED BRIDGES

Final Report

PennDOT/MAUTC Partnership, Work Order No. 2
Research Agreement No. 510401

November 30, 2006

By D. G. Linzell, V. P. Nadakuditi and D. L. Nevling

PENNSTATE

Pennsylvania Transportation Institute

The Pennsylvania State University
Transportation Research Building
University Park, PA   16802-4710
(814) 865-1891   www.pti.psu.edu

PREDICTION OF MOVEMENT AND STRESSES IN CURVED AND SKEWED BRIDGES

Final Report

PennDOT/MAUTC Partnership, Work Order No. 2
Research Agreement No. 510401

Prepared for

Bureau of Planning and Research
Commonwealth of Pennsylvania
Department of Transportation

By

Daniel G. Linzell, Ph.D., P.E.
Venkata Pavan Nadakuditi
Deanna L. Nevling

Pennsylvania Transportation Institute
The Pennsylvania State University
Transportation Research Building
University Park, PA 16802-4710

November 30, 2006

PTI 2007-05

1. Report No. FHWA-PA-2006-014-510401-02	2. Government Accession No.	3. Recipient's Catalog No.

4. Title and Subtitle Prediction of Movement and Stresses in Curved and Skewed Bridges	5. Report Date November 30, 2006
	6. Performing Organization Code

7. Author(s) Daniel G. Linzell, Ph.D., P.E., Venkata Pavan Nadakuditi, and Deanna L. Nevling	8. Performing Organization Report No. PTI 2007-05

9. Performing Organization Name and Address The Pennsylvania Transportation Institute The Pennsylvania State University 201 Transportation Research Building University Park, PA 16802	10. Work Unit No. (TRAIS)
	11. Contract or Grant No. 510401, Work Order No. 2

12. Sponsoring Agency Name and Address The Pennsylvania Department of Transportation Bureau of Planning and Research Commonwealth Keystone Building 400 North Street, 6th Floor Harrisburg, PA 17120-0064	13. Type of Report and Period Covered Final Report 6/30/2005 – 9/30/2006
	14. Sponsoring Agency Code

15. Supplementary Notes
COTR: Tom Macioce, 717-787-7504

16. Abstract
Although the use of curved and skewed bridges continues to increase steadily throughout the country, certain aspects of their behavior during construction and while in service still are not well understood. The effects of design, fabrication, and construction on the geometry and load distribution in a curved or skewed bridge system are areas in which further study and understanding are required. The construction of both curved and skewed bridges in the I-99 Advanced Technology Test Bed provides a unique opportunity to investigate curved and skewed structures not only during their construction but also while in-service. Two objectives were defined for this project: (1) the development and maintenance of data acquisition capabilities for instruments on two structures in the I-99 corridor identified as bridges 207 and 314; and (2) the development and comparison of accuracy of three different numerical models to construction data and/or to each other.

17. Key Words Curved bridge, skewed bridge, design, fabrication, construction, geometry, load distribution	18. Distribution Statement No restrictions. This document is available from the National Technical Information Service, Springfield, VA 22161

19. Security Classif. (of this report) Unclassified	20. Security Classif. (of this page) Unclassified	21. No. of Pages 93	22. Price

Form DOT F 1700.7   **(8-72)**   **Reproduction of completed page authorized**

Table of Contents

List of Figures

List of Tables

1 INTRODUCTION

1.1 BACKGROUND

Horizontally curved steel bridges and bridges supported by skewed substructure units, with either steel or concrete superstructures, continue to see increased utilization in the United States as both new or replacement bridges at interchanges or river crossings. Explanations for their increased usage are, in many instances, directly tied to the economy that these types of structures can provide. Constructing bridges that align with the roadway rather than attempting to align the roadway with the bridge helps reduce the amount of grading work required for the entire traffic system and allows for smoother and safer roadway alignments. In addition, utilizing curved superstructure members and/or piers and abutments that are not orthogonal to the superstructure can reduce the number of required substructure units and can considerably lower the volume of earthwork necessary to place those units, thereby lowering construction time and reducing costs.

Information provided in this report document summarizes incremental findings from the latest of an ongoing series of projects related to studying horizontally curved steel bridges and skewed steel and concrete bridges within the I-99 Advanced Technology Test Bed in central Pennsylvania. This work has been funded by various entities at the Pennsylvania Department of Transportation (PennDOT). Additional background information and details related to tasks and findings from the earlier projects be found in other reports and publications (Bennett 2004, Hiltunen et al. 2004, Linzell et al. 2003, Linzell et al. 2001, Shura 2005). This report focuses on work that occurred after construction of the structures was completed and prior to their being opened to traffic.

1.2 PROBLEM STATEMENT

Although the use of curved and skewed bridges continues to increase steadily throughout the country, certain aspects of their behavior during construction and while in service still are not well understood. The effects of design, fabrication, and construction on the geometry and load distribution in a curved or skewed bridge system are areas in which further study and understanding are required. The construction of both curved and skewed bridges in the I-99 Advanced Technology Test Bed provides a unique opportunity to investigate curved and skewed structures not only during their construction but also while in-service.

1.3 OBJECTIVES

Two objectives were defined for this project: (1) the development and maintenance of data acquisition capabilities for instruments on two structures in the I-99 corridor identified as bridges 207 and 314; and (2) the development and comparison of accuracy of three different numerical models to construction data and/or to each other.

1.4 SCOPE

The following scope (i.e., series of tasks) was developed based upon the objectives discussed in

the previous section:

Task 1: Bridge Instrumentation. Replace damaged/missing instruments measuring strain and deformations on beams, diaphragms and cross frames to measure bridge response during and after construction. Completion of this task is contingent upon PennDOT providing access to damaged/missing instrument locations.

Task 2: Hard-wiring of Instruments. Hard-wire instruments to acquisition systems that will permit remote monitoring of structure response by Penn State personnel.

Task 3: Data Collection and Numerical Study. Collect, compile and summarize data recorded throughout duration of project. Compare data to numerical results from: a grillage model, a full-shell 3D finite element model and a 3D finite element model containing a combination of frame members and shell and brick elements. Comparisons will be completed for the construction sequences that were used. In addition, an analysis for a single HS20 truck placed at the location generating maximum positive moment in the exterior/largest radius girder will be completed for each model and results will be compared. Deliverable: Draft Final Report - 2 copies.

Task 4: Final Report. A final report will be prepared taking into consideration feedback from PennDOT's technical advisor. Deliverable: Final Report – 5 copies.

Task 5: Summarize the problem statement, findings and recommendations.
Deliverable: IDEAs HAVE CONSEQUENCES – 1 electronic copy.

2   BRIDGE DESCRIPTIONS

Prior to discussing work that was completed in association with the scope/task items mentioned earlier, descriptions of the structures being examined will be provided in this section along with a summary of the instrumentation, and in the section that follows. Additional detailed descriptions of the structure, instrumentation and monitoring can be found elsewhere (Hiltunen et al. 2004, Linzell et al. 2003, Linzell and Laman 2001, Shura 2005). The structure descriptions provide general information related to overall bridge geometry, with an emphasis placed on the bridge's superstructure.

2.1   STRUCTURE #207

Structure #207 is a two-span, continuous, composite steel plate girder bridge with a total length of 146.53 m (480′-9″). The superstructure utilizes five ASTM A709 Grade 50 singly symmetric steel plate girders that are 2.74 m (108″) deep and spaced at 3.25 m (10′-8″) center-to-center. Flange plate dimensions vary along the length of the girders. Spans 1 and 2 measure 65.38 m (214′-6″) and 81.5 m (266′-3″) along the arc, respectively, and the radius of curvature to the center girder is 585.48 m (1920′-10 5/16″). Lateral bracing is provided using K-shaped cross-frames containing WT sections and oriented radially along both spans. For shipping purposes, each girder consists of five sections that are bolted at four field splices. Table 1 outlines the geometry of the five girders. Figure 1 and Figure 2 detail the plan view and typical cross-section of the superstructure.

Table 1: Girder Lengths, Radii, and Field Splice Locations (see Figure 1).

Girder ID (1)	Radius m (ft) (2)	L1 m (ft) (3)	L2 m (ft) (4)	L3 m (ft) (5)	L4 m (ft) (6)	L5 m (ft) (7)	Span 1 m (ft) (8)	Span 2 m (ft) (9)	Total m (ft) (10)
G1	579.98 (1899.53)	15.84 (51.98)	32.93 (108.03)	36.59 (120.05)	36.57 (119.99)	26.20 (85.95)	64.62 (212.02)	83.50 (273.96)	148.13 (486.08)
G2	582.22 (1910.17)	15.84 (51.98)	32.57 (106.86)	36.59 (120.05)	36.12 (118.49)	26.20 (85.95)	64.28 (210.88)	83.05 (272.46)	147.42 (483.42)
G3	585.48 (1920.86)	15.84 (51.98)	32.21 (105.69)	36.59 (120.05)	35.66 (116.98)	26.20 (85.95)	63.92 (209.70)	82.59 (270.95)	146.50 (480.75)
G4	588.73 (1931.53)	15.84 (51.98)	31.86 (104.52)	36.59 (120.05)	35.20 (115.48)	26.20 (85.95)	63.56 (208.54)	82.13 (269.46)	145.69 (478.13)
G5	591.98 (1942.19)	15.84 (51.98)	31.50 (103.35)	36.59 (120.05)	34.74 (113.98)	26.20 (85.95)	63.21 (207.37)	81.67 (267.96)	144.87 (475.42)
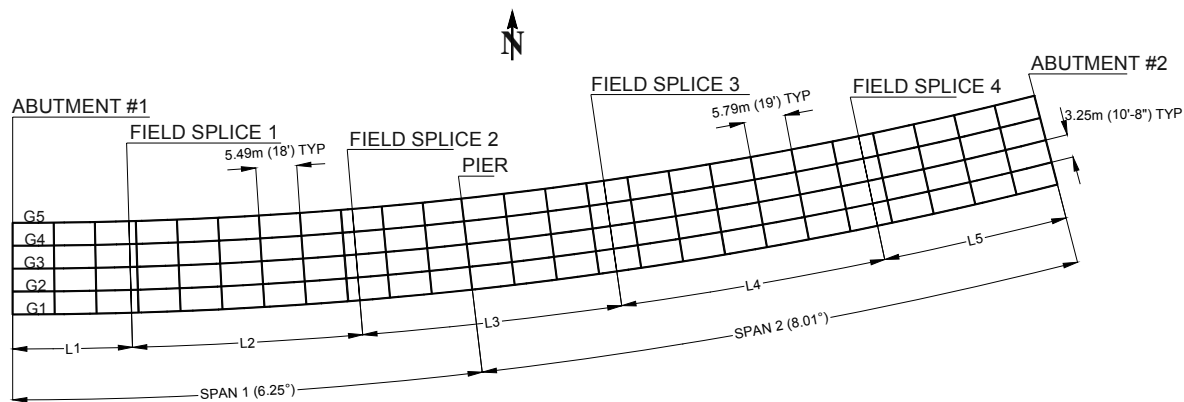
Figure 1. Plan View, Structure #207.
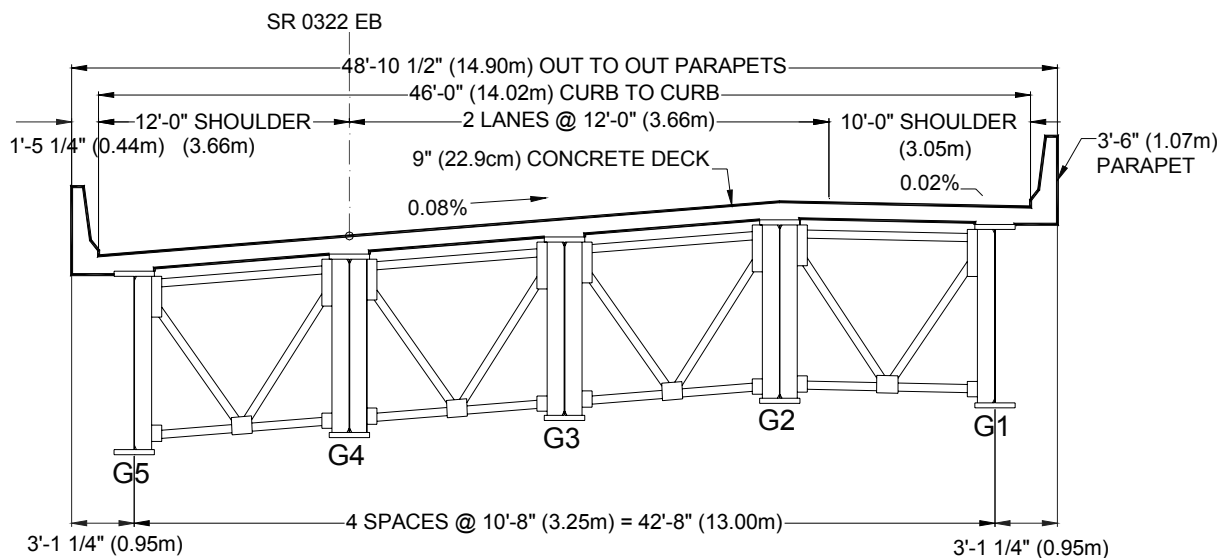
Figure 2. Typical Cross-Section, Structure #207.

2.2 STRUCTURE #314

Structure #314 is a two-span, live-load continuous, skewed bridge consisting of 12 prestressed concrete I-girders supporting a cast-in-place concrete deck (see Figure 3). The total bridge length is 76.20 m (250.00 ft). The abutments and piers are skewed at 44º relative to the bridge centerline. The bridge structure slopes longitudinally at 8.25% and the deck is superelevated. The lateral slope varies from 2% to 7.8%. A 1,067 mm (42 in) high cast-in-place parapet is located along both edges of the bridge deck.

The superstructure is flared and, as a result, girder depth and spacing as well as deck overhang

length and horizontal deck curvature vary between spans. Prestressed girders in each span have a design strength of 55.16 MPa (8 ksi) and a minimum strength of 46.88 MPa (6.8 ksi) at release of prestressing force. The cast-in-place concrete deck's design strength is 27.58 MPa (4 ksi).
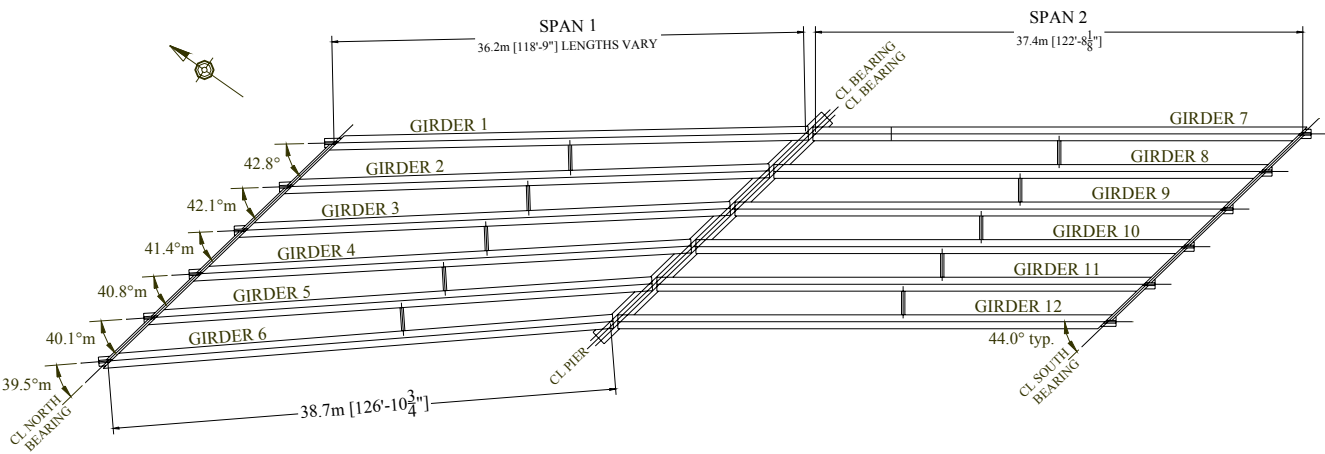
Figure 3. Plan View, Structure #314.

The northern span, Span 1, consists of six 1,828 mm (72 in) deep prestressed I-girders that contain normal reinforcement in the web and top flange. Girder spacing varies from 3.38 m (11.09 ft) at the northern abutment to 2.92 m (9.58 ft) at the interior pier. Girder skews vary from 39.50º for the westernmost girder to 42.82º for the easternmost girder relative to the span centerline. The westernmost girder spans 38.68 m (126.90 ft) from bearing to bearing while the easternmost girder spans 36.20 m (118.75 ft). Roadway curvature causes deck overhangs on both sides to vary between 0.76 m (2.5 ft) and 1.23 m (4 ft) along the length of the span. Jacking force for the prestressed girders in Span 1 is 10.83 MN (2435 k) per girder. A two-point drape pattern is used to alleviate stresses near the girder ends (Figure 4). Locations of drape points for each girder are given in Table 2.
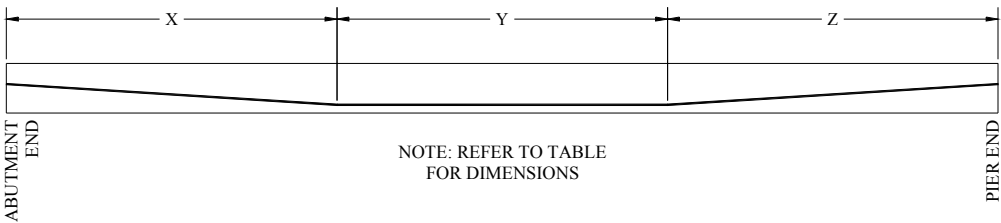
Figure 4. Span 1 Prestressing Strand Profile.

5

Table 2. Span 1 Prestressing Strand Drape Point Location.

Girder	X		Y		Z	
	m	ft	m	ft	m	ft
(1)	(2)	(3)	(4)	(5)	(6)	(7)
1A	12.60	41.33	12.19	40.00	12.29	40.33
2B	12.84	42.14	12.19	40.00	12.54	41.14
3C	12.92	42.40	12.52	41.08	12.62	41.40
4D	13.17	43.21	12.52	41.08	12.87	42.21
5E	13.25	43.46	12.85	42.17	12.94	42.46
6F	13.51	44.32	12.85	42.17	13.20	43.32

The southern span, Span 2, consists of six 1,676 mm (66 in) deep prestressed I-girders that contain normal reinforcement in the web and top flange. Span 2 girders have constant spacing of 2.91 m (9.55 ft) and constant skew of 44° relative to the span centerline. Girder lengths are 37.80 m (124.00 ft). Constant deck overhangs of 1.14 m (3.74 ft) occur on each side. Jacking force for girders in Span 2 is 12.04 MN (2705 k) per girder. Strands are straight but debonded near the girders ends to alleviate stresses at these locations.

Cast-in-place diaphragms are present at several locations on the structure, at the abutments, near the midspan of both spans and at the intermediate pier. Cast-in-place concrete diaphragms at both abutments extend downward from the bottom of the slab to 533 mm (21 in) above the bearing elevation of the adjacent beam and are 305 mm (12 in) thick. Diaphragms are also provided near mid-span between each girder. Mid-span diaphragms extend from the bottom of the slab downward to 533 mm (21 in) above the beam bottom and are 254 mm (10 in) thick. The diaphragm at the pier is full depth and extends from the bottom of the deck to the top of the pier. The pier diaphragm is 1.22 m (4 ft) wide.

3   INSTRUMENTATION AND MONITORING

Summaries of instrumentation used on Structures 207 and 314 are provided herein. Additional detailed instrumentation and monitoring descriptions are found elsewhere (Bennett 2004, Hiltunen et al. 2004, Linzell et al. 2003, Linzell et al. 2001, Shura 2005). Information provided herein focuses on the fabrication and construction phases for both structures. Data that were recorded consisted primarily of strains and rotations recorded from the beams/girders, although laser scanning of Structure #207 was conducted by Greenman-Pederson, Inc. using Cyrax Laser Technology. Summaries of the laser scans can be found elsewhere (Hiltunen et al. 2004, Linzell et al. 2003, Linzell and Laman 2001, Shura 2005).

3.1   STRUCTURE #207

3.1.1   Instrument Information

Normal strains are measured at the anticipated points of maximum positive and negative bending. Geokon Model VK-4100 vibrating wire strain gages, shown in Figure 5, were used for this purpose. The instruments have a gage length of 50.8 mm (2 in), a range of 2500 miorostrain, and a sensitivity of 0.5-1.0 microstrain. The gages were welded to the top and bottom flanges of the girders, 25 mm (1 in) from the flange tips.
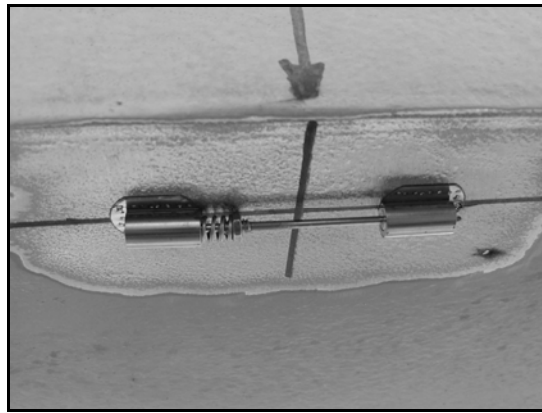
Figure 5. Geokon Model VK-4100 Vibrating Wire Strain Gage.

Geokon 6350 vibrating wire tiltmeters (Figure 6) are used to measure longitudinal rotations at Abutment 2, and torsion of the entire superstructure near the point of anticipated maximum positive bending in Span 2. These instruments have a range of ±10° and a resolution of 10 arc seconds. The tiltmeters were affixed to the girder webs using a bracket bolted to the web at the non-composite neutral axis.

Figure 6. Geokon Model 6350 Vibrating Wire Tiltmeter.

3.1.2 Instrument Statistics

A total of 65 vibrating wire strain gages, 4 vibrating wire tiltmeters, and 10 laser targets are being used to monitor the bridge at any given time. The majority of the instruments are placed on the exterior girders and cross-frames because these were known to be the critical elements within a curved girder system. Table 3 summarizes instrument quantities on the cross-frames and each girder. Instrument locations are summarized in Figure 7 and Figure 8 and Table 4 through Table 6. Note that girder and section numbers in the tables reference relevant figure IDs for Structure #207.

Table 3. Instrument Quantities (Linzell et al., 2003).

Instrument Type (1)	Location (2)	Quantity (3)
Vibrating Wire Strain Gages	Girder 1	12
	Girder 2	9
	Girder 3	11
	Girder 4	9
	Girder 5	12
	Cross Frames	12
	Total	**65**
Vibrating Wire Tiltmeters	Girder	4
	Total	**4**
Laser Targets	Girder	10
	Total	**10**
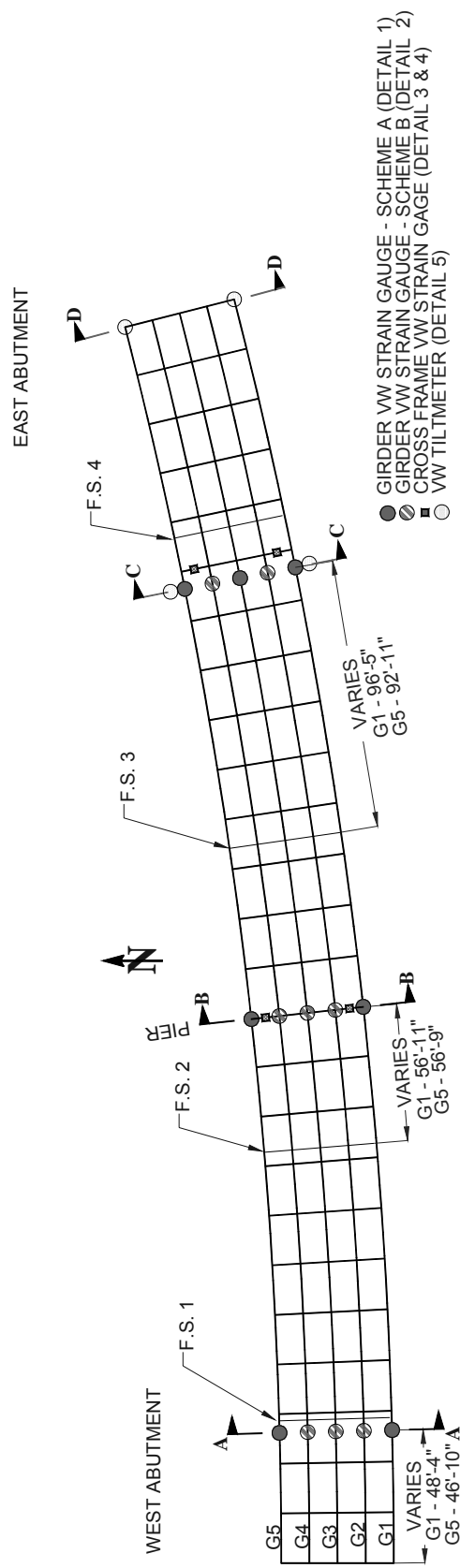
BRIDGE S-207 - INSTRUMENT LOCATION PLAN

Figure 7. **Instrument Locations on Bridge Plan View (Linzell et al. 2003).**
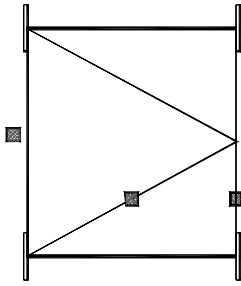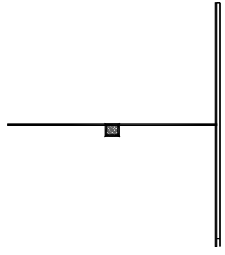
DETAIL 1

TYPICAL SECTION
WITH FOUR
STRAIN GAGES

DETAIL 2

TYPICAL SECTION
WITH THREE
STRAIN GAGES

DETAIL 3

TYPICAL CROSS-
FRAME WITH THREE
STRAIN GAGES

DETAIL 4

CROSS-FRAME
CHORD DETAIL
(WT-SECTION)

DETAIL 5

TYPICAL SECTION
WITH TILT-
METER

Figure 8. Instrument Details (Linzell et al. 2003).

Table 4. Girder Positive Moment Vibrating Wire Strain Gage Locations (Linzell et al. 2003).

Girder	Section (Fig. 6)	Distance From Abutment #1		Distance from Field Splice #1		**Cross Frame No. From Abutment #1	Distance from Cross-Frame		Quantity
		m.	Ft.	m.	Ft.		m.	Ft.	
G1A	A-A	14.73	48′-4″	1.12	3′-8″	3	2.95	9′-8″	4
G2A	A-A	14.63	48′-0″	1.22	4′-0″	3	2.92	9′-7″	3
G3A	A-A	14.58	47′-10″	1.27	4′-2″	3	2.92	9′-7″	3
G4A	A-A	14.48	47′-6″	1.37	4′-6″	3	2.90	9′-6″	3
G5A	A-A	14.27	46′-10″	1.45	4′-9″	3	2.87	9′-5″	4

Girder	Section	Distance From Field Splice #3		Distance From Field Splice #4		**Cross Frame No. From Abutment #1	Distance from Cross-Frame		Quantity
		m.	Ft.	m.	Ft.		m.	Ft.	
G1D	C-C	29.39	96′-5″	7.18	23′-7″	20	2.39	7′-11″	4
G2D	C-C	29.14	95′-7″	6.98	22′-11″	20	2.40	7′-10″	3
G3D	C-C	28.86	94′-9″	6.79	22′-3″	20	2.38	7′-10″	4
G4D	C-C	28.58	93′-10″	6.62	21′-8″	20	2.36	7′-9″	3
G5D	C-C	28.30	92′-11″	6.44	21′-1″	20	2.34	7′-8″	4

NOTE: Cross Frames counted from Abutment #1. Diaphragms at abutment and pier are counted

Table 5. Girder Negative Moment Vibrating Wire Strain Gage Locations (Linzell et al. 2003).

Girder	Section (Fig. 6)	Distance From Field Splice #2		Distance From Field Splice #3		**Cross Frame No. From Abutment #1	Distance from Cross-Frame		Quantity
		m.	Ft.	m.	Ft.		m.	Ft.	
G1C	B-B	17.35	56′-11″	19.25	63′-2″	12	1.50	4′-11″	4
G2C	B-B	17.35	56′-11″	19.25	63′-2″	12	1.50	4′-11″	3
G3C	B-B	17.32	56′-10″	19.28	63′-3″	12	1.47	4′-10″	3
G4C	B-B	17.32	56′-10″	19.28	63′-3″	12	1.47	4′-10″	3
G5C	B-B	17.30	56′-9″	19.30	63′-4″	12	1.45	4′-9″	4

NOTE: Cross Frames counted from Abutment #1. Diaphragms at abutment and pier are counted

Table 6. Cross Frame Vibrating Wire Strain Gage Locations (Linzell et al. 2003).

Girder (Fig. 1)	Cross Frame Number (From Abutment 1)	Quantity
G1B-G2B	12	3
G4B-G5B	12	3
G1C-G2C	21	3
G4C-G5C	21	3

NOTE: Cross Frames counted from Abutment #1. Diaphragms at abutment and pier are counted

3.1.3 Instrument Installation and Monitoring – Fabrication and Construction

Detailed information related to instrument installation and monitoring during fabrication and construction, which occurred prior to initiation of the project described herein, can be found elsewhere (Hiltunen et al. 2004, Linzell et al. 2003, Linzell and Laman 2001, Shura 2005). An abridged, tabular summary of the installation and monitoring procedures followed during fabrication and construction is presented in Table 7.

Table 7. VW Instrumentation and Monitoring Plan – Fabrication and Construction (Shura 2005).

Event	Location	Instruments	Action
(1) Initial Girder VW Gage Placement and Monitoring Plan	Fabrication Shop	VW Strain Gages at Section C-C (Qty – 18)	Girders were blocked to curvature and VW Gages were welded to the flange tips. Benchmark readings were recorded with portable readout box.
(2) Girder VW Gage Pre-Shipment Readings	Fabrication Shop	VW Strain Gages at Section C-C	Girder strains were recorded upon placement on trucks.
(3) Girder VW Gage Post-Shipment Readings	Project Site	VW Strain Gages at Section C-C	Girder strains were recorded before girders were offloaded from trucks
(4) Girder VW Gage Site Storage Placement and Readings	Project Site	VW Strain Gages at Sections A-A and B-B, (Qty – 19)	Girders were blocked to curvature and VW Gages were welded to the flange tips. Benchmark readings were taken with the portable readout box.
(5) Girder VW Gage Erection Readings	Project Site	VW Strain Gages previously installed	Strain readings were taken at the end of each working day using the portable readout box.
(6) Final VW Strain Gage and Tiltmeter Placement	Project Site	VW Strain Gages at all Sections and Cross-frames (Qty – 28) VW Tiltmeters (Qty – 4)	Remaining VW Strain Gages were welded to the flange tips and Cross-Frames. Tiltmeters were bolted to the girder webs near the non-composite neutral axis. Benchmark readings were taken with the portable readout box.
(7) VW Instrument Hard Wiring	Project Site	VW Gages and Tiltmeters	CR10X was installed onto bridge pier and 64 instruments were hardwired. Solar panel was also installed at this time.
(8) Construction Monitoring – Normal Construction Activities	Project Site	All VW Gages and Tiltmeters	CR10X was used to monitor the VW Gages during normal construction activities, i.e. placement of deck pans, reinforcing steel, and formwork. Readings were taken at ½ hour intervals.
(9) Construction Monitoring – Concrete Deck and Parapet Placement	Project Site	All VW Gages and Tiltmeters	CR10X was used to monitor VW Gages during placement of concrete deck and parapet walls. Readings were taken at 5 minute intervals.

3.1.4 Instrument Installation and Monitoring – Current Project

All instruments had been placed onto Structure #207 and wired into the data-logger before the

start of the current project. These instruments were investigated using a PennDOT Snooper to determine if any were missing or had stopped working. Three instruments were replaced on Structure 207. Figure 9 through Figure 11 detail the instrumentation replacement and wiring process and Figure 12 through Figure 14 show the instruments that were replaced. After the three instruments were replaced the data-logger was programmed to record data once an hour.

Figure 9. PennDOT Snooper Used Structure 207 Field Work.

Figure 10. Inspection of Structure 207 Gages.

Figure 11. Inspection of Structure 207 Data-Logger.

Figure 12. Replacement for Gage G1 A-A TF South.
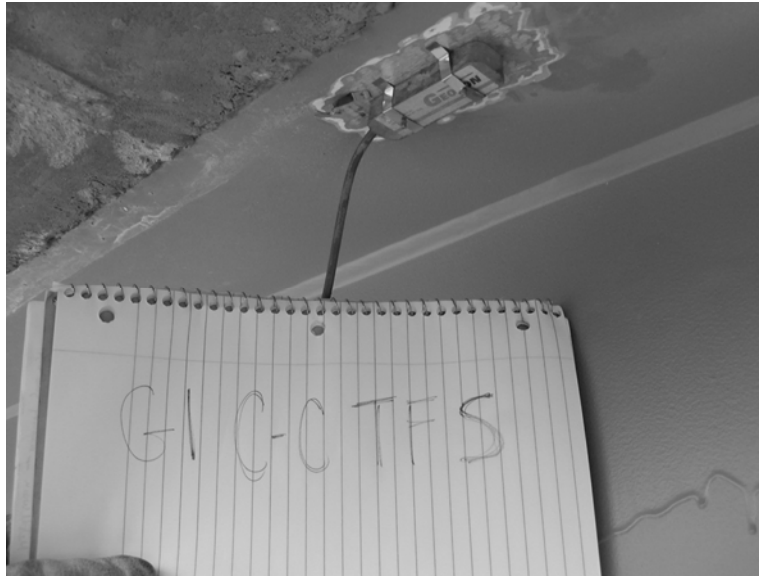
Figure 13. Replacement Gage for G1 C-C TF South.
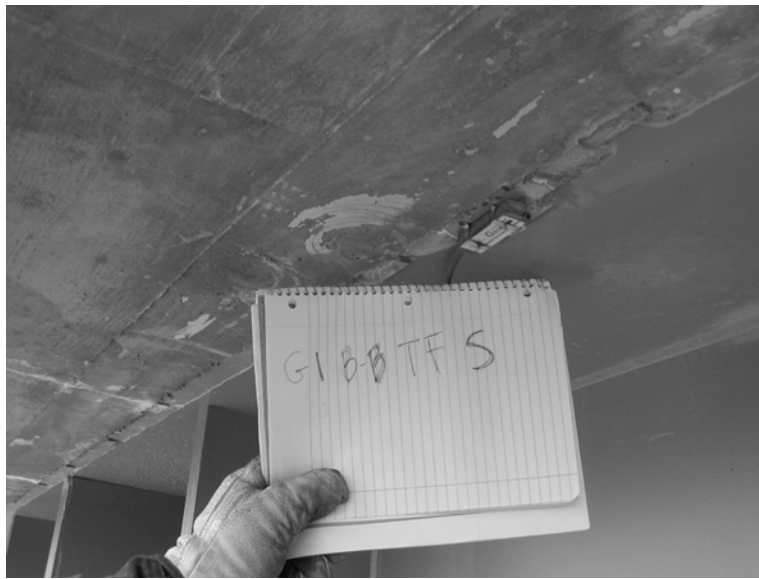
Figure 14. Replacement Gage for G1 B-B TF South.

3.2 STRUCTURE #314

3.2.1 Instrument Information

Normal and shear strains in the girders and diaphragms are measured using Geokon VSM-4000 vibrating wire strain gages, which have a gage length of 152.4 mm (6 in), a range of 3,000 microstrain and a sensitivity of 0.5-1.0 microstrain. Three gages were typically placed at a given girder section measuring normal strains near the flange tips. On at least one section per girder, a single gage measuring shear strains was placed at the non-composite neutral axis at a 45˚ angle relative to the longitudinal axis. On the diaphragms, the gages were mounted to measure axial

and shearing strains. Tiltmeters are placed at the non-composite neutral axis at certain locations as well. Figure 15 details all possible instrument locations at a girder section and Figure 16 depicts a VSM-4000 gage mounted to the bottom flange of a girder at the precasting facility. Figure 17 shows a typical diaphragm elevation.
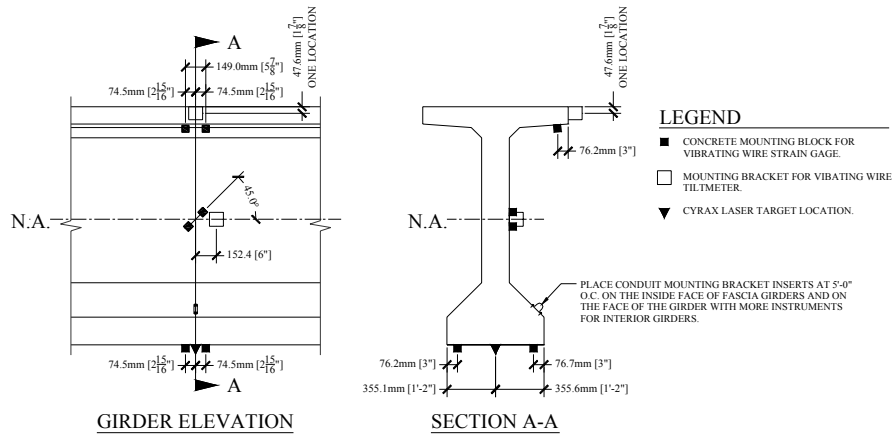
Figure 15. Typical Instrument Location and Orientation (Bennett 2004).
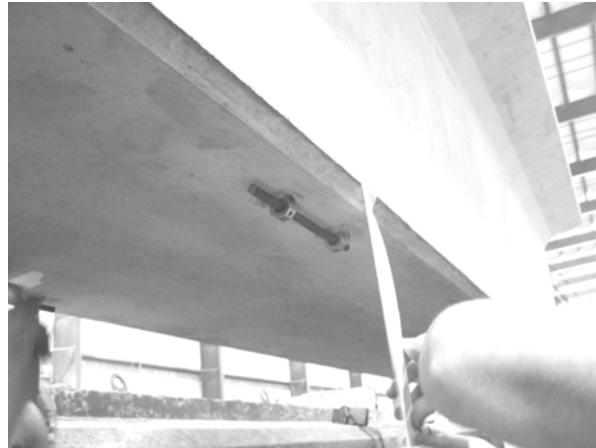
Figure 16. VSM-4000 mounted to girder (Bennett 2004).

■ VIBRATING WIRE STRAIN GAGE
  PLACED IN FIELD
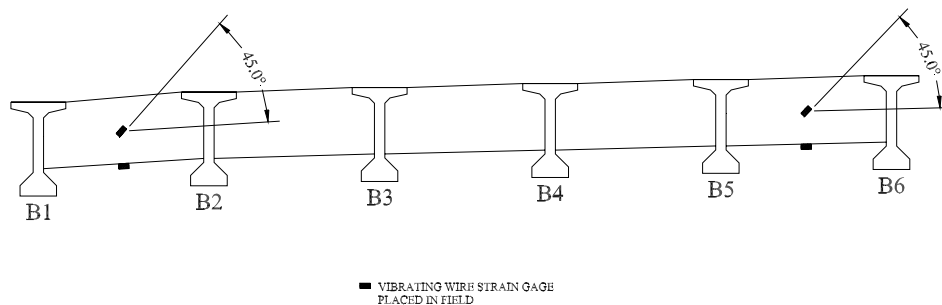
Figure 17. Span 1 Section at Interior Diaphragm (Bennett 2004).

Rotation of the girders (Figure 15) is measured using Geokon Model 6350 vibrating wire tiltmeters (Figure 6), which have a resolution of 10 arc seconds and a total range of ±10°. As shown in Figure 15, it was also originally planned to have global rotations monitored at various instances using a Cyrax laser measurement system supplied by PennDOT personnel from either District 12-0 or the Photogrammetry and Survey Division of the Bureau of Design. However, this system was not made available and laser scans of Structure #314 did not occur.

3.2.2 Instrument Statistics

Upwards of 70 strain gages and 10 tiltmeters are available for monitoring at any given time. The total number of instruments is summarized in Table 8. Instrument locations for the entire structure are depicted in Figure 18 and shown for a representative girder in Figure 19 and Figure 20. Table 9 through Table 11 provide numerical summaries of the instrumentation.

Table 8. Instrument Quantity Summary, Structure No. 314 (Bennett 2004).

Instrument Type	Location	Quantity
Vibrating Wire Strain Gages	Girder	60
	Diaphragm	8
	Total	**68**
Vibrating Wire Tiltmeters	Girder	9
	Total	**9**
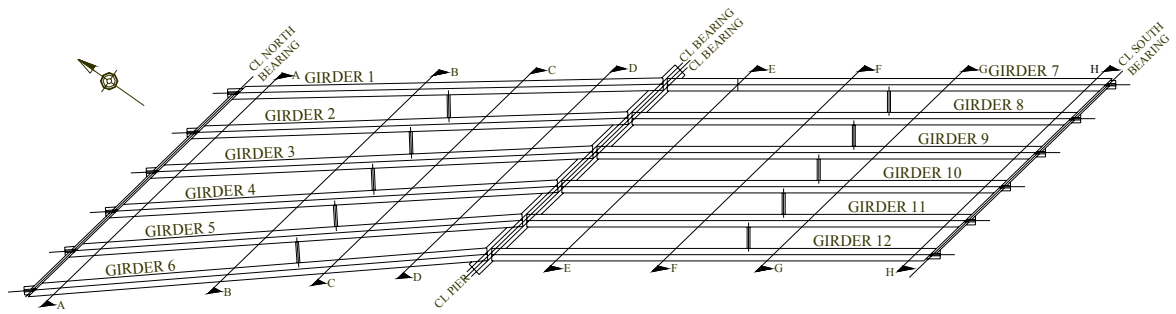
Figure 18. Instrument Locations on Bridge Plan View (Bennett 2004).
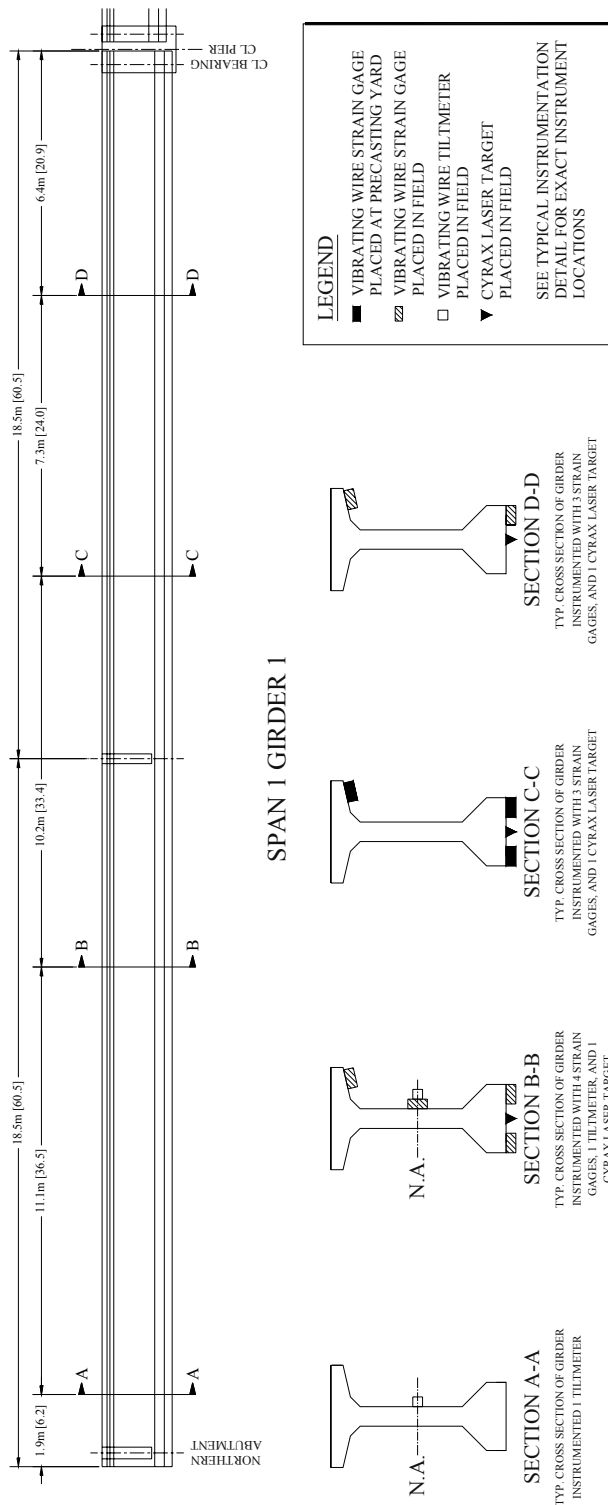
Figure 19. Representative Girder Instrument Locations (Bennett 2004).

19

Figure 20. Typical Girder Isometric View Detailing Flange Instruments.

Table 9. Girder Instrument Locations (Linzell and Laman 2001).

Girder	Section	Dist from North Bearing		Quantity
		m	**ft**	
G1	B-B	13.0	42.7	4
G1	C-C	23.2	76.1	3
G1	D-D	30.5	100.1	3
G3	B-B	13.4	43.8	4
G3	C-C	24.4	79.9	3
G3	D-D	31.7	103.9	3
G6	B-B	15.2	49.9	4
G6	C-C	25.9	84.8	3
G6	D-D	33.2	108.8	3
G7	E-E	5.3	17.4	3
G7	F-F	14.4	47.4	3
G7	G-G	21.8	71.8	4
G9	E-E	5.3	17.4	3
G9	F-F	14.4	47.4	3
G9	G-G	21.8	71.8	4
G12	E-E	5.3	17.4	3
G12	F-F	14.4	47.4	3
G12	G-G	21.8	71.8	4

NOTE: Distances are measured along the centerline of the girder from north to south.

20

Table 10 Diaphragm Instrument Locations (Linzell and Laman 2001).

Girder	Span Number	Diaphragm Number (From North End of Bridge)	Quantity
G1-G2	1	2	2
G5-G6	1	2	2
G7-G8	2	4	2
G11-G12	2	4	2

NOTE: Diaphragms at abutment and pier are included.

Table 11. Rotation Instrument Locations (Linzell and Laman 2001).

Girder	Section	Distance from North Bearing Going South m	ft	Quantity
G1	A-A	1.9	6.2	1
G1	B-B	13.0	42.7	1
G6	A-A	2.0	6.7	1
G6	B-B	15.2	49.9	2
G7	G-G	21.8	71.8	1
G7	H-H	36.0	118.3	1
G12	G-G	21.8	71.8	1
G12	H-H	36.0	118.3	1

NOTE: Distances are measured along the centerline of the girder from north to south.

3.2.3   Instrument Installation and Monitoring – Fabrication and Construction

Detailed information related to instrument installation and monitoring during fabrication and construction, which occurred prior to initiation of the project described herein, can be found elsewhere (Hiltunen et al. 2004, Linzell et al. 2003, Linzell and Laman 2001, Shura 2005). A brief summary is provided herein.

A detailed instrument installation and monitoring plan was developed and implemented during girder fabrication at the precasting facility. This plan involved the girder strain gages mentioned in the previous section and some additional strain gages and thermistors used only during fabrication to track girder top flange strains and internal temperature changes during the casting and curing process. Vibrating wire instrument placement and data acquisition started before prestressing release and continued throughout girder fabrication and storage with vibrating wire (VW) strain gages being used in conjunction with length, temperature, and camber measurements and material property tests to determine deformations, stresses, and long-term prestressing losses in the girders. Table 12 provides a timeline for the activities that occurred during instrumentation and monitoring at the precasting yard.

Table 12. Fabrication Instrumentation and Monitoring Schedule for a Typical Precast Girder (Bennett 2004).

Day	1			3			6	7	14	21	28	+14
Action	Pre-Casting	Casting	Post-Casting	Pre-Release	Release	Post-Release						
(1)	(2)	(3)	(4)	(5)	(6)	(7)	(8)	(9)	(10)	(11)	(12)	(13)
Install Atkins Thermistors	●											
Cast Concrete Cylinders		●										
Place Strain Gage Mounting Brackets			●				●					
Install VW Strain Gages in Girder Top Flange				●								
Modulus of Elasticity Tests at Penn State					●						●	
Install VW Gages at Flange Tips and N.A.								●				
Record Gage Measurements				●		●		●	●	●	●	●
Record Survey Measurements				●		●		●	●	●	●	●

Remaining instruments discussed in the previous section, consisting largely of the tiltmeters on the girders and strain gages on the cast-in-place diaphragms, were installed as specified at the construction site. Figure 21 shows a photograph of the instrumented girders during the construction process.

Figure 21. Structure #314 Girders During Construction.

3.2.4   Instrument Installation and Monitoring – Current Project

Sixty-four instruments from Structure #314 were selected and wired into the waterproof cabinet containing the data-logger (Figure 22). The data-logger was programmed to record data once an

hour. The data-logger initially collected three weeks of data and then the battery and one of the boards in the logger needed to be replaced and/or repaired. The data-logger is now continuously monitoring Structure #314, performing a scan once every hour.

Figure 22. Wiring Structure #314 Gages into Data-Logger.

4 NUMERICAL MODELING

Data produced during field monitoring of Structure #207 and Structure #314 were compared to results produced by three different types of numerical models: a grillage model, a full-shell 3D finite element model and a 3D finite element model containing a combination of frame members and shell and brick elements. Discussions of these models for each structure follow. More detailed discussions of the models can be found elsewhere (Bennett 2004, Hiltunen et al. 2004, Linzell et al. 2003, Linzell and Laman 2001, Shura 2005).

4.1 STRUCTURE #207

4.1.1 Model Descriptions

4.1.1.1 Grillage Model

The Structure #207 grillage model was developed in SAP2000 and had the steel superstructure modeled as a true grillage using SAP2000 frame elements with the concrete deck modeled using a series of offset shell elements with varying stiffness to more accurately depict placement of the wet concrete onto the steel superstructure. Therefore, the model may not be a true grillage but was referred to as such since the steel superstructure was modeled in a single, two-dimensional plane.

The grillage model that was developed was run using the small displacement and staged construction analysis capabilities in SAP2000 to attempt to accurately mimic effects of the final construction procedure on structure response. Support conditions shown on the design plans at the pier and abutments were reproduced numerically and the SAP2000 self-weight function was used to apply all dead loads for these analyses while point loads were used to apply the HS20 truck loads to the deck. An isometric view of the model is shown in Figure 23.
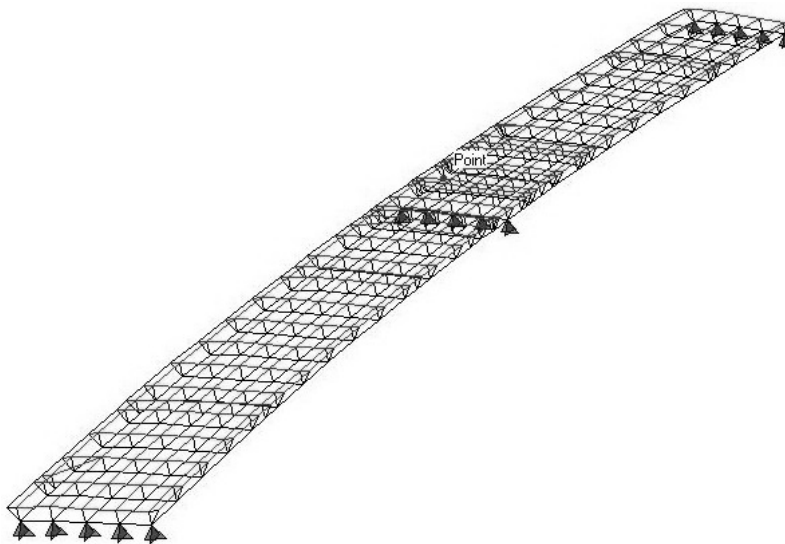

Figure 23. Structure #207 SAP2000 Grillage Model (Shura 2005).

Nodes were placed at all cross-frame and flange transitions along the girder lines. Girders were modeled as straight SAP2000 frame members between these nodes. All flange and web transitions were considered, as well as elevation changes along the length and cross-section of the structure. Geometric properties of these elements were calculated directly by SAP using inputted flange and web plate dimensions. Intermediate stiffeners were not considered by the grillage model.

The K-frames between girders were modeled as straight frame members and assigned equivalent stiffness values. Geometric properties required for a typical cross-frame member included strong and weak axis moments of inertia, vertical and horizontal shear areas, torsional constants, and an equivalent area for self-weight calculations. Because no published procedures are available for estimating properties of cross-frames, an additional numerical analysis in SAP2000 was used to obtain the moment of inertia about the strong axis for a representative cross-frame (Shura 2005). The weak axis moment of inertia was calculated by summing the local strong axis moments of inertia for the cross-frame members since the vertical axis of the cross-frame coincided with the local strong axis of the members. Similarly, the torsional constant of the cross-frame was determined by summing torsional constants of the members.

The concrete deck was modeled using 3 and 4-noded shell elements. Wet concrete was modeled using a thick plate with pure plate characteristics and the material density of concrete. These elements have 6 degrees of freedom at each node and no in-plane stiffness. Translational stiffness for these elements was reduced to zero to ensure that non-composite behavior of the girders was achieved. These elements were used primarily to apply the self-weight of the wet concrete, and subsequently would contribute no stiffness to the girder frame elements. Concrete that had set was modeled using shells with full shell behavior but a material density equal to zero since self-weight is accounted for using the pure plate elements. At any location, these two types of elements could be superimposed to account for changing material properties (i.e. modulus) during construction.

Composite action was achieved by offsetting the shell elements above the girder frame members and using stiff, weightless, rigid frame members to connect the two. These members connected the two meshes and transferred loads from the deck to the girders. The portion of the deck cantilevered outside the fascia girders was modeled in the same manner as the rest of the deck, except that false supports were needed in the SAP2000 model to stabilize the cantilever when modeling the wet concrete. These false supports consisted of hinged frame elements capable of transferring axial loads, shown in Figure 24, which represented the overhang brackets installed on the actual structure to support the weight of the wet concrete.
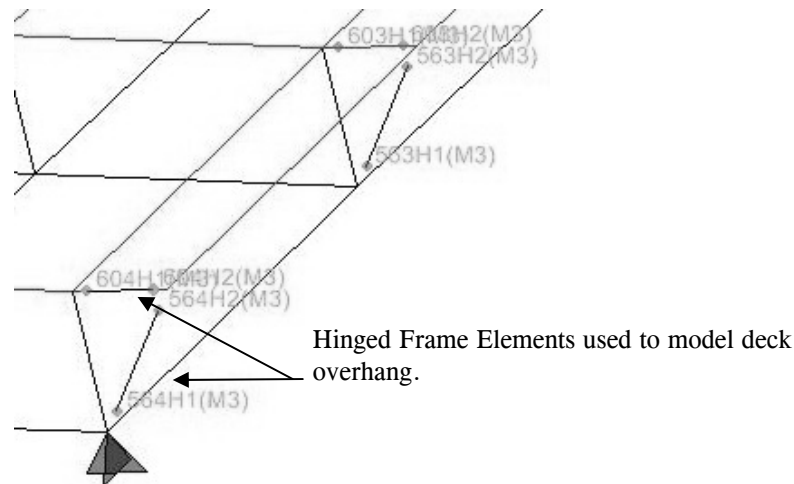
Hinged Frame Elements used to model deck overhang.

Figure 24. False Members Used to Support Cantilevered Slab at Abutment, Structure #207 (Shura 2005).

Prior to running analyses related to the scope of work described herein, staged construction analyses that accounted for actual girder erection and deck placement procedures were run to account for construction effects on response. These analyses were completed using 14 stages as listed in Table 13.

Table 13. SAP2000 Construction Stages (Shura 2005).

	STAGE	EVENT
Superstructure Erection	1	Addition of Girders G4A-C, G5A-C, and cross-frames
	2	Addition of Girders G3A-C and cross-frames
	3	Addition of Girders G2A-C and cross-frames
	4	Addition of Girders G1A-C and cross-frames
	5	Addition of Girders G4D & E, G5D & E, and cross-frames
	6	Addition of Girders G3D & E and cross-frames
	7	Addition of Girders G2D & E and cross-frames
	8	Addition of Girders G1D & E and cross-frames
Concrete Deck and Parapet Placement	9	Addition of wet concrete over positive moment region in Span 1 (Thick Plate Elements)
	10	Addition of shell elements accounting for the stiffness of the deck over the positive moment region in Span 1 (Full Shell Elements)
	11	Addition of wet concrete over positive moment region in Span 2
	12	Addition of full shell elements over positive moment region in Span 2
	13	Addition of wet concrete over negative moment region
	14	Application of parapet dead load

During each stage, the corresponding frame or shell elements were added to the structure's deformed shape, and an analysis was performed for that stage. All relevant information such as

26

node deformations, frame and shell forces, support reactions, etc. was retained from each previous stage. A series of analyses were completed to ascertain the effects of loose verse rigid splices on structure response. Details of these analyses are provided elsewhere (Shura 2005) and they indicated that rigid connections should be used.

4.1.1.2 Full-Shell 3D Finite Element Model

The full shell finite element model of Structure #207 was created using ABAQUS/Standard. ABAQUS was selected as the modeling tool because of its ability to model complex structures in the elastic and inelastic ranges at both small and large deflections and because of the large element library that is available to the user. Figure 25 depicts the model that was created.
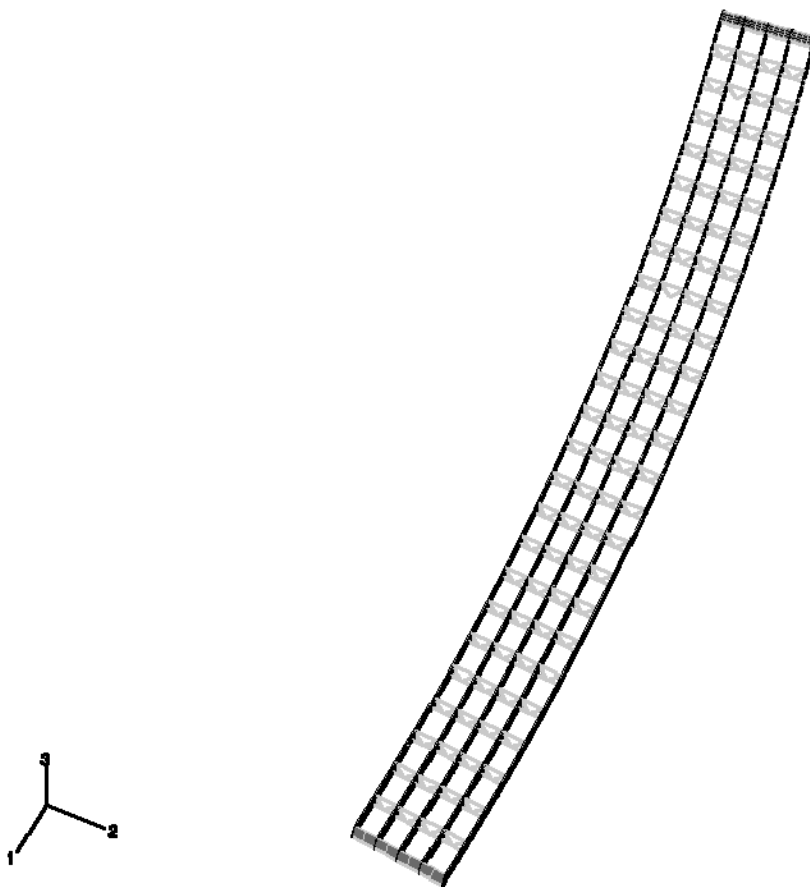
Figure 25. Full Shell Model of Superstructure, Structure #207.

Girder camber was included in the model. Webs were modeled with 18 nodes through the web depth with the location of nodes along the girder arc being selected as a function of the element height so that the elemental aspect ratio remained close to 1:1. The shell general section option in ABAQUS was used to define these elements. The shell general section option requires that the thickness of the section, the material properties, and the orientation of the section be defined by the user. The S4R element was selected from the ABAQUS element library. The S4R

element is a conventional, four-noded shell element that allows displacement and rotational degrees of freedom and uses reduced integration to calculate shell section behavior. It accounts for finite membrane strains and large rotations along with transverse shear stiffness. Super-elevation was not included in the model.

Girder flanges were also modeled using S4R elements. Flange nodes correspond with the web nodes along the length of the girders. Flange element aspect ratios did not exceed 2:1.

Radial cross-frame members between adjacent girders were modeled using beam elements, with the diagonals and the top and bottom chords being modeled as separate members for cross frame. ABAQUS B31OS beam elements were selected for all cross-frame members. The B31OS element is an open section, three-dimensional beam element that uses linear interpolation between end nodes with 6 degrees of freedom at each node. The element is formulated so that transverse shear deformation is permitted. All cross frames were assumed to be rigidly connected to the girder webs.

Girder web stiffeners were also modeled using beam elements. The ABAQUS B31 element was used to model the web stiffeners. The B31 is a three-dimensional beam element using linear interpolation between end nodes with 6 degrees of freedom at each node. The element is formulated so that transverse shear deformation is permitted.

The slab was modeled using S4R shell elements. Slab element nodes were selected to correspond to an aspect ratio of 2:1. The slab thickness of 228.6 mm (9.0 in) was inputted into the model.

All components of the model were assigned the nominal material and geometric properties of structural steel. In addition, the assumption was made that all parts of the model will remain in the elastic range using small displacement response. Boundary conditions were inputted to match what was observed from the design plans and during erection. Loads consisted of bridge component dead loads and point loads representing wheels from an HS20 truck.

4.1.1.3   Frame, Shell, Brick 3D Finite Element Model

An additional model was created using brick elements for the slab. The ABAQUS C3D8R brick element (Figure 26) was used to model the slab. This element has 8 nodes and is a linear brick element with reduced integration. The brick finite element model used beam elements to model the girder flanges and shell elements for the webs. The brick element model was analyzed under dead load and point load representing the wheels from an HS20 truck.
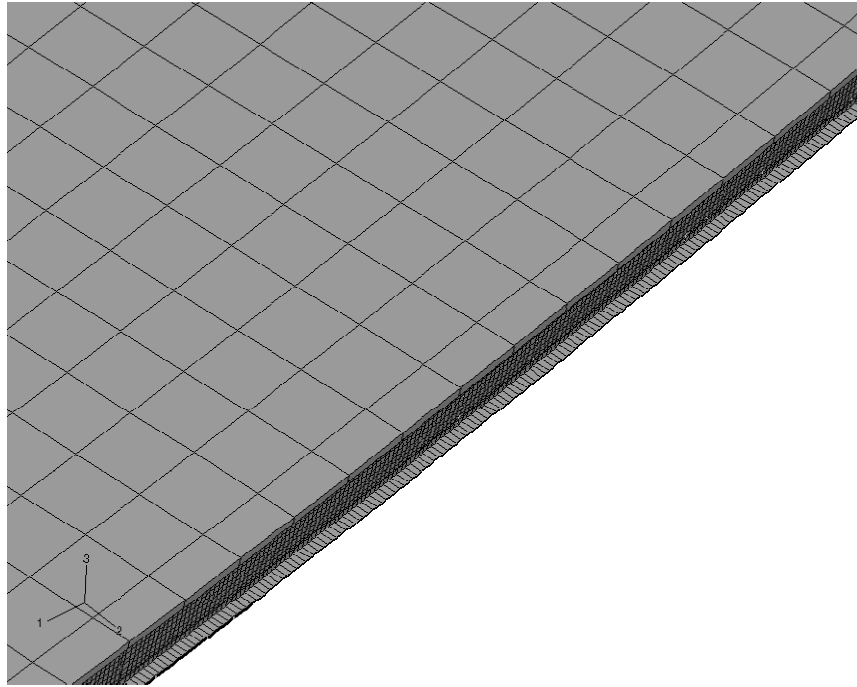
Figure 26. ABAQUS Shell and Brick Finite Element Model.

STRUCTURE #314

4.1.2 Model Descriptions

4.1.2.1 Grillage Model

The Structure #314 grillage model was developed in ABAQUS/Standard and included the geometric nonlinearity options available within that program. The model consisted of a planar grid containing the girders and deck with any camber, super-elevation and other out-of-plane effects being ignored.

Frame elements were used to model prestressed concrete girders, prestressed concrete girders composite with the cast-in-place concrete deck, and the cast-in-place concrete diaphragms. Longitudinal frame elements were intended to model non-composite girders or composite beam-slab girders depending on the construction or in-service stage. Cross sections of individual girders are modeled as I-sections and rectangular sections were used for cast-in-place diaphragms.

Transverse frame elements connected at a skewed angle between adjacent girders were intended to represent the deck and permit load sharing between girders. Additional transverse frame elements, used to represent the diaphragms, were also placed at the abutments, near the mid-span of both spans, and at the pier. Diaphragms at the abutments and pier matched the skew angle while those near the mid-span were placed perpendicular to the girders. The existence of these transverse frame elements was dependent on the construction or in-service stage. Measured section and material properties were used for the elements. A plan view of the model is shown in Figure 27.
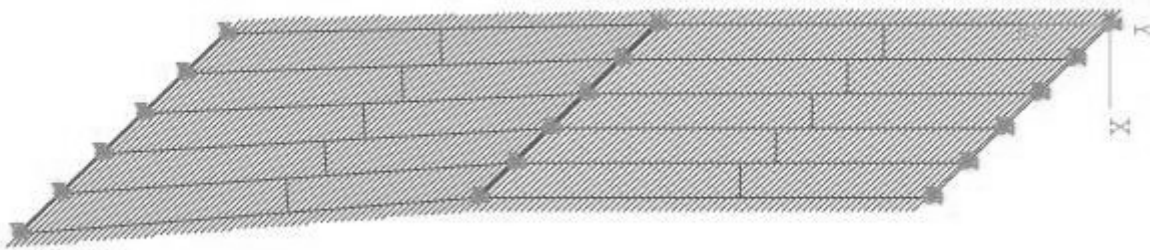
Figure 27. Structure #314 ABAQUS Grillage Model.

Each span of the deck slab was modeled as six individual strips with the width of each strip being constant. The development of composite action was modeled by varying elastic moduli as the pour progressed. Boundary conditions were taken as simply supported for all the piers and abutments. Load balancing was used to apply prestressing forces to the grillage model. Therefore, these forces were applied at an eccentricity from the neutral axis of each girder to account for their eccentricity from the design plans. As such, additional moments were also applied at the ends of the girders to account for the eccentricity.

4.1.1.2 Full-Shell 3D Finite Element Model

The full shell finite element model of Structure #314 was created using ABAQUS/Standard. Girders, including web and flanges, and deck were modeled using S4R element selected from the ABAQUS element library. The shell general section option in ABAQUS was used to define girder elements with web node locations being defined corresponding to the non-composite elastic neutral axis for each girder. Girder cross sections consisted of eight shell elements as they were modeled so that their elemental aspect ratios remained as close to 1:1 as possible. Each flange consisted of two elements and the web had four elements.

Diaphragms were also composed of four-noded S4R shell element. Partial-depth diaphragms located at mid-span were connected to adjacent girders at their non-composite neutral axis and at the top web node. Full-depth diaphragms at the piers and abutments were connected to adjacent girders along the entire web depth.

To represent the documented pour sequence for the deck, it was divided into six sections along the length of the structure. Each section was modeled using shell elements with varying moduli to represent setting of the concrete. Deck slab and top flange shells were connected using a series of tie-constraints defined in ABAQUS/Standard.

Special care was taken with the boundary conditions to imitate the design supports. Support conditions mimicking elastomeric bearings for all girders were created using ABAQUS C3D8R eight-noded brick elements with dimensions and properties matching those from the design plans. The top surfaces of the bearing elements were connected to the bottom flange shells with their bottom surfaces being restrained using fixed support conditions. Figure 28 depicts the model that was created.
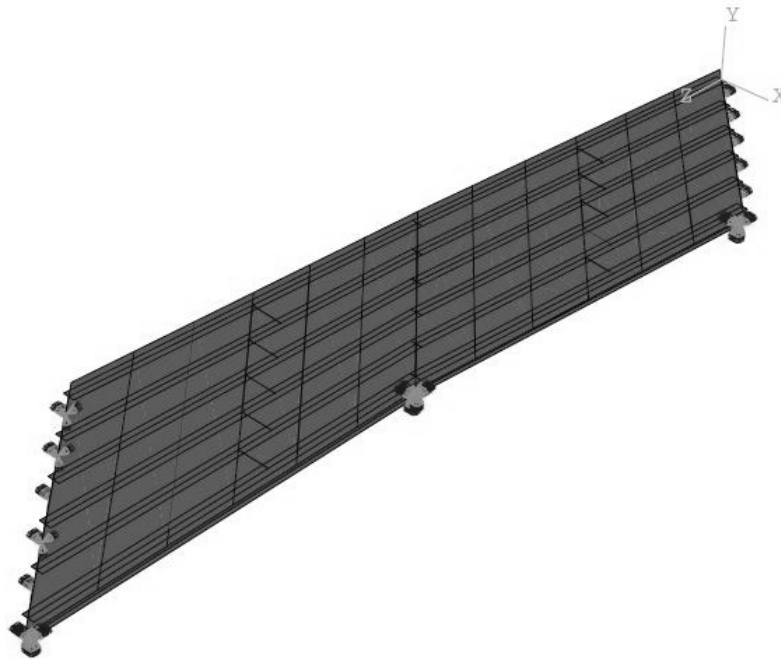
Figure 28. Full Shell Model of Superstructure, Structure #314.

All components of the model were assigned nominal material and geometric properties. In addition, the assumption was made that all parts of the model will remain in the elastic range. Loads consisted of bridge component dead loads and point loads representing wheels from an HS20 truck.

4.1.2.2   Frame, Shell, Brick 3D Finite Element Model

A combination of elements was used for the final model of Structure #314. This model was again created using ABAQUS/Standard.

Similar to the shell model, the girders consisted of eight S4R shell elements with aspect ratios close to 1:1. The concrete deck in spans 1 and 2 was similar in global geometry to the shell model but was comprised of 3D bricks, constructed using ABAQUS C3D8R elements. Tied constraints were again used to link the deck elements to the girder top flanges. Diaphragms in the present model were also constructed using C3D8R elements. Bearings were modeled and meshed using a similar procedure to the shell model.

All components of the model, as mentioned earlier, were assigned nominal material and geometric properties. In addition, the assumption was made that all parts of the model will remain in the elastic range. Loads consisted of bridge component dead load and point loads representing wheels from an HS20 truck. Figure 29 depicts the model that was created.
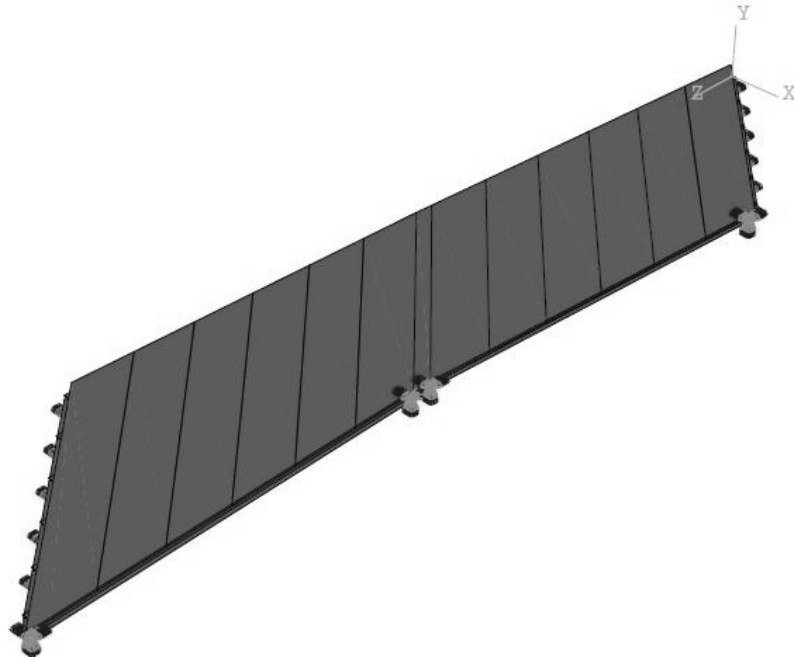
Figure 29. **4.2.1.2** **Frame, Shell, Brick 3D Model of Superstructure, Structure #314.**

5   DATA COLLECTION

A summary of field data collected during the current project is provided herein.

5.1   STRUCTURE #207

Figures 30 through 41 show representative plots collected for bridge 207. The figures show the data that was collected starting March 31, 2006 at 11 a.m. and continuing until May 4, 2006 at 8 a.m. These plots, which show limited variation in the recorded stresses due to temperature variations, are representative of the entire data set, which lasted from March 31 to August 1, 2006. As a result, plots for the remainder of the collected data are not included herein. The following plots show similar magnitudes in the change in stress for both the top and bottom flange. The change in stress for the top and bottom flanges in based solely on the change in temperature. The temperature plots show that the change in temperature for the top and bottom flanges is very similar, indicating a uniform heating or cooling of the girders and, subsequently, somewhat similar magnitudes for the change in stress throughout the cross section.
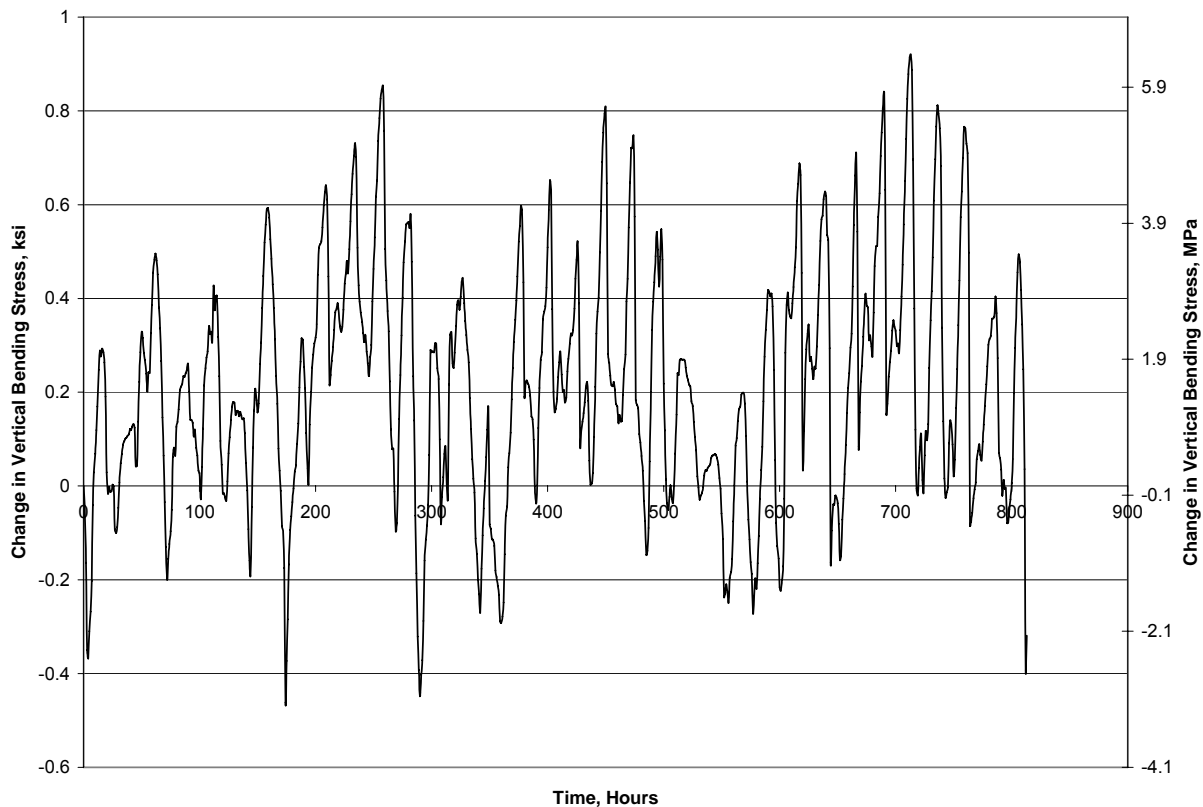
**Figure 30. Vertical Bending Field Results (1st Set) for Girder 5
Bottom Flange Section C-C (Fig. 7).**
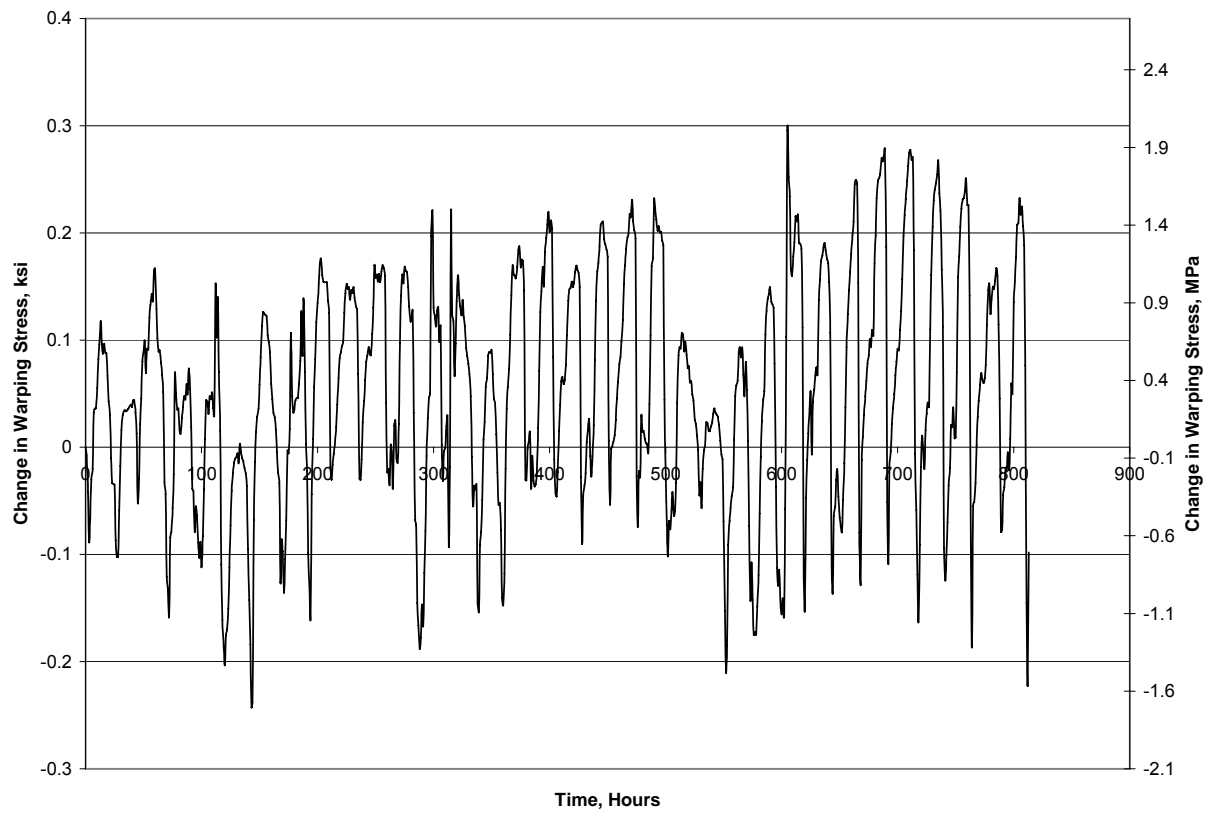
Figure 31. Lateral Bending Field Results (1st Set) for Girder 5 Bottom Flange Section C-C (Fig. 7).
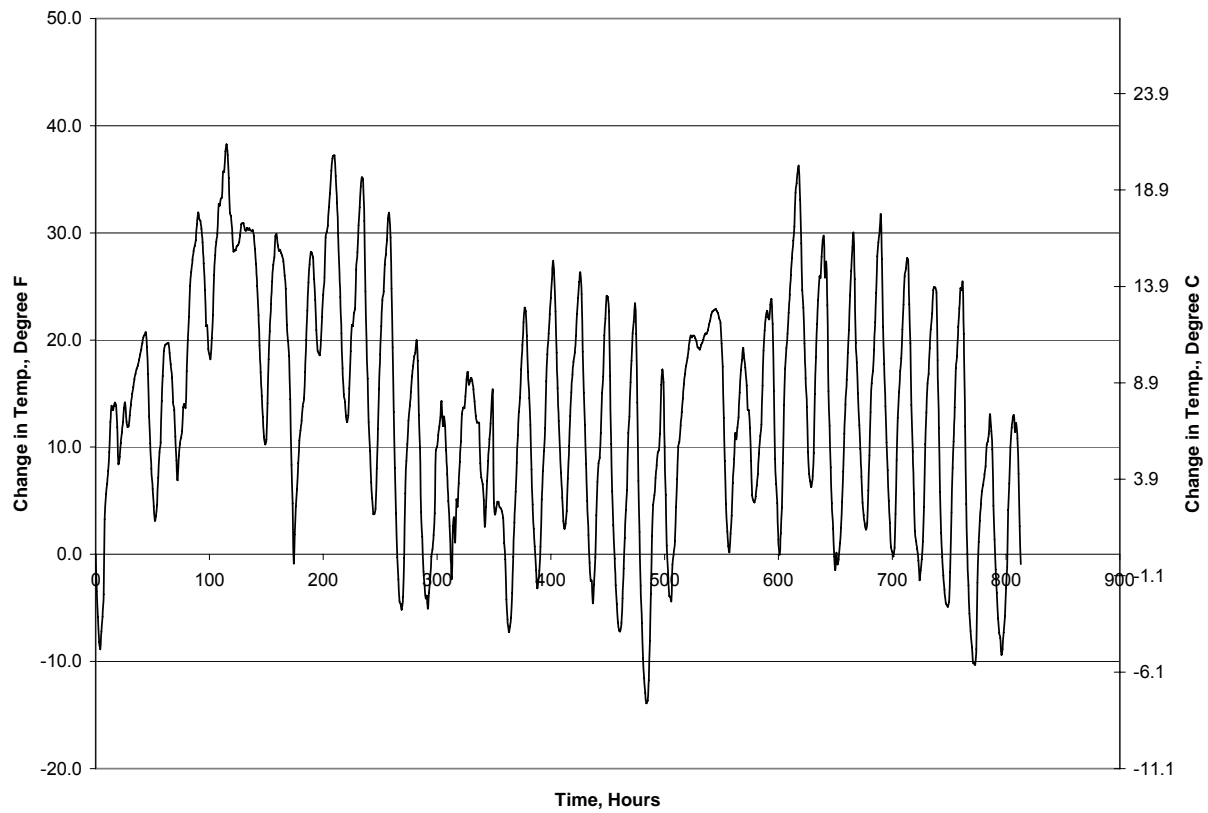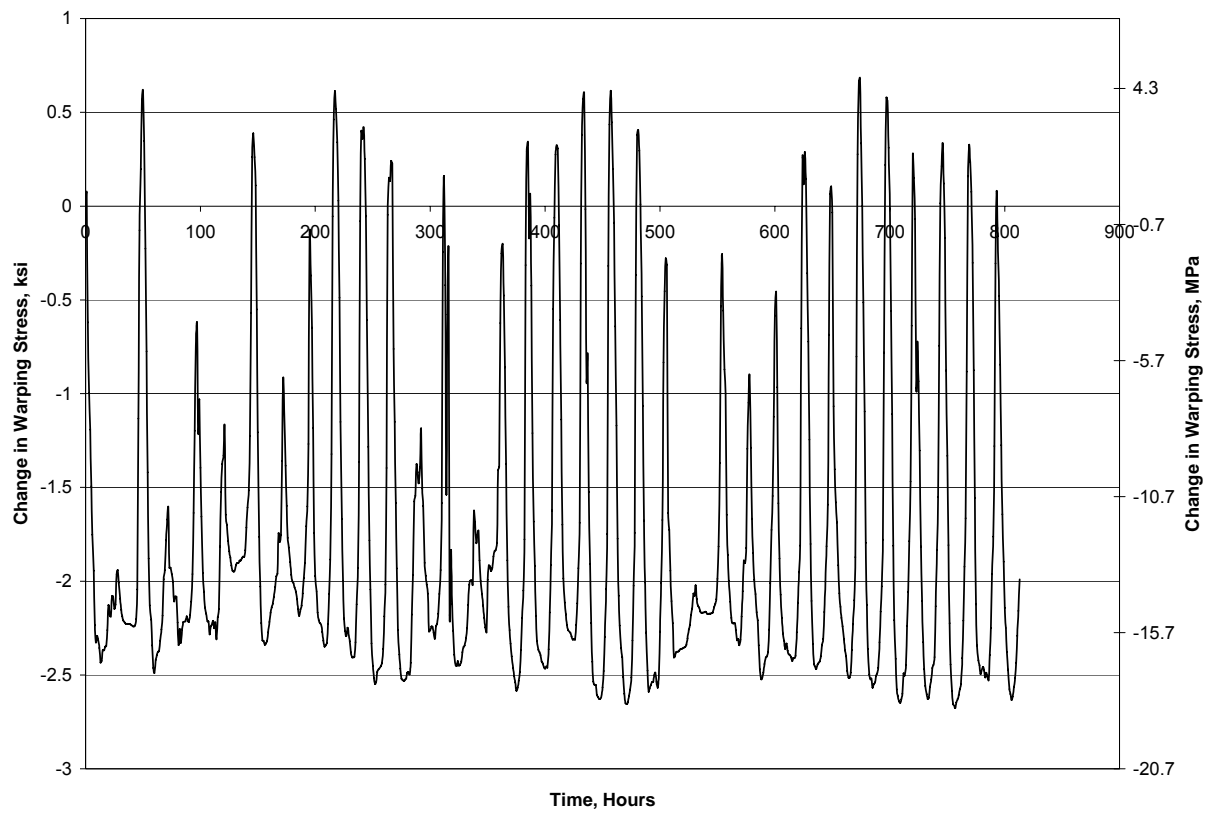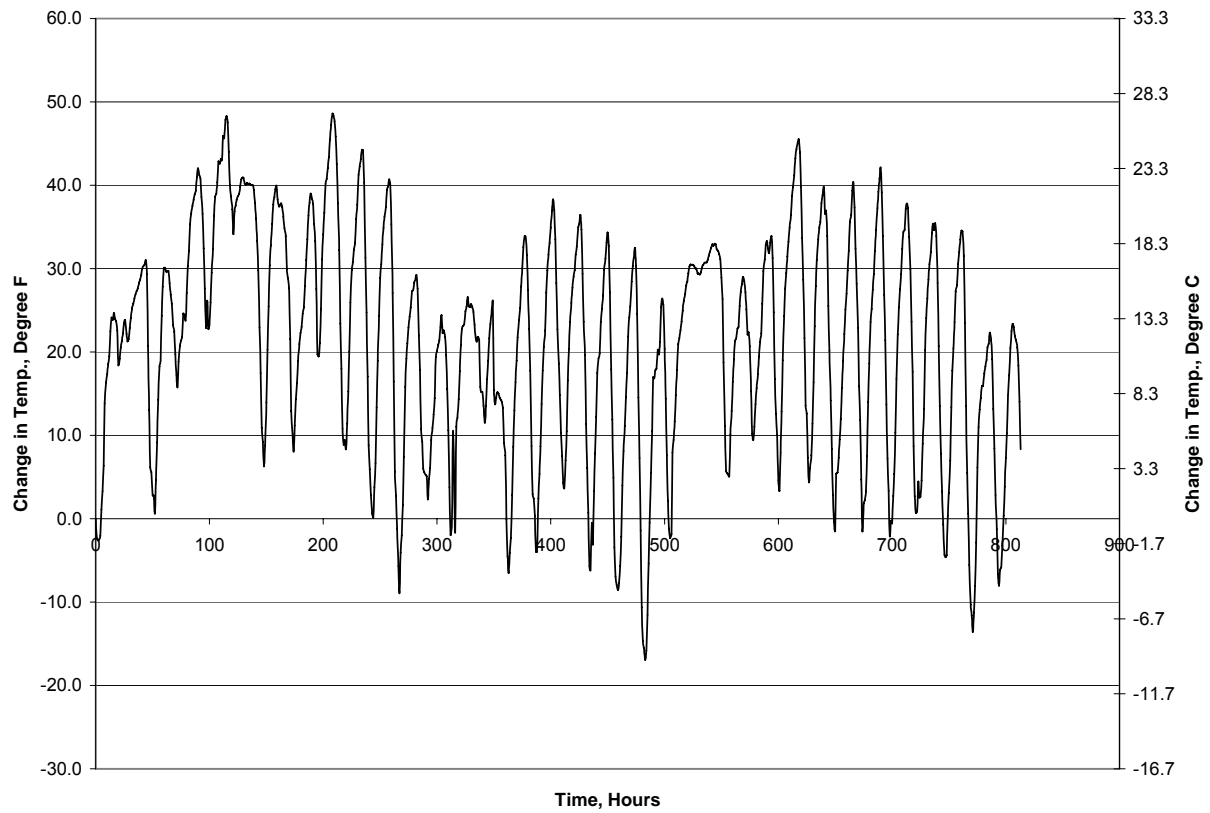
Figure 32. Temperature Field Results (1st Set) for Girder 5 Bottom Flange Section C-C (Fig. 7).
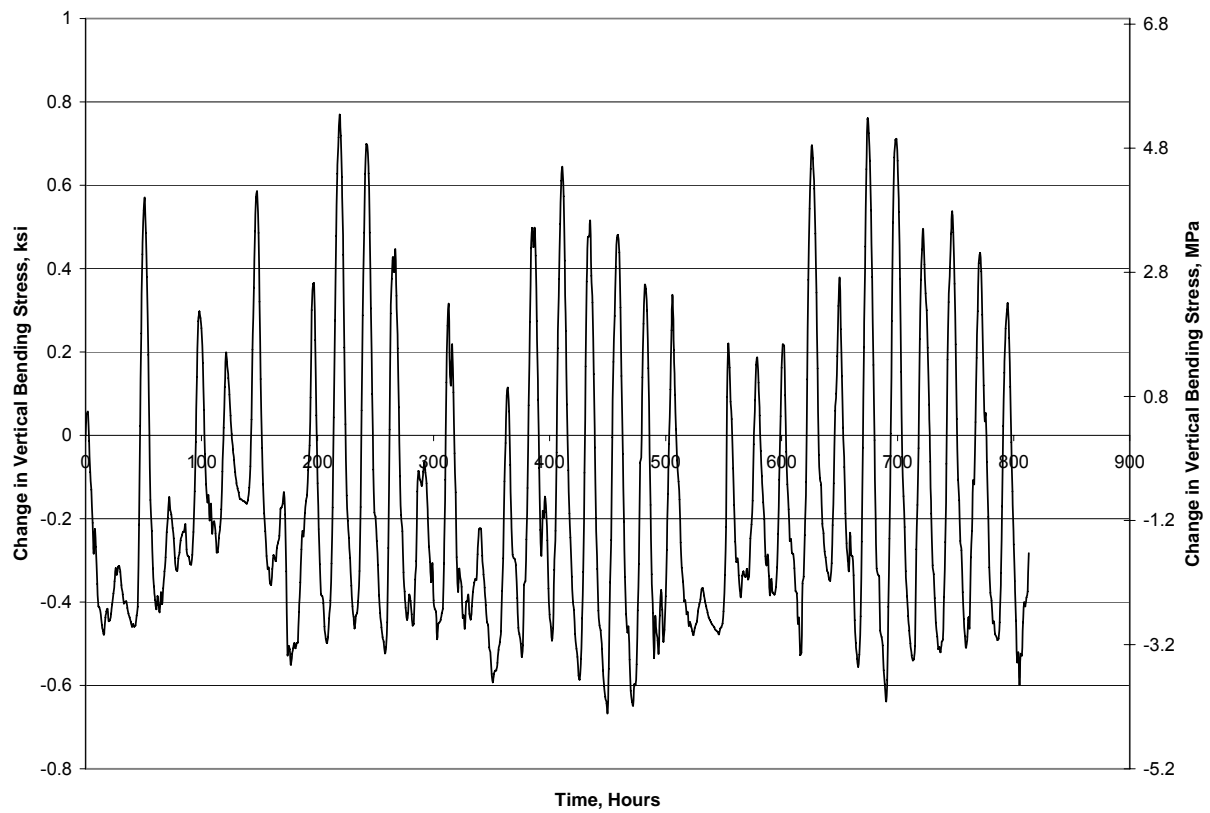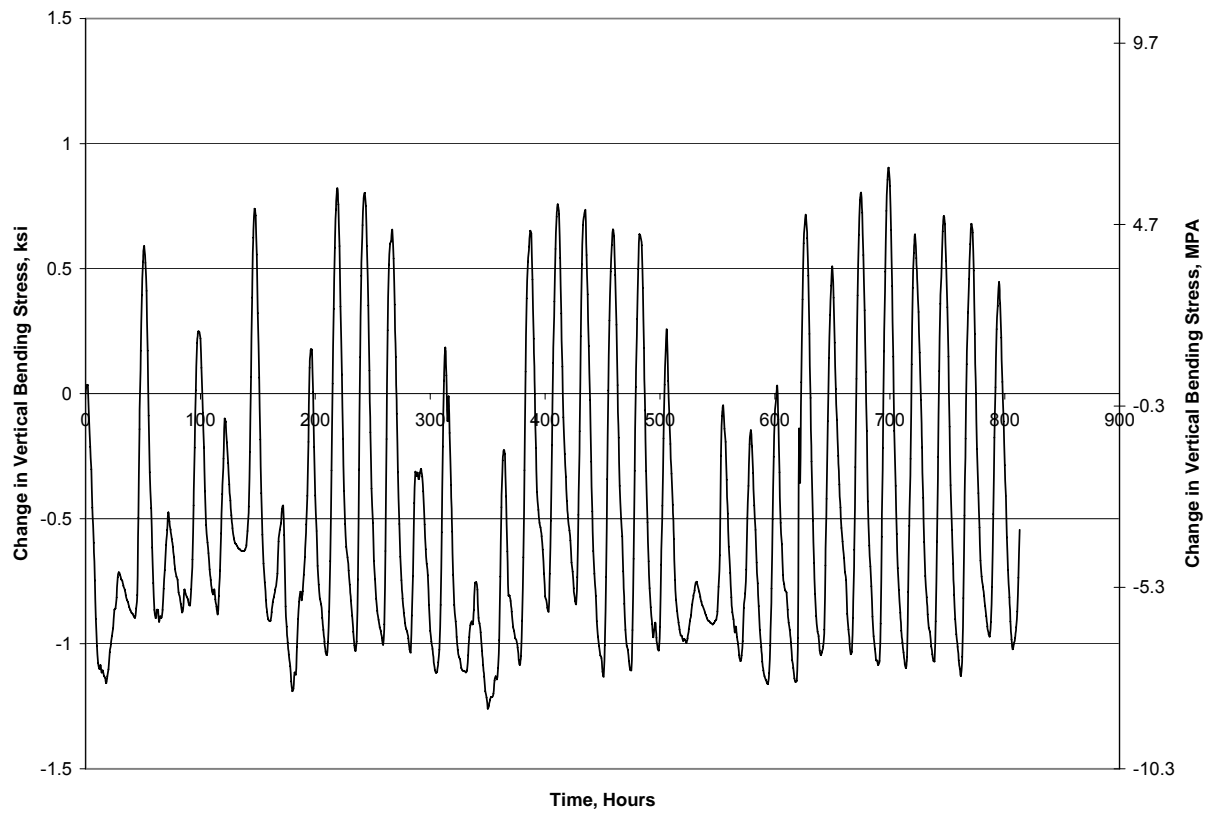
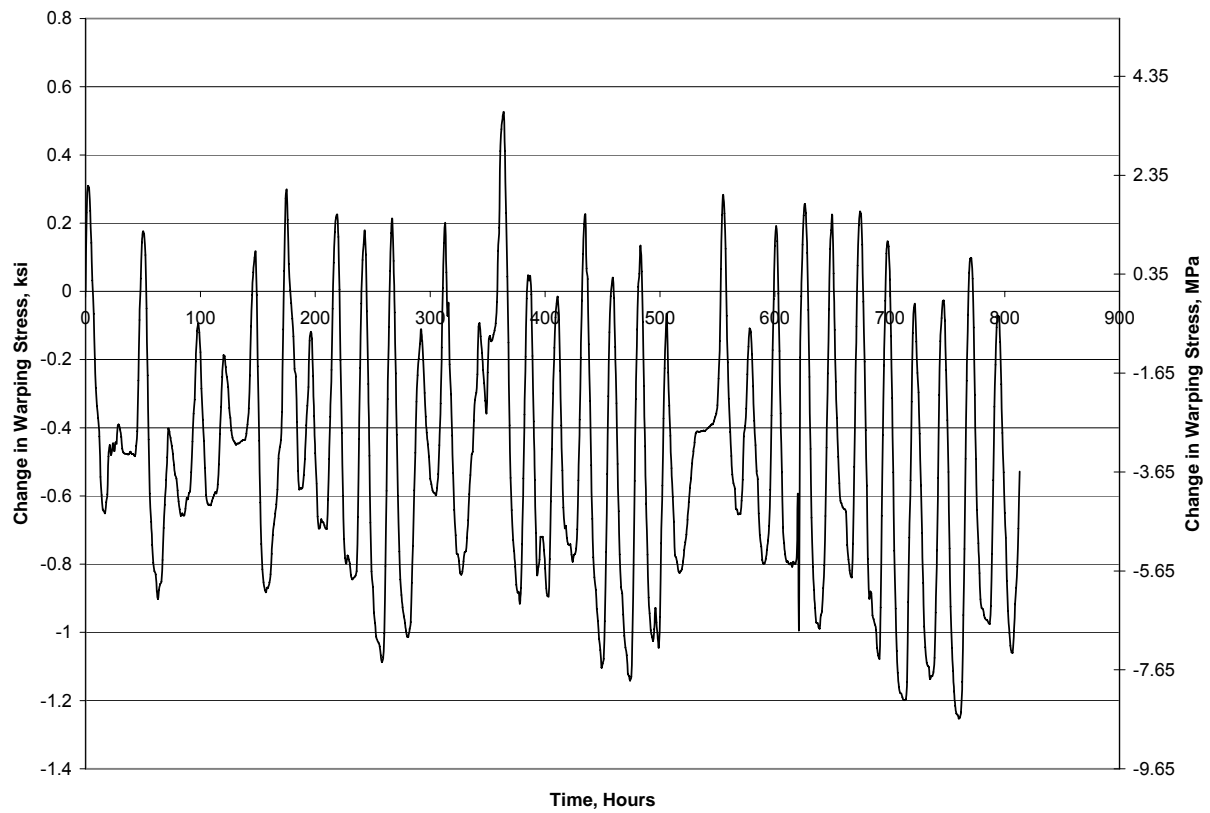**Figure 33. Vertical Bending Field Results (1st Set) for Girder 5 Top Flange Section C-C (Fig. 7).**
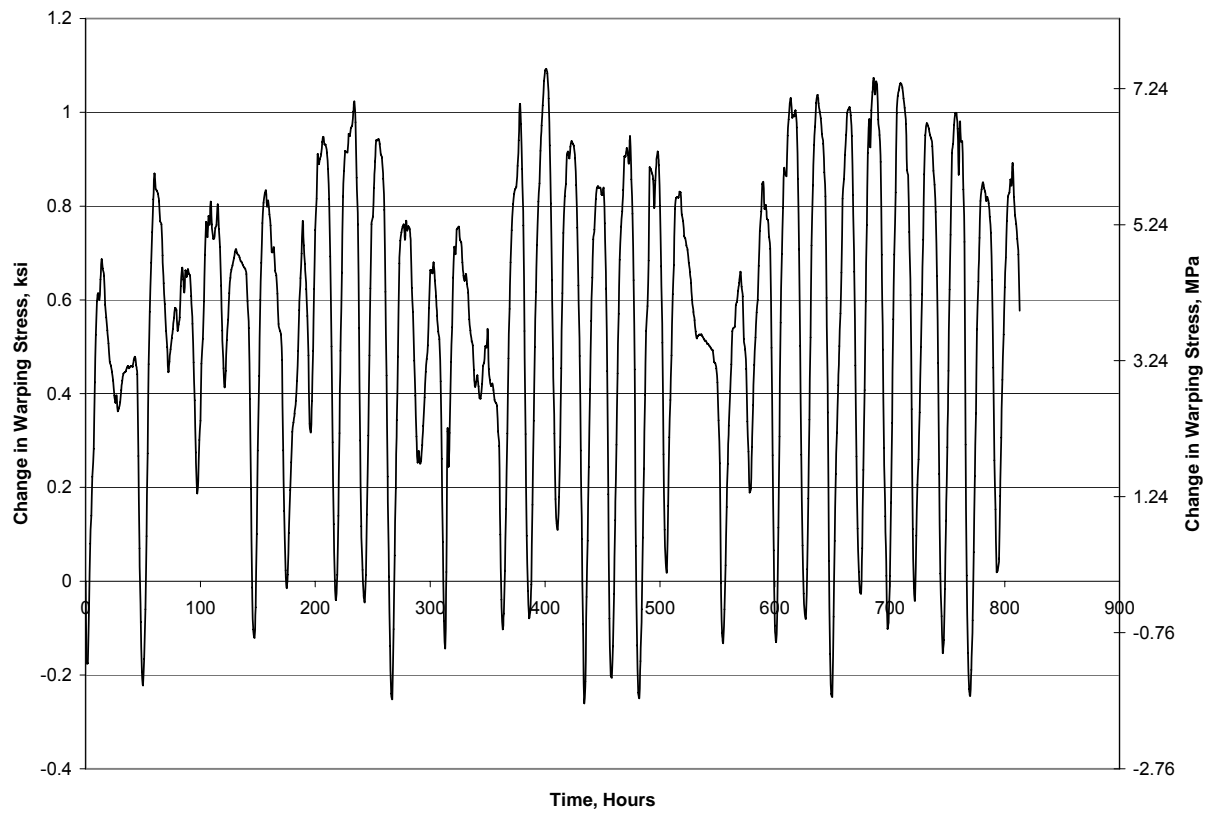
Figure 34. Lateral Bending Field Results (1st Set) for Girder 5 Top Flange Section C-C (Fig. 7).
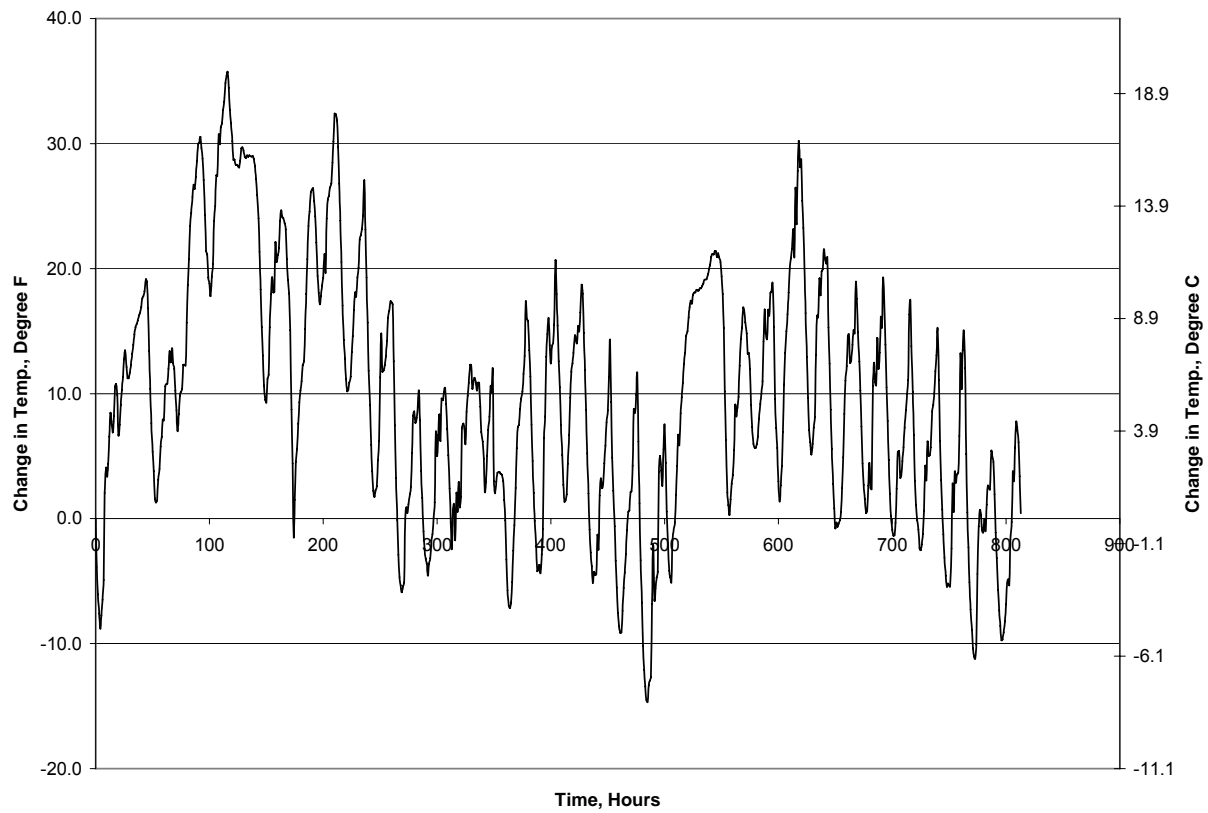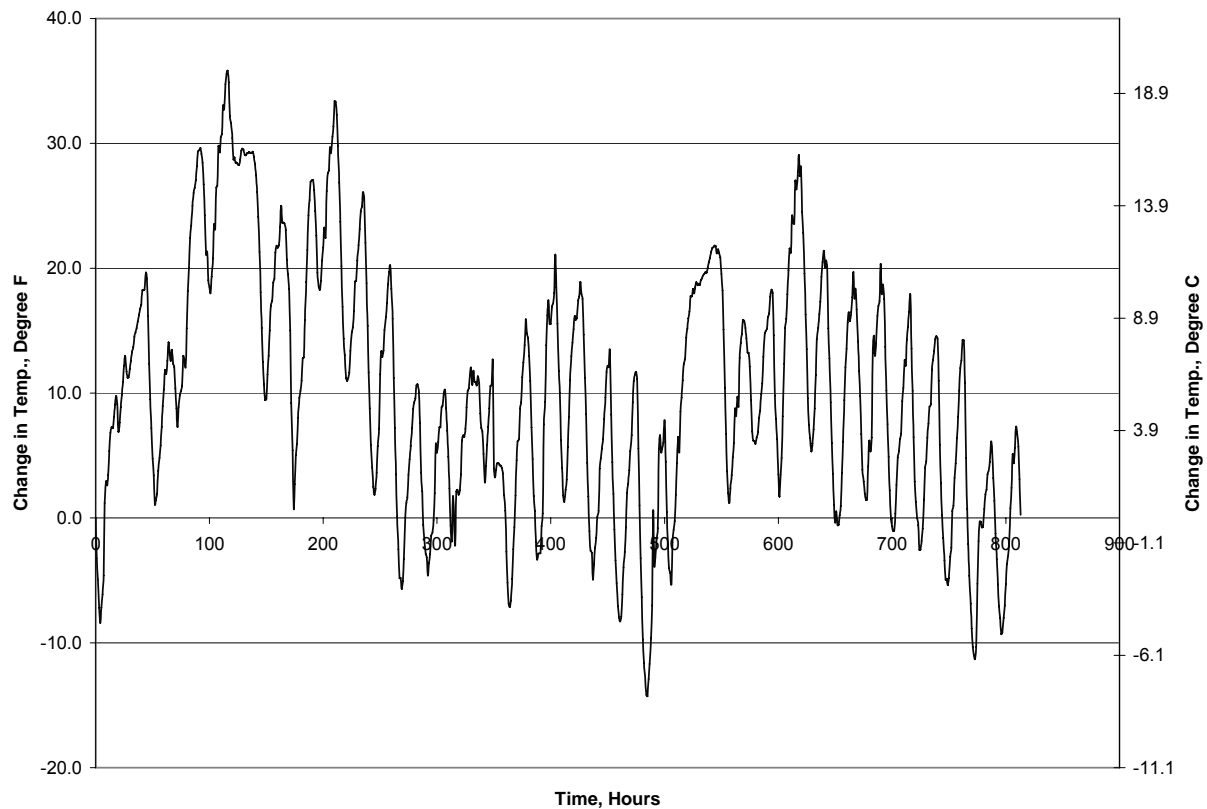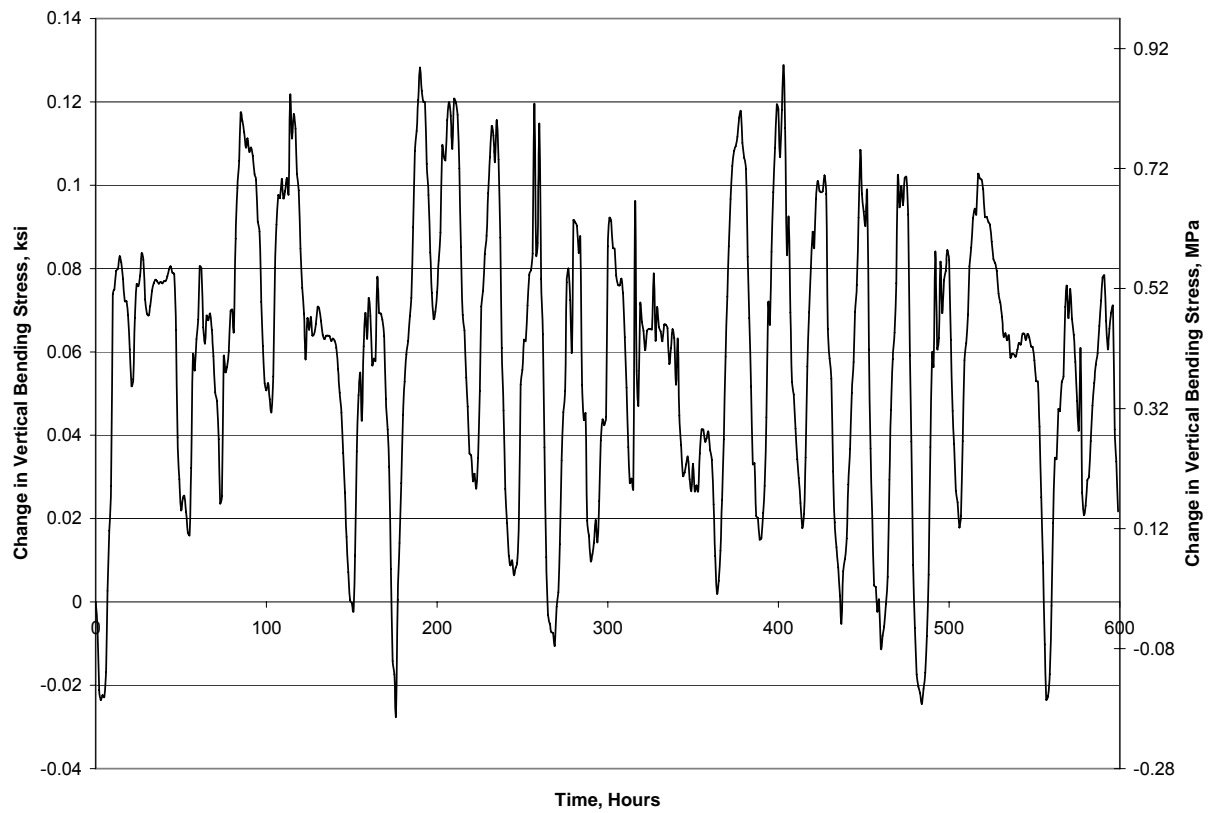
Figure 35. Temperature Field Results (1st Set) for Girder 5 Top Flange Section C-C (Fig. 7).
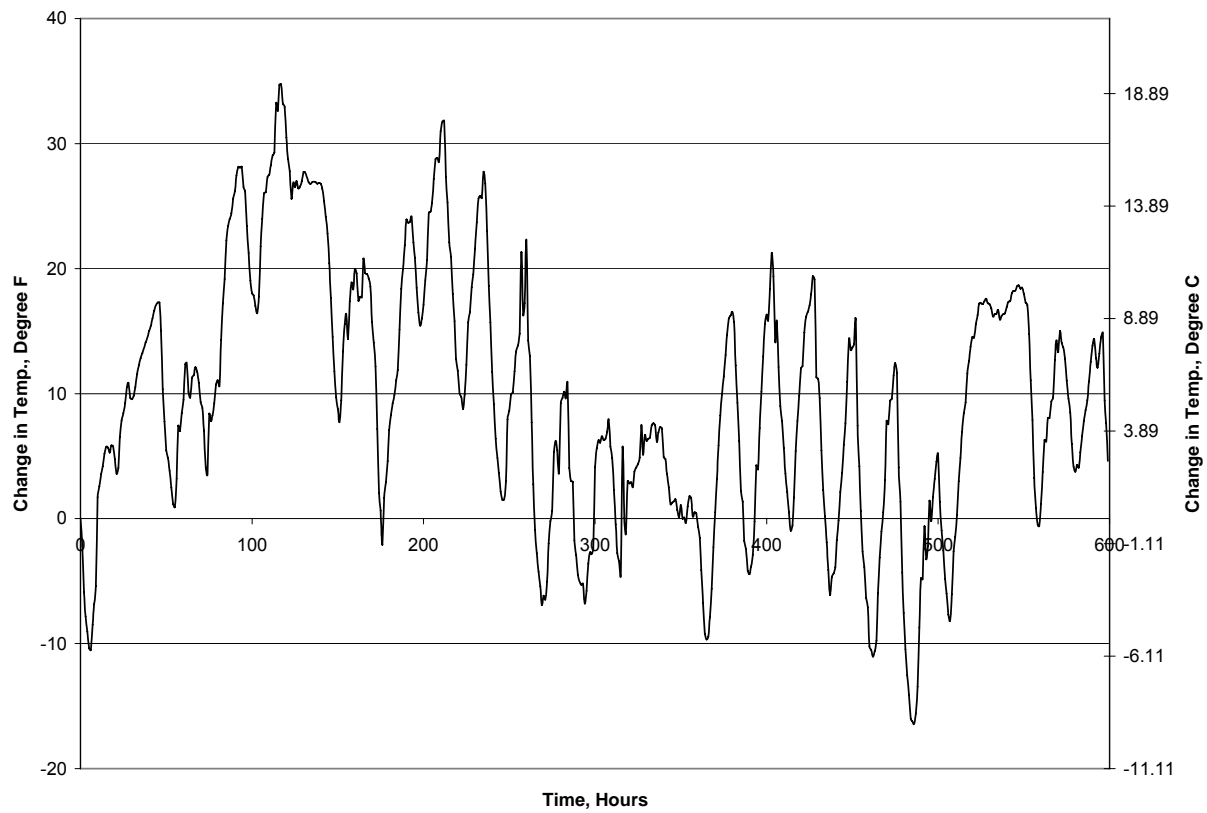
39
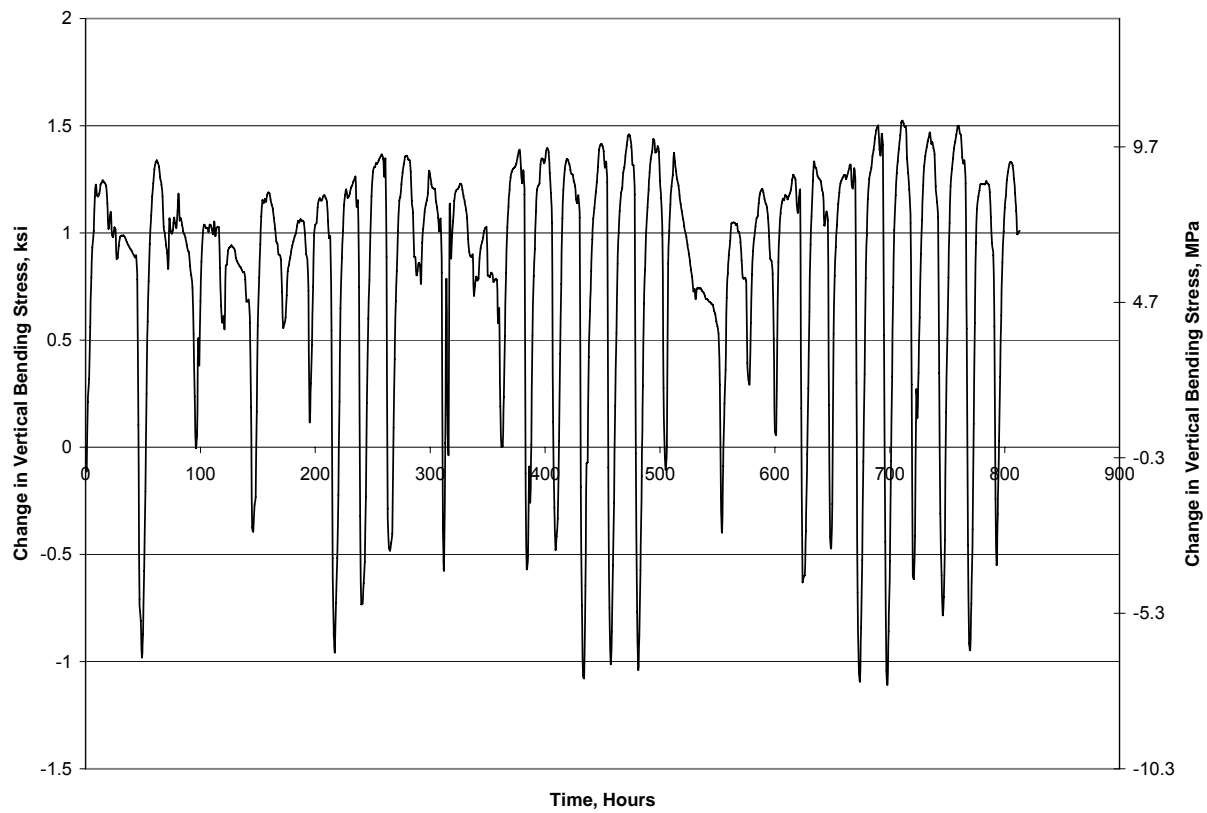
Figure 36. Vertical Bending Field Results (1st Set) for Girder 2 Bottom Flange Section B-B (Fig. 7).

**Figure 37. Lateral Bending Field Results (1st Set) for Girder 2
Bottom Flange Section B-B (Fig. 7).**

**Figure 38. Temperature Field Results (1st Set) for Girder 2
Bottom Flange Section B-B (Fig. 7).**

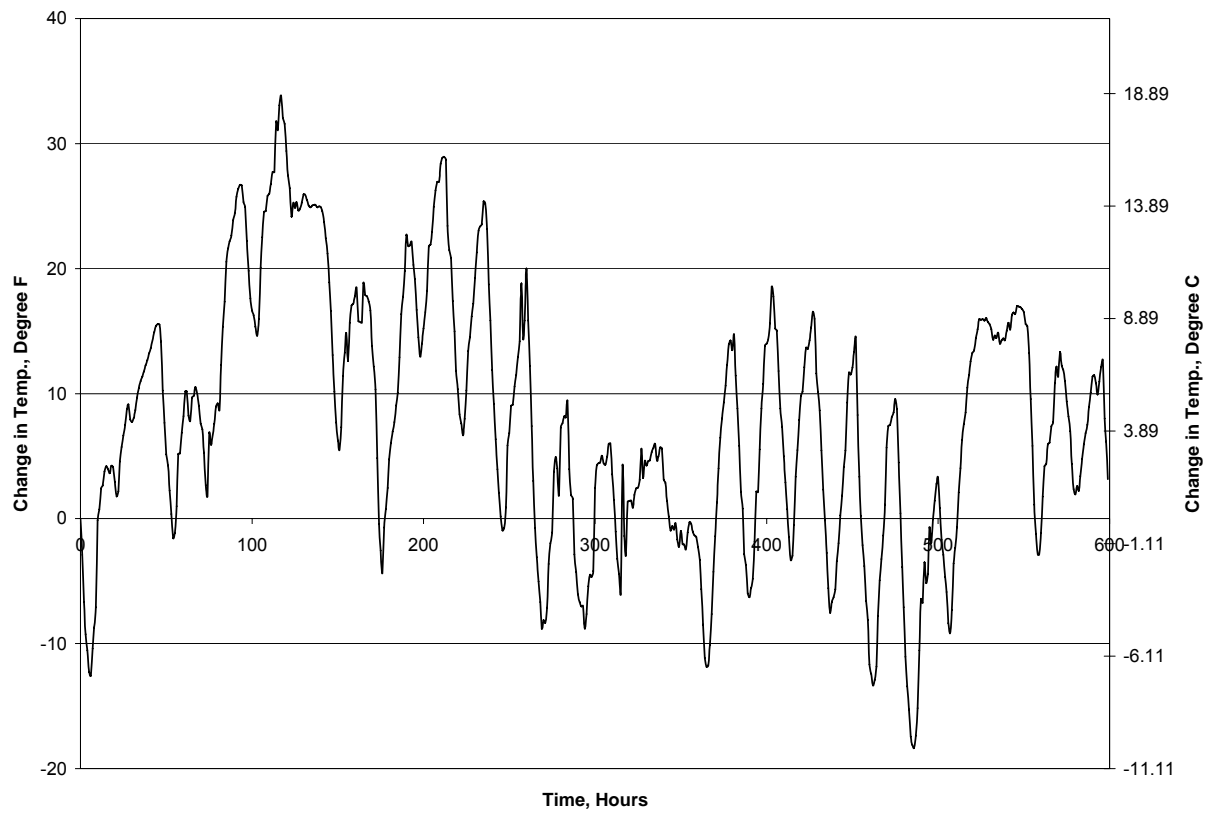**Figure 39. Vertical Bending Field Results (1st Set) for Girder 1 Top Flange Section B-B (Fig. 7).**

Figure 40. Lateral Bending Field Results (1st Set) for Girder 1 Top Flange Section B-B (Fig. 7).

Figure 41. Temperature Field Results (1st Set) for Girder 1 Top Flange Section B-B (Fig. 7).

5.2   STRUCTURE #314

Figures 42 through 57 show representative plots collected for Structure #314. The figures show the data that were collected starting March 31 at 11 a.m. and continuing until April 25 at 10 a.m., when the data-logger battery and board experienced trouble and had to be replaced/repaired. These plots, which show extremely limited variation in the recorded stresses due to temperature variations, are representative of the entire data set, which lasted from March 31 to August 1. As a result, plots for the remainder of the collected data are not included herein.

45

**Figure 42. Vertical Bending Field Results (1st Set) for Girder 1
Bottom Flange Section B-B (Fig. 18).**

**Figure 43. Temperature Field Results (1st Set) for Girder 1
Bottom Flange Section B-B (Fig. 18).**

47
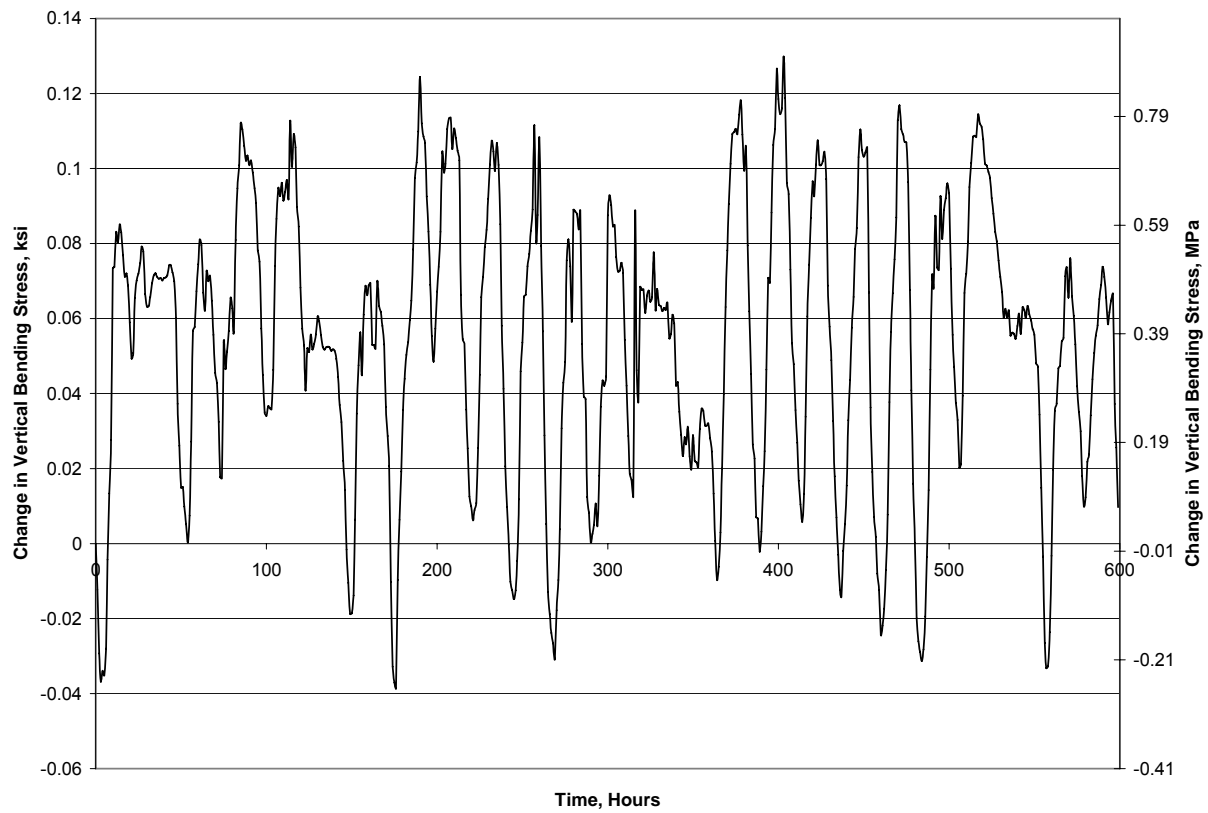
Figure 44. Vertical Bending Field Results (1st Set) for Girder 3 Bottom Flange Section C-C (Fig. 18).

Figure 45. Temperature Field Results (1st Set) for Girder 3 Bottom Flange Section C-C (Fig. 18).
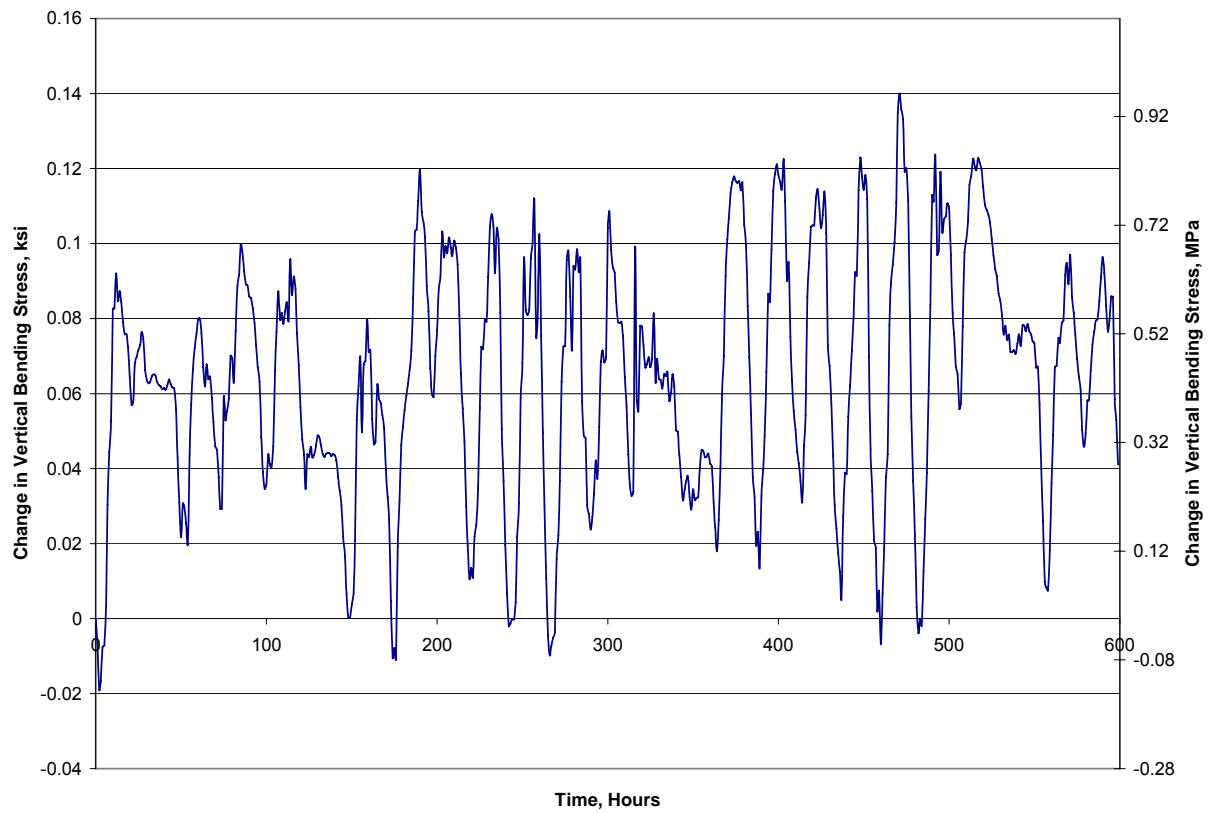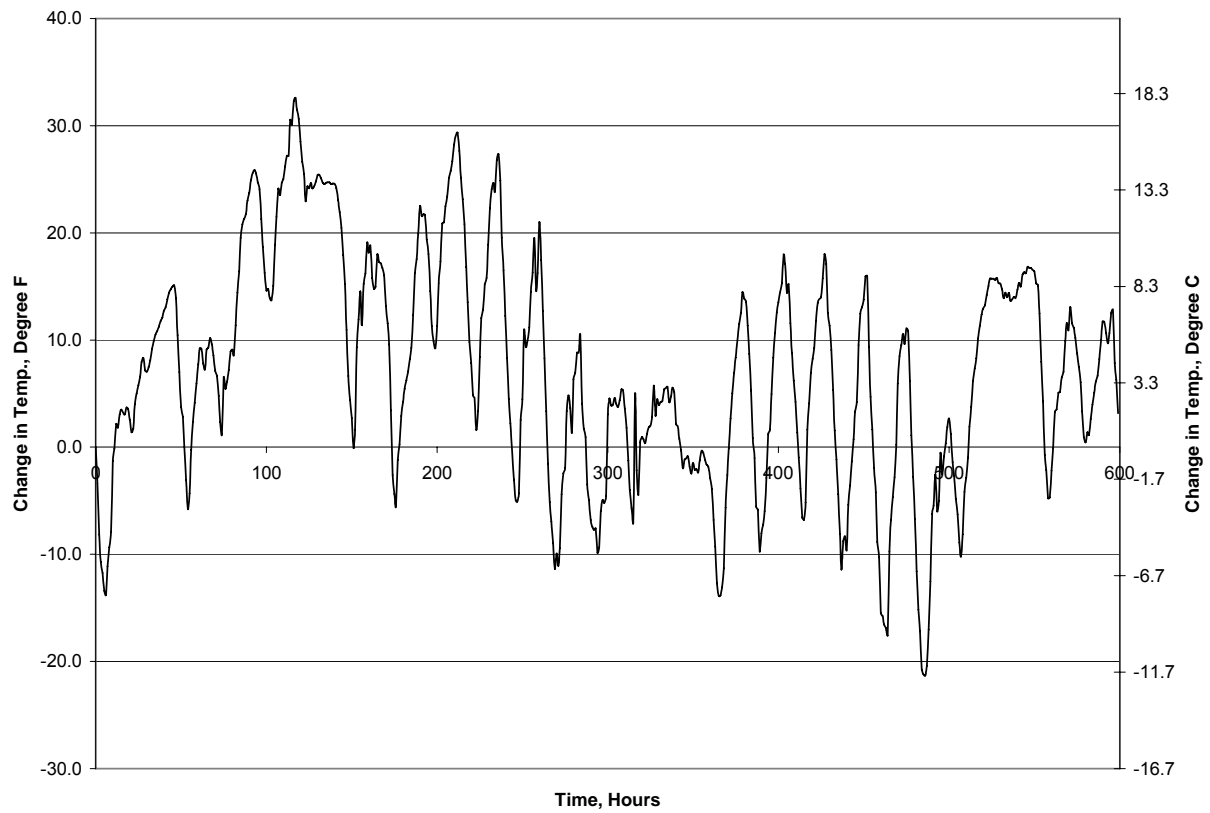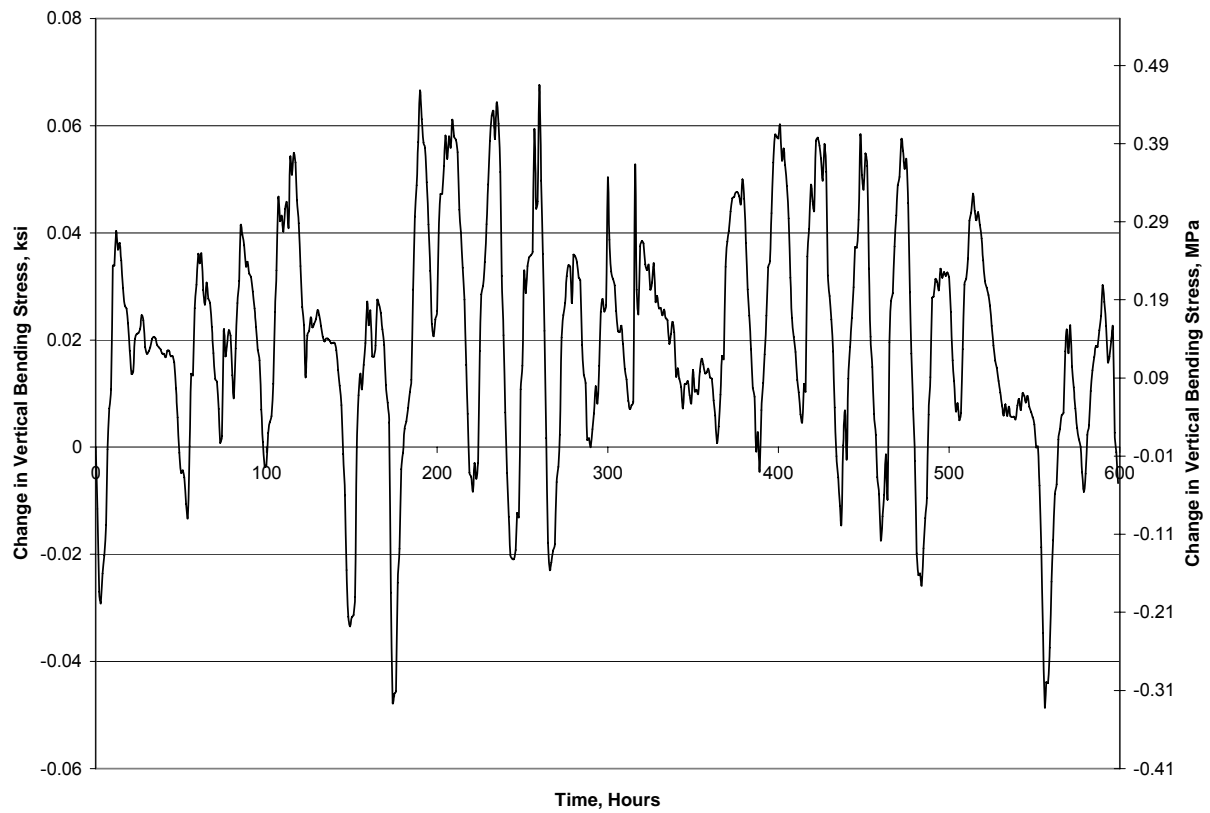
49

Figure 46. Vertical Bending Field Results (1st Set) for Girder 6 Bottom Flange Section B-B (Fig. 18).

**Figure 47. Temperature Field Results (1st Set) for Girder 6
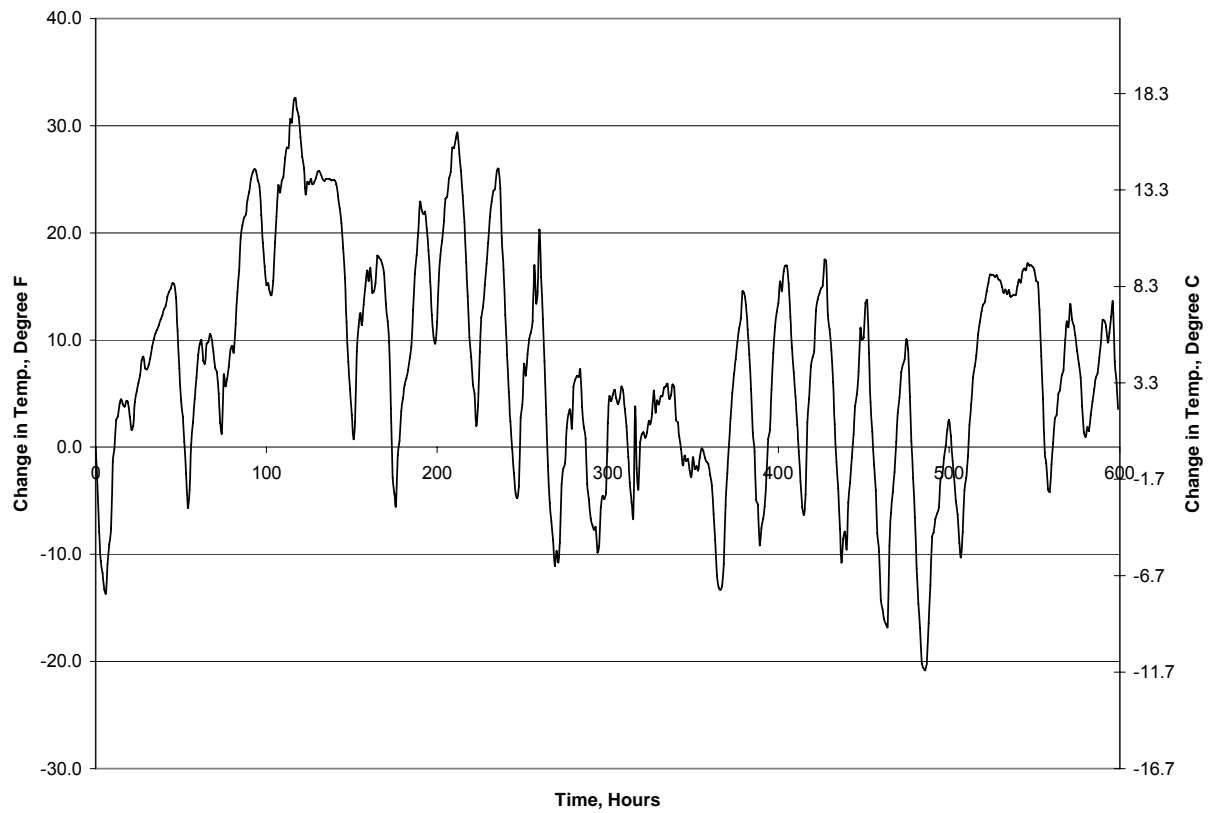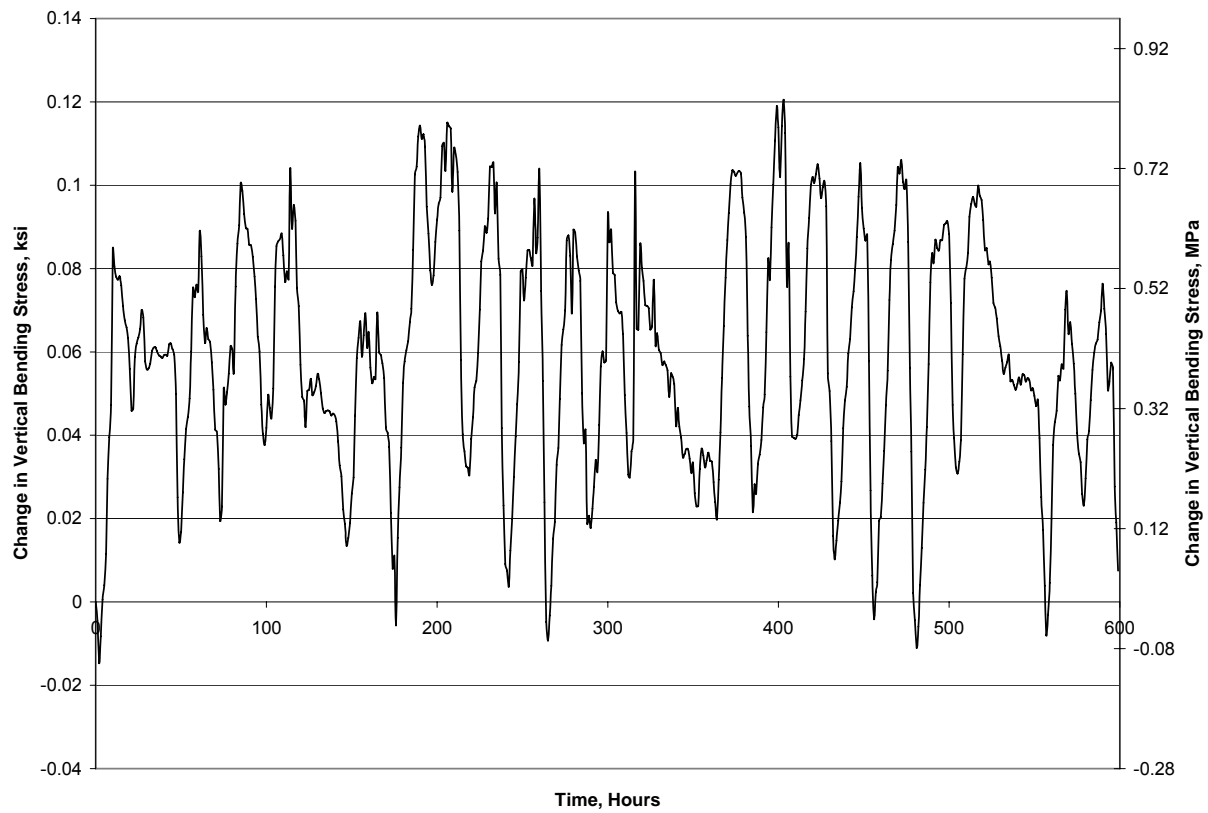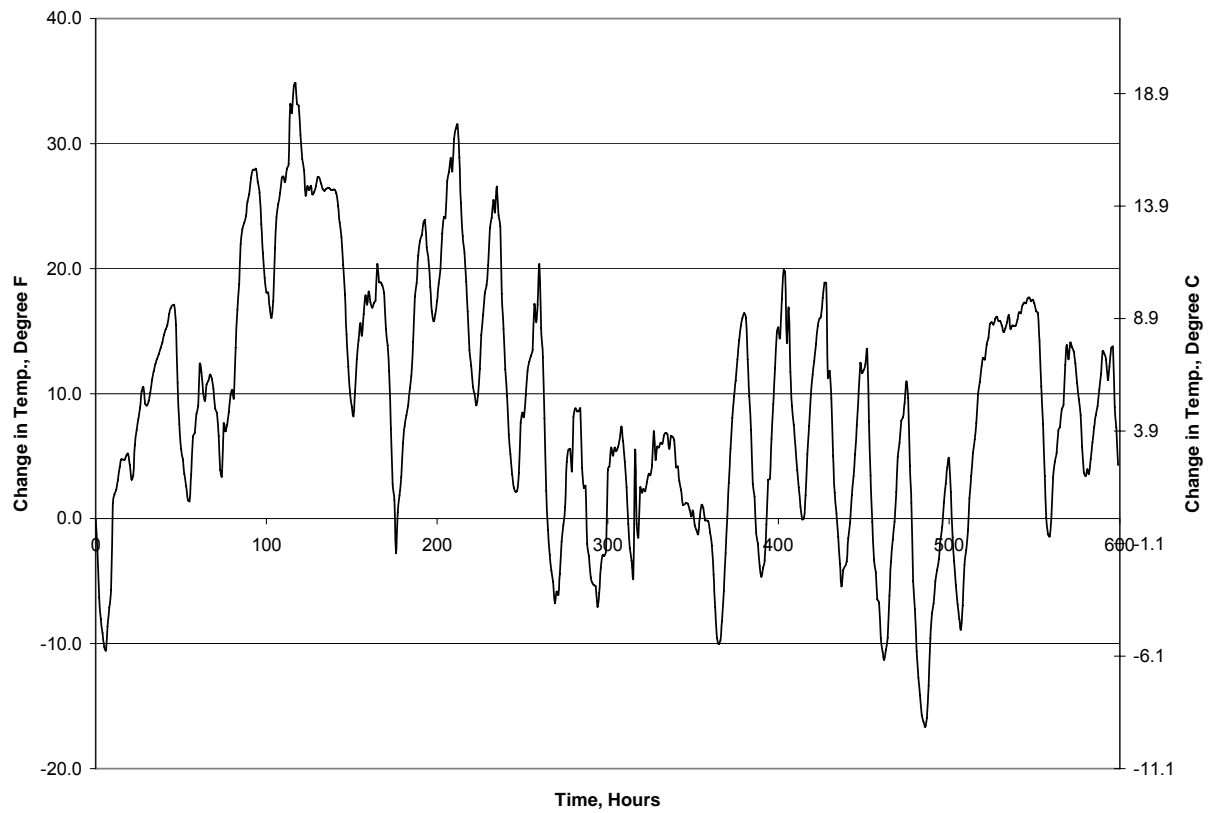Bottom Flange Section B-B (Fig. 18).**

Figure 48. Vertical Bending Field Results (1st Set) for Girder 6 Bottom Flange Section D-D (Fig. 18).
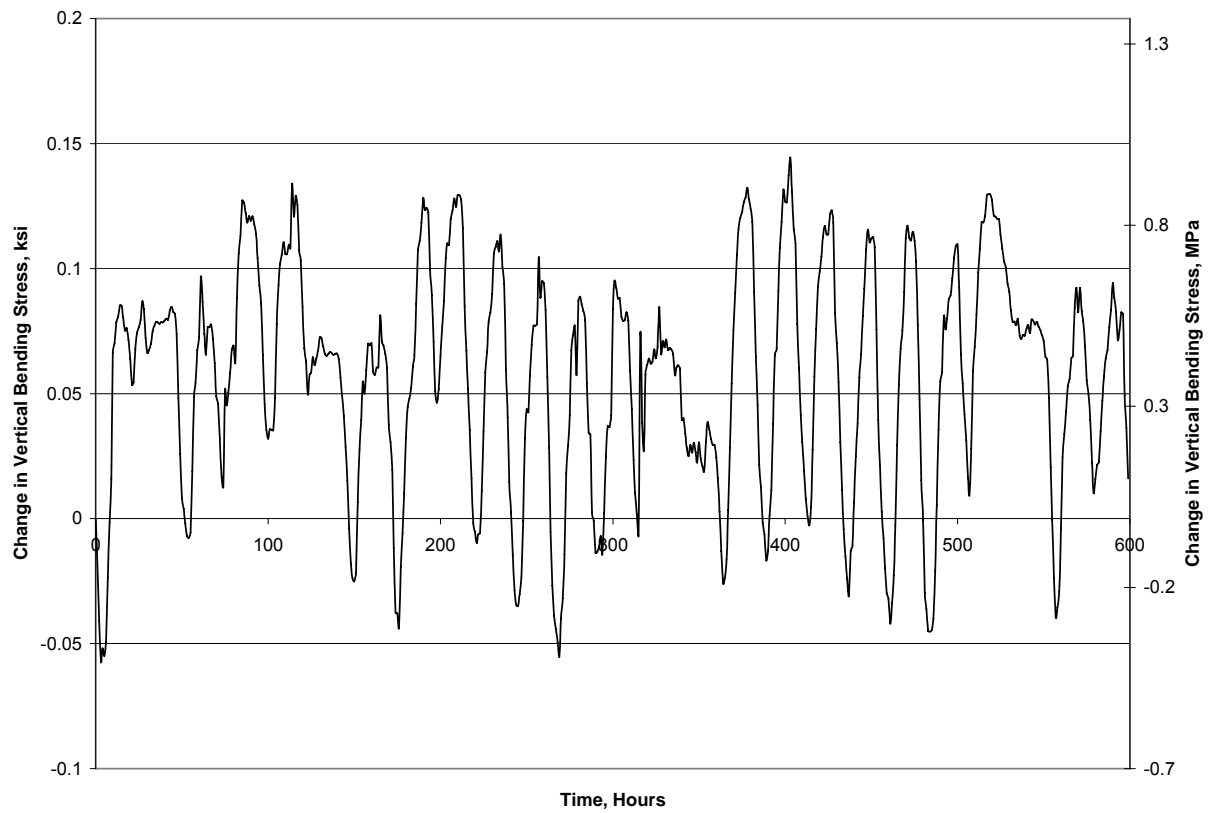
**Figure 49. Temperature Field Results (1st Set) for Girder 6
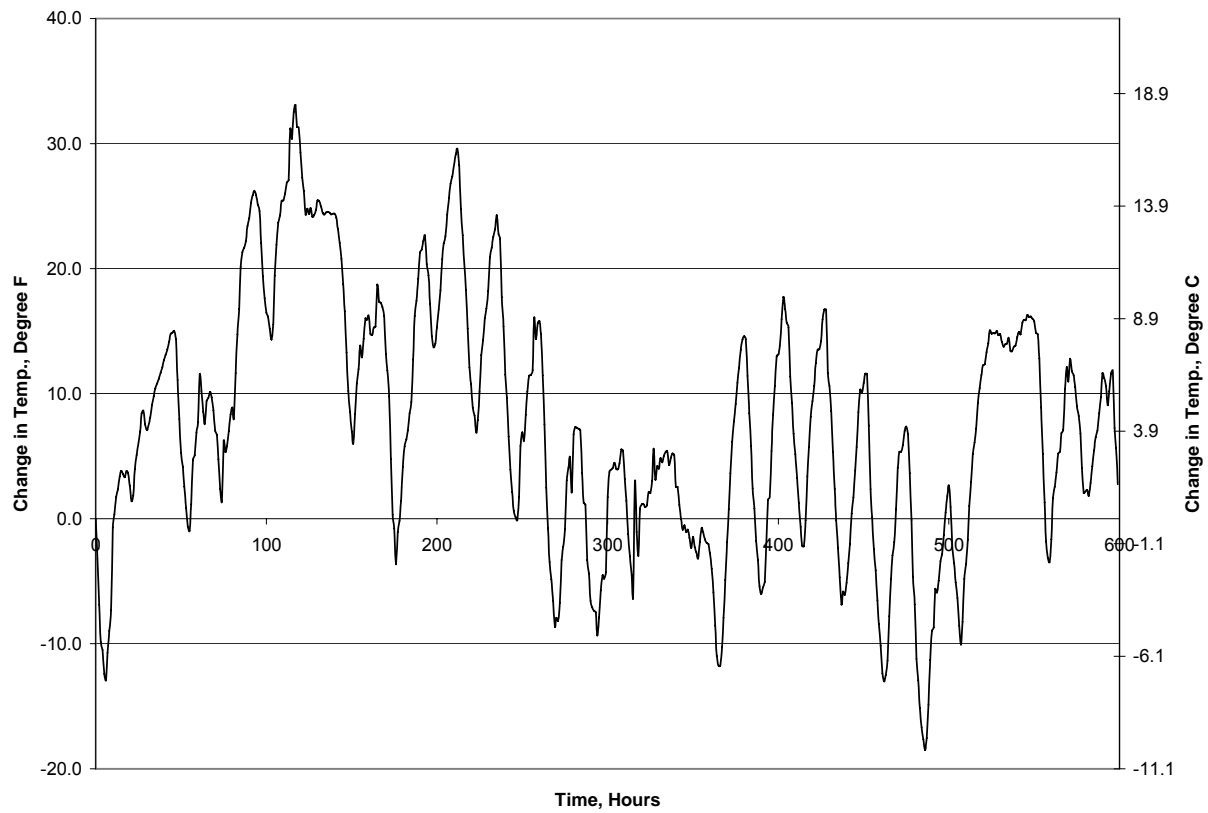Bottom Flange Section D-D (Fig. 18).**

**Figure 50. Vertical Bending Field Results (1st Set) for Girder 7
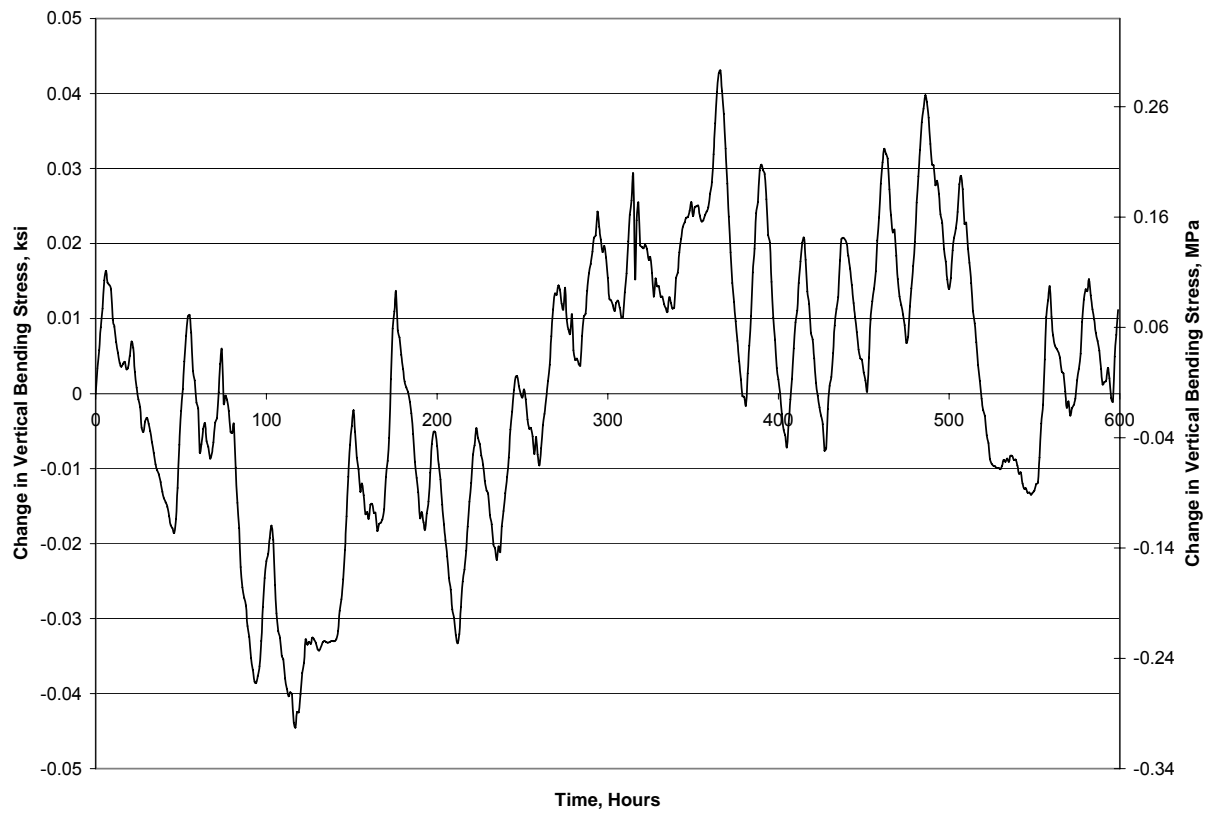Bottom Flange Section E-E (Fig. 18).**

**Figure 51. Temperature Field Results (1st Set) for Girder 7
Bottom Flange Section E-E (Fig. 18).**

**Figure 52. Vertical Bending Field Results (1st Set) for Girder 9
Bottom Flange Section G-G (Fig. 18).**

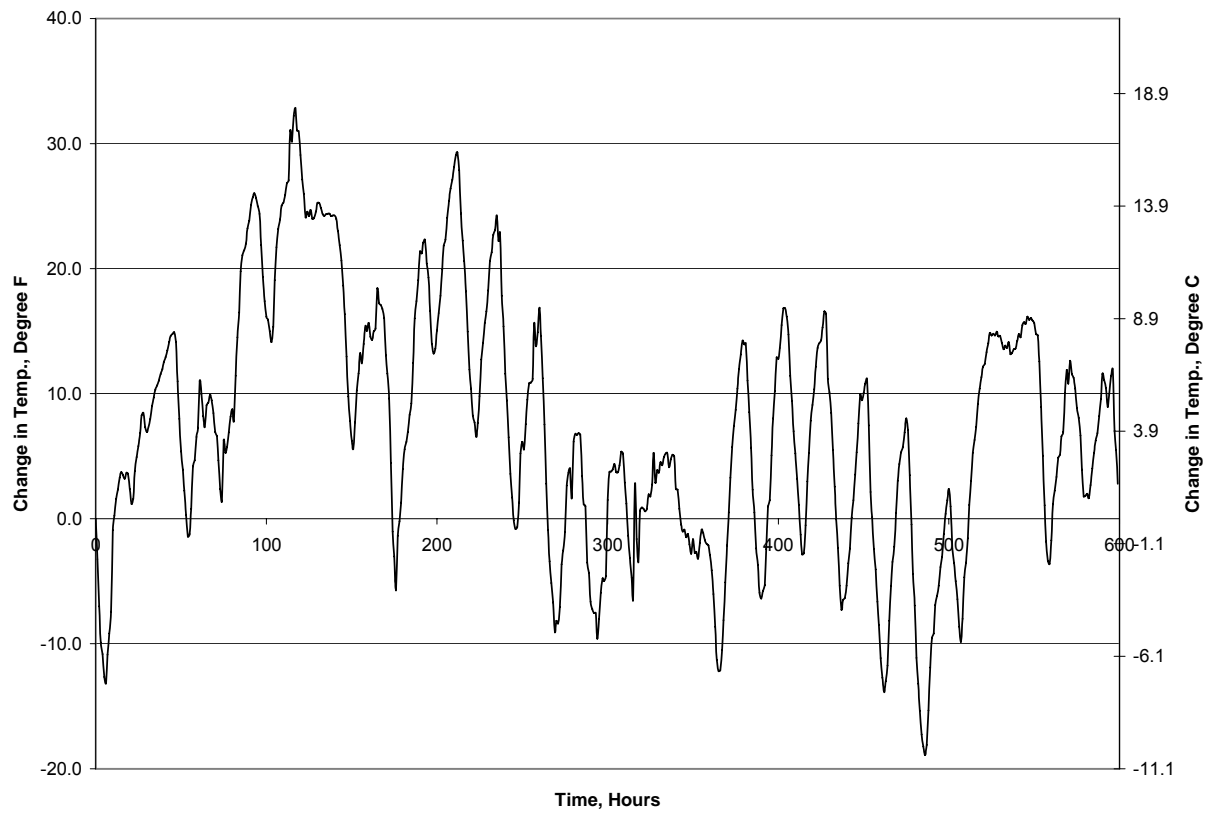**Figure 53. Temperature Field Results (1st Set) for Girder 9 Bottom Flange Section G-G (Fig. 18).**

Figure 54. Vertical Bending Field Results (1st Set) for Girder 9 Bottom Flange Section F-F (Fig. 18).
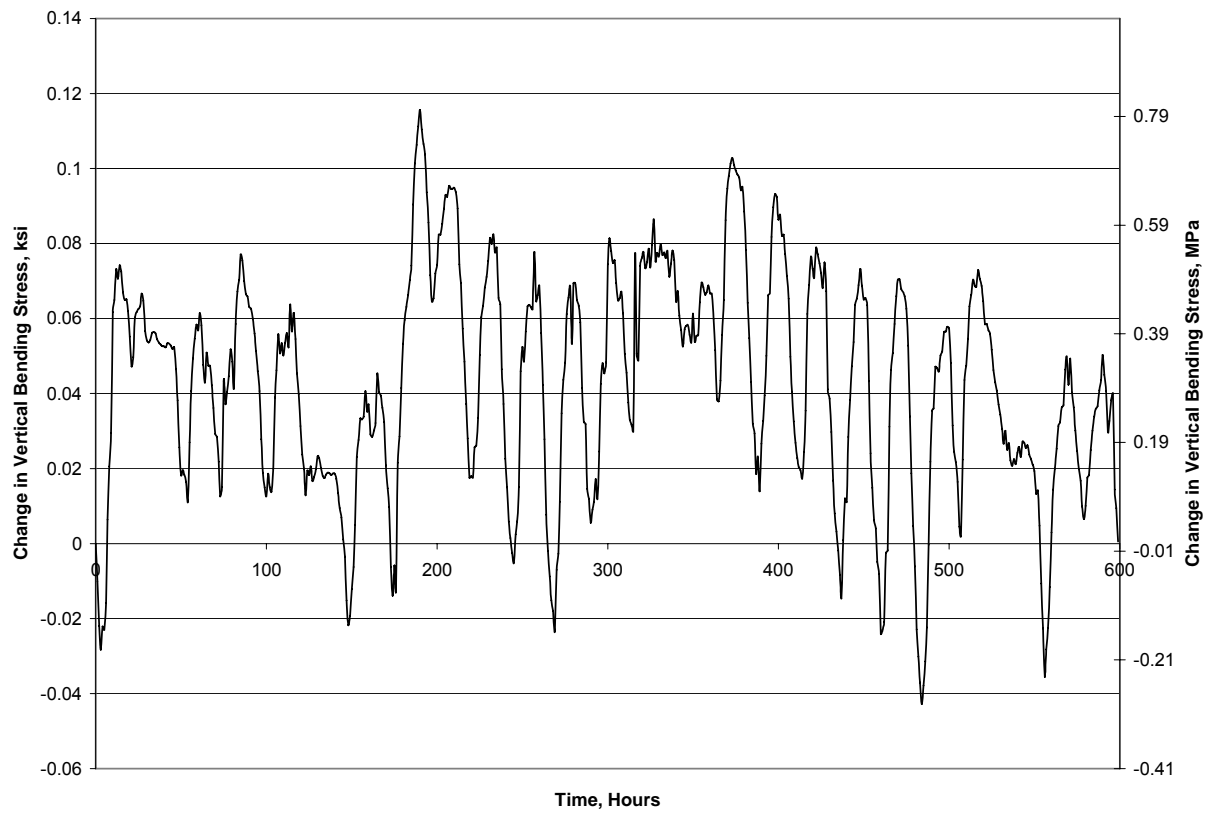
**Figure 55. Temperature Field Results (1st Set) for Girder 9
Bottom Flange Section F-F (Fig. 18).**

Figure 56. Vertical Bending Field Results (1st Set) for Girder 12 Bottom Flange Section G-G (Fig. 18).

60

**Figure 57. Temperature Field Results (1st Set) for Girder 12
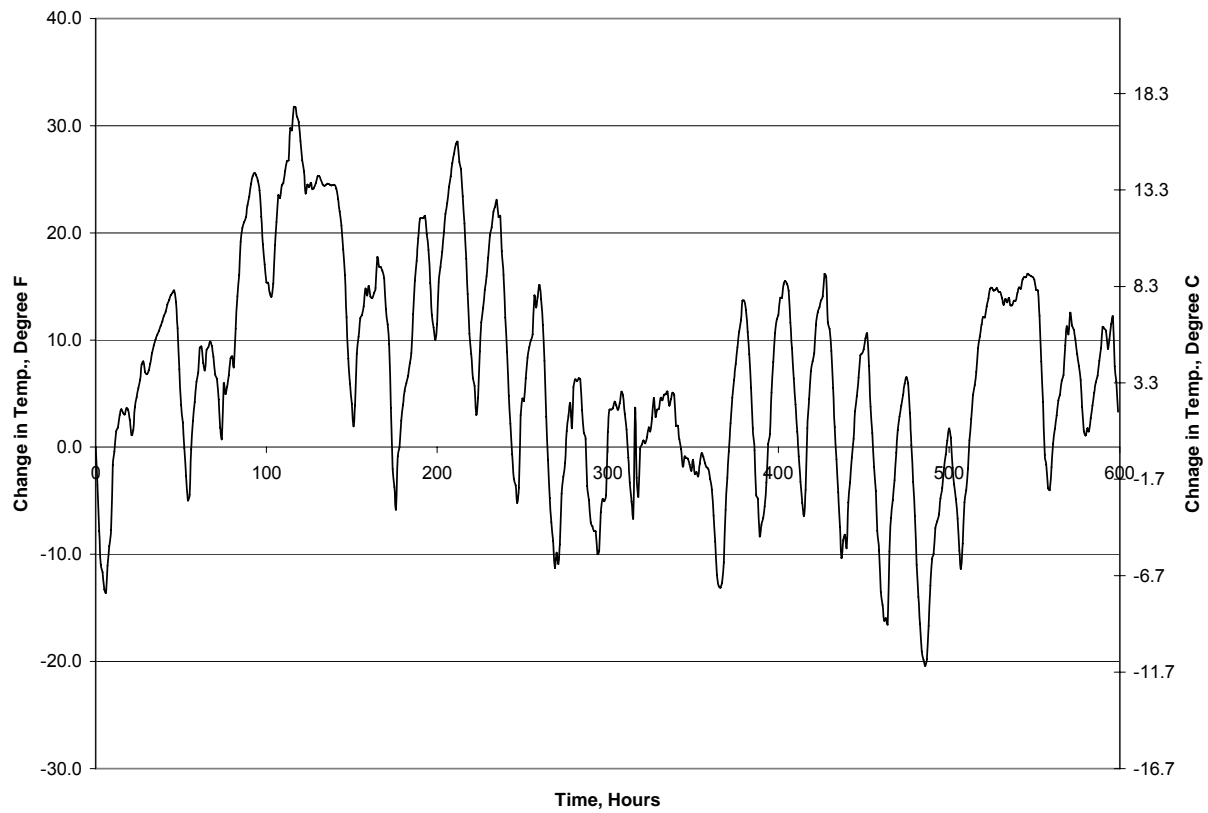Bottom Flange Section G-G (Fig. 18).**

6 NUMERICAL ANALYSES COMPARISONS

Comparisons between the collected field data and select results from the grillage, full-shell 3D and 3D finite element model containing a combination of frame members and shell and brick elements are provided herein. Comparisons are completed for construction sequences and for a single HS20 truck placed at the location generating maximum positive moment in the exterior/largest radius girder.

6.1 STRUCTURE #207

6.1.1.1 Results for Staged Construction (Steel Only)

This section compares the finite element model results from the ABAQUS shell model to the field test data and grillage model results for the erection of the steel superstructure. For all of the figures in this section Stage 8a represents the construction stage where all steel components are erected, but the bolts have not been tightened. Stage 8b represents the construction stage where all bolts have been tightened.

Figure 58 shows the vertical bending results for the bottom flange of Girder 5 at location C-C. The figure shows that for Stage 8 the ABAQUS model produced results that more accurately portrayed the field test results than the SAP2000 grillage model. The figure also shows that for Stage 5 the SAP2000 model predicted the field behavior more accurately than the ABAQUS model.   Figure 59 shows the vertical bending stress results for the top flange of Girder 5 at Section C-C. This figure shows that both the ABAQUS model and the SAP2000 model do not predict the general trend of the field behavior. It also shows that the ABAQUS model and the SAP 2000 model results predict different stresses for Stage 8.
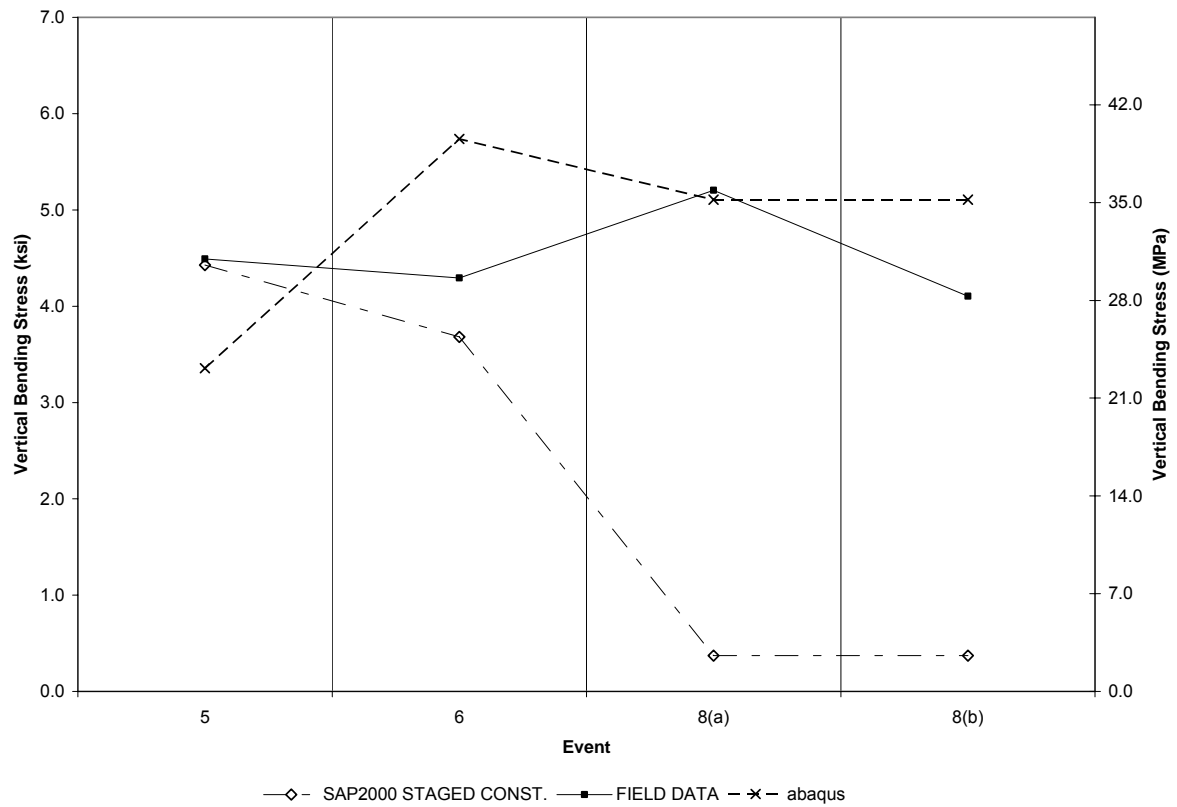
Figure 58. Results Comparison for Girder 5 Bottom Flange Section C-C (Fig. 7).
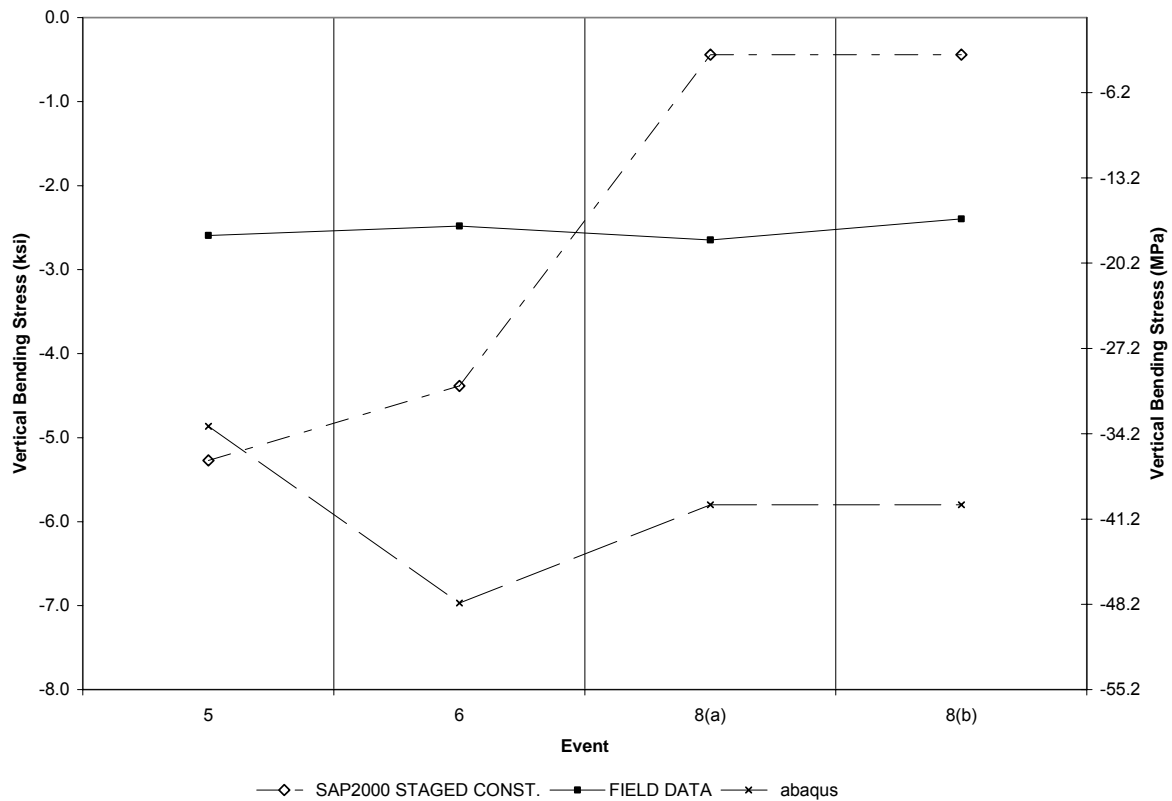
Figure 59. Results Comparison for Girder 5 Top Flange Section C-C (Fig. 7).

Figure 60 shows the results for the vertical bending stress of the north top flange of Girder 4. The figure shows that ABAQUS appears to predict behavior of the girder in the field more accurately than the SAP2000 model. However the ABAQUS results do not correspond precisely with the field test data. Figure 61 shows that neither the ABAQUS model nor the SAP 2000 model predicts the trends of the behavior of the bottom flange of Girder 4 in the field at Section C-C.
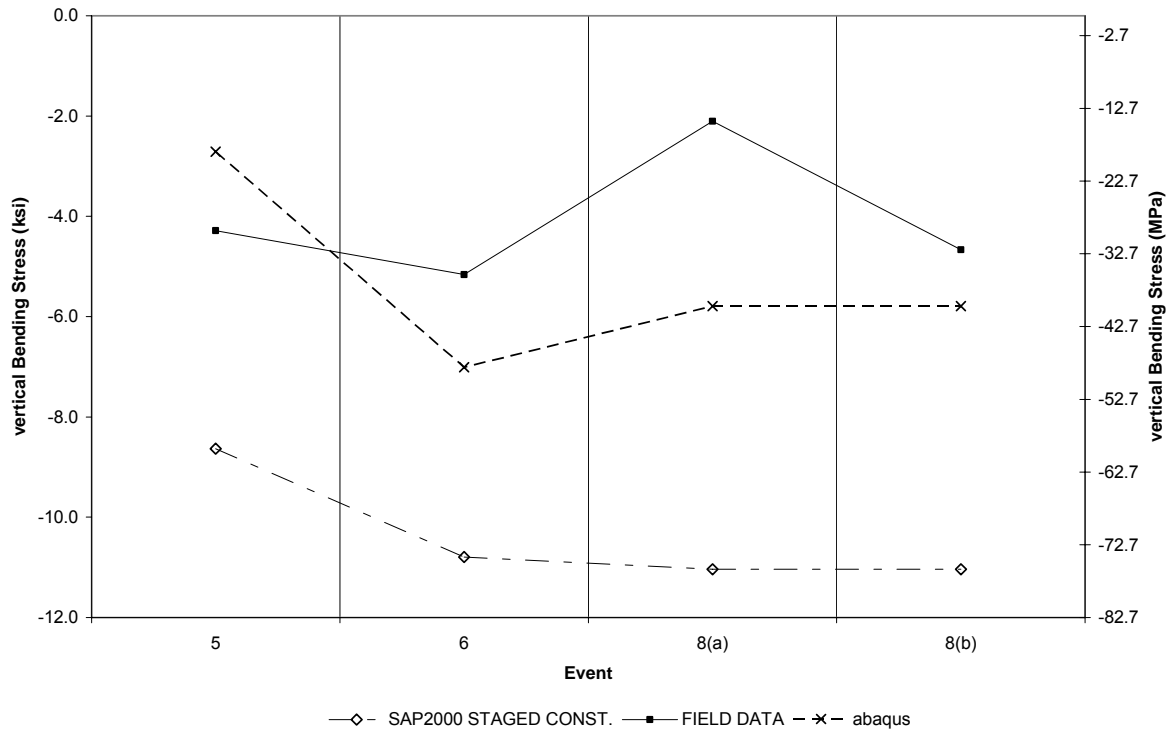
Figure 60. Results Comparison for Girder 4 Top Flange Section C-C (Fig. 7).
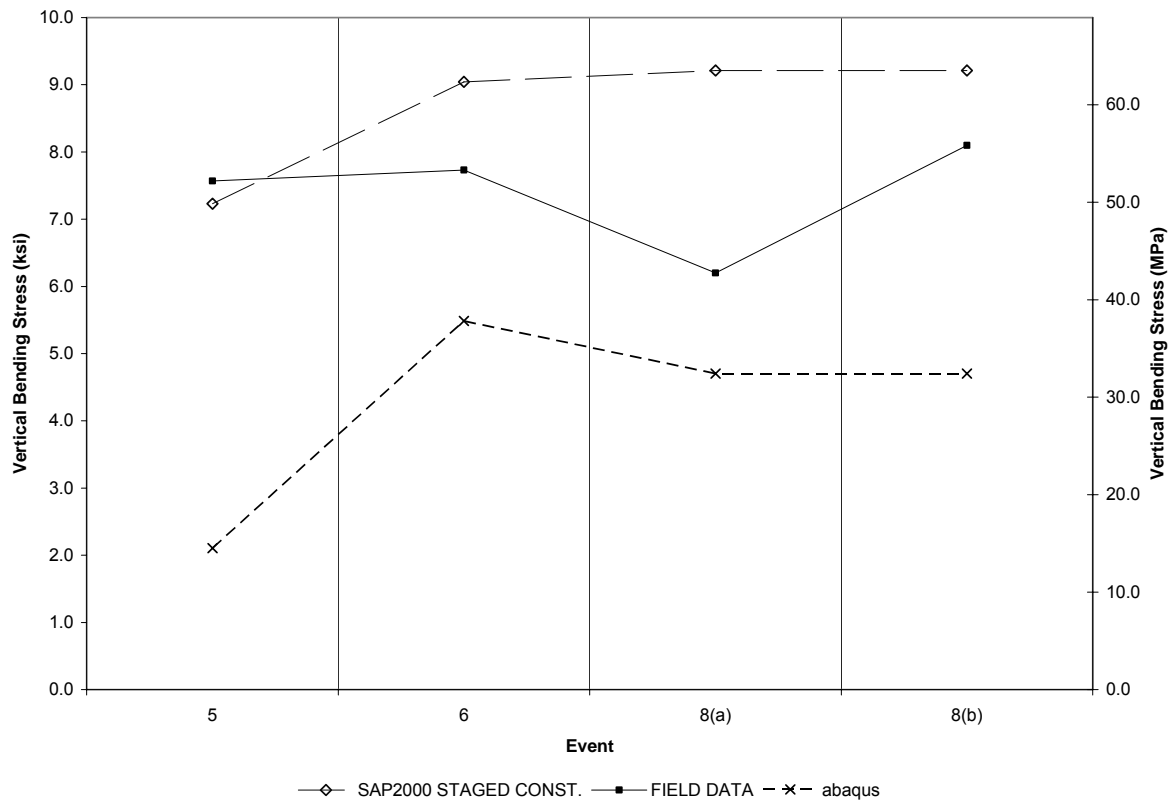
Figure 61. Results Comparison for Girder 4 Bottom Flange Section C-C (Fig. 7).

Figure 62 shows that the ABAQUS model predicts the general trend of the behavior of the bottom flange of Girder 1 at Section B-B. The SAP2000 model does not predict the behavior of the girder in the field as accurately as the ABAQUS model. Figure 63 shows that the ABAQUS model predicts the behavior of the top flange of Girder 5 at Section B-B more accurately than the SAP 200 model. Figure 63 shows that for the instrumented section the SAP 2000 model appears to follow the general trend of the field data but predicts a different magnitude than the field test data.
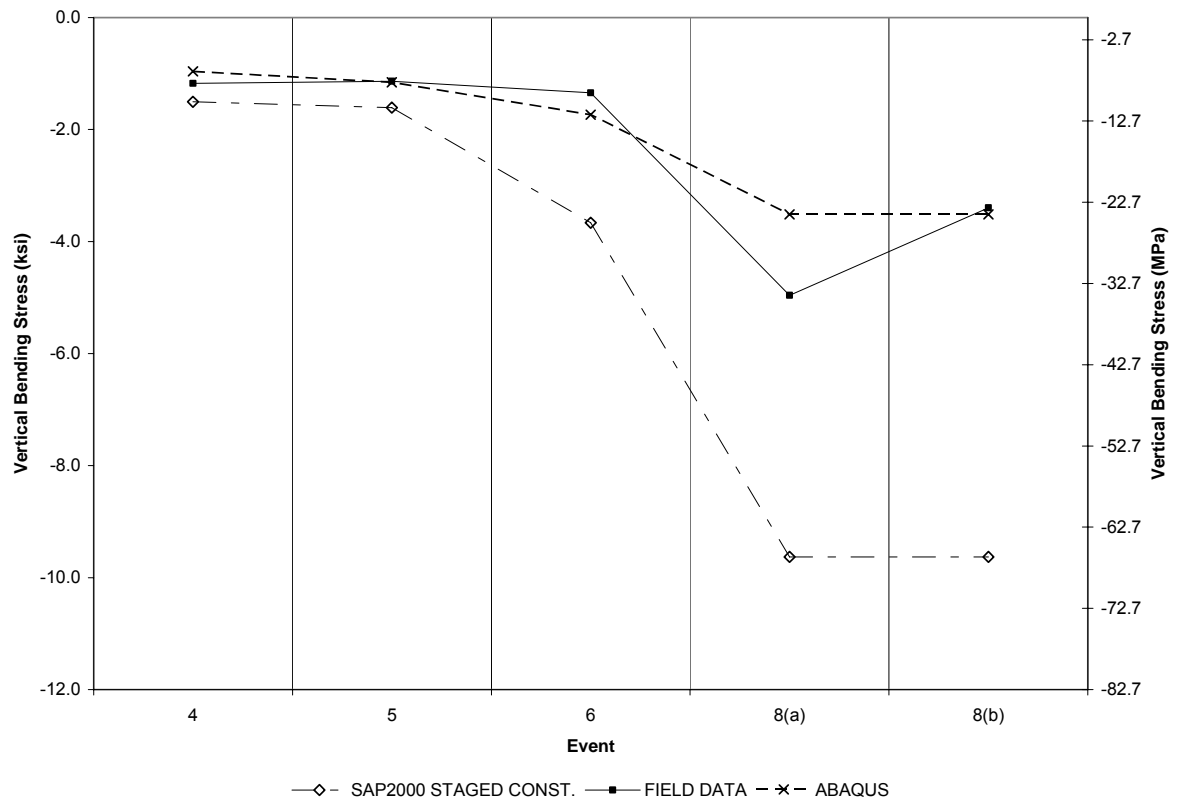
Figure 62. Results Comparison for Girder 1 Bottom Flange Section B-B (Fig. 7).
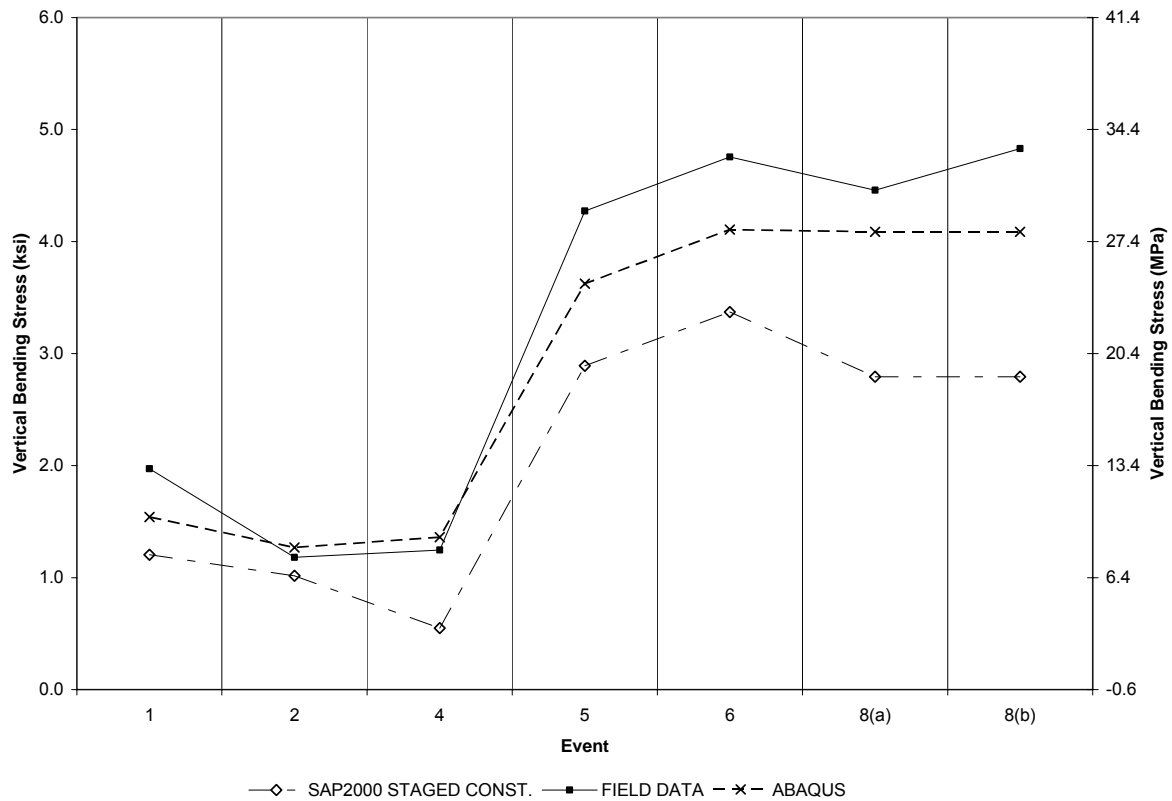
Figure 63. Results Comparison for Girder 5 Top Flange Section B-B (Fig. 7).

Results for the lateral bending of the steel superstructure throughout steel erection are shown starting with Figure 64. This figure shows that the ABAQUS model accurately predicts the general trend of the field data. However, field data magnitudes are larger than those predicted by the ABAQUS model. The figure also shows that the SAP2000 model predicts small values of lateral bending stresses. Figure 65 shows that neither the ABAQUS nor the SAP2000 models predict the general lateral bending stress behavior trend of the top flange of Girder 5 at Section C-C. The SAP2000 model predicts the value at Stage 8 accurately; however, the SAP2000 model does not accurately predict the behavior observed in the field at Stage 5. The ABAQUS model predicts the behavior observed in the field well for Stage 5; however, the ABAQUS results for Stage 8 are higher than those observed in the field.
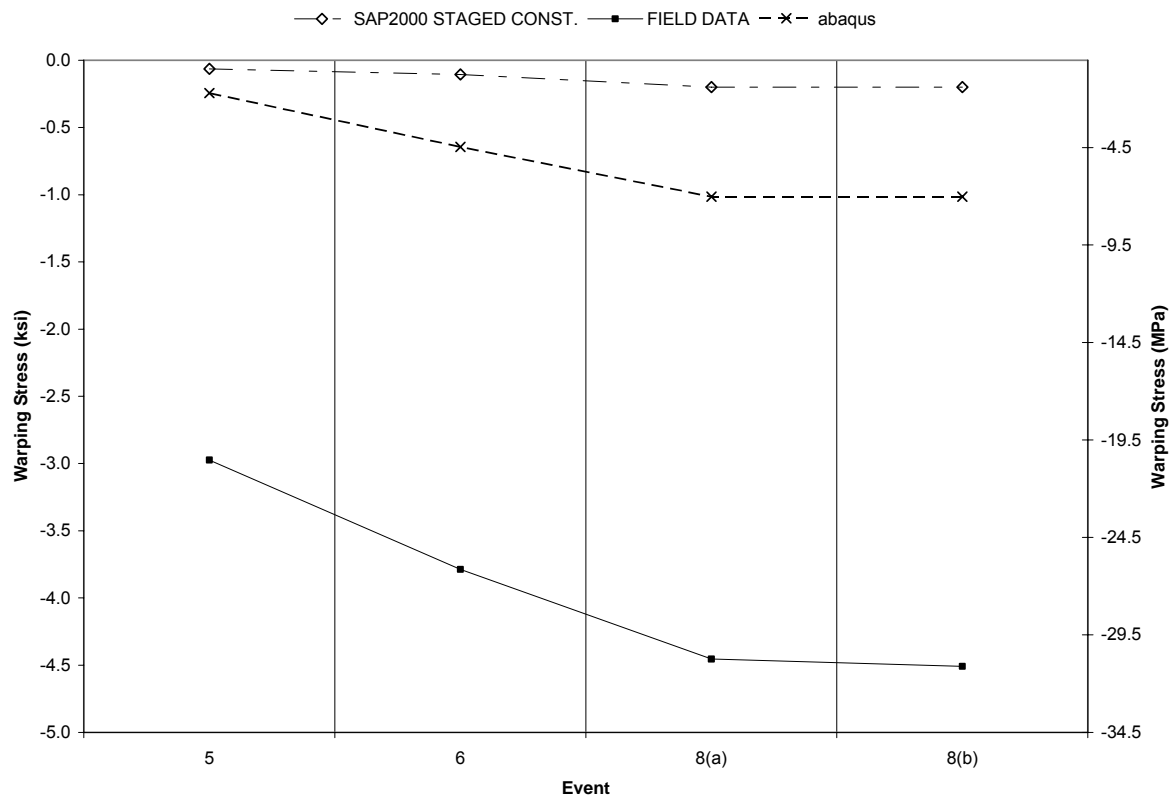
Figure 64. Results Comparison for Girder 5 Bottom Flange Section C-C (Fig. 7).
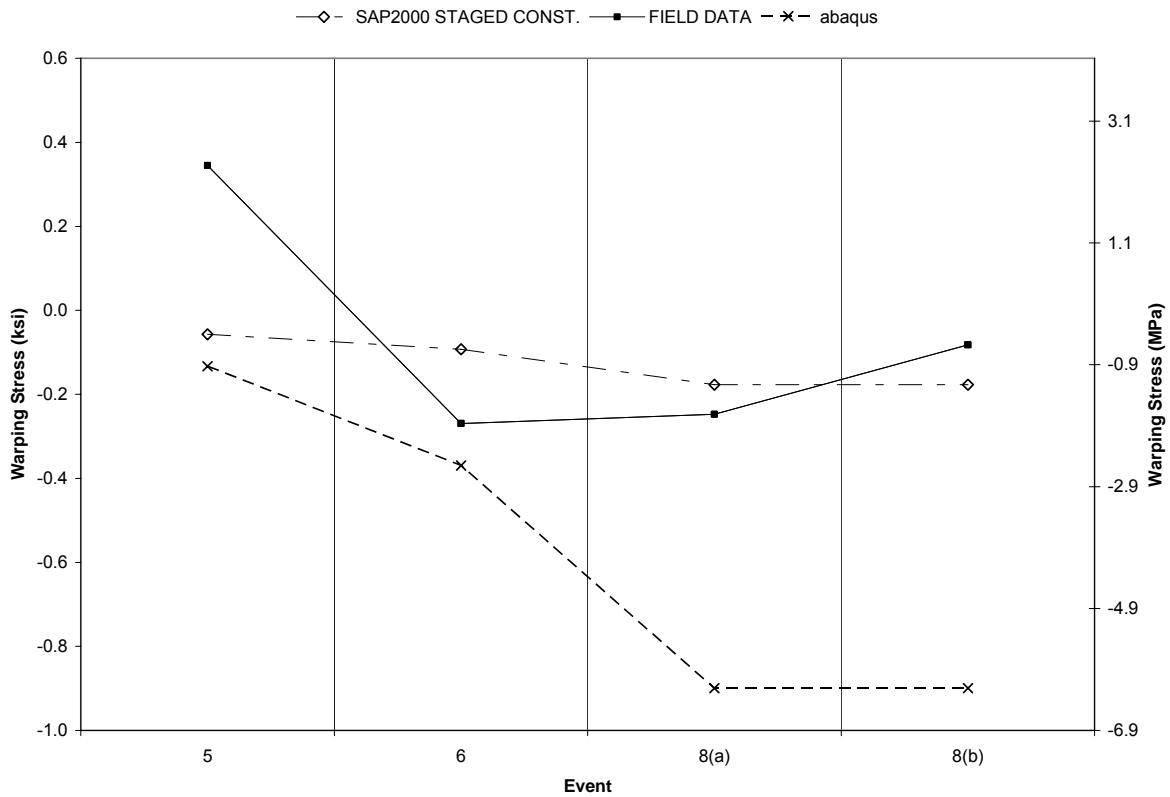
Figure 65. Results Comparison for Girder 5 Top Flange Section C-C (Fig. 7).

Figure 66 shows that neither the SAP2000 model nor the ABAQUS model accurately portrays the behavior observed in the field. The field data warping stresses have larger magnitudes than those predicted by the SAP2000 model and the ABAQUS model. Figure 67 shows that neither the SAP2000 model nor the ABAQUS model accurately predict the behavior observed in the field for the warping stresses of the top flange of Girder 5 at Section B-B.

70

Figure 66. Results Comparison for Girder 1 Bottom Flange Section B-B (Fig. 7).

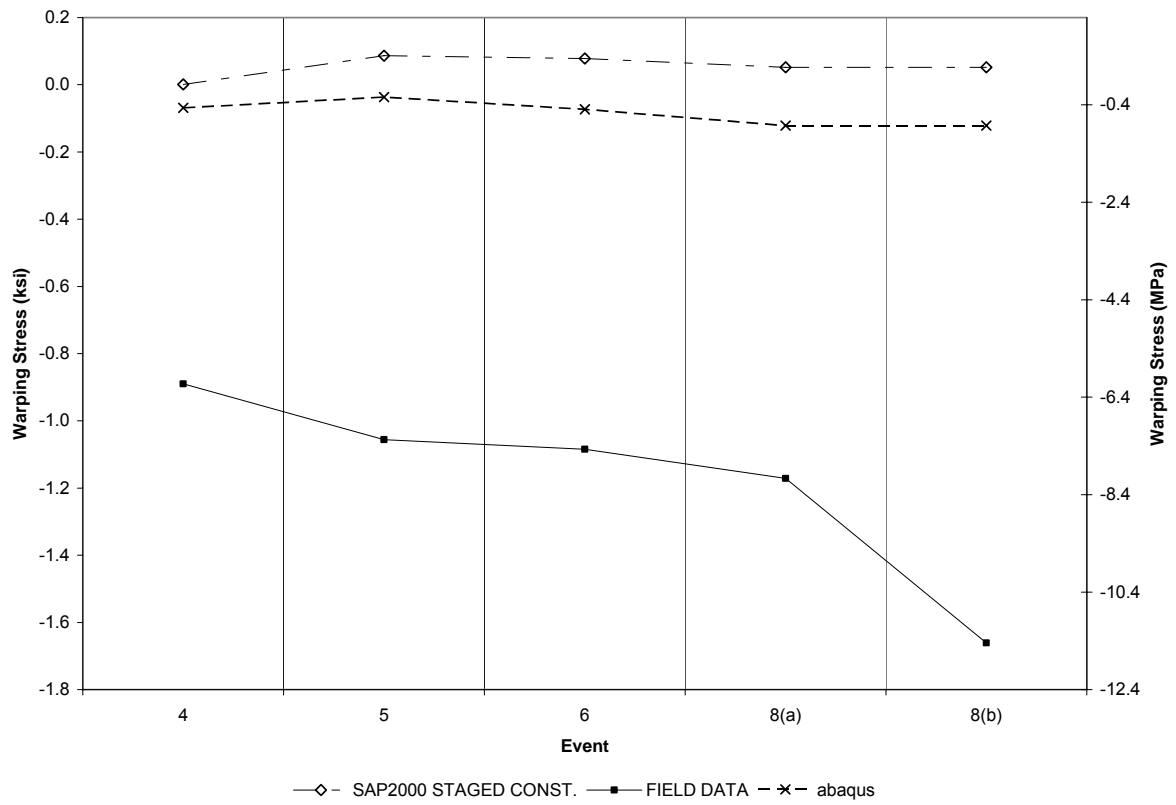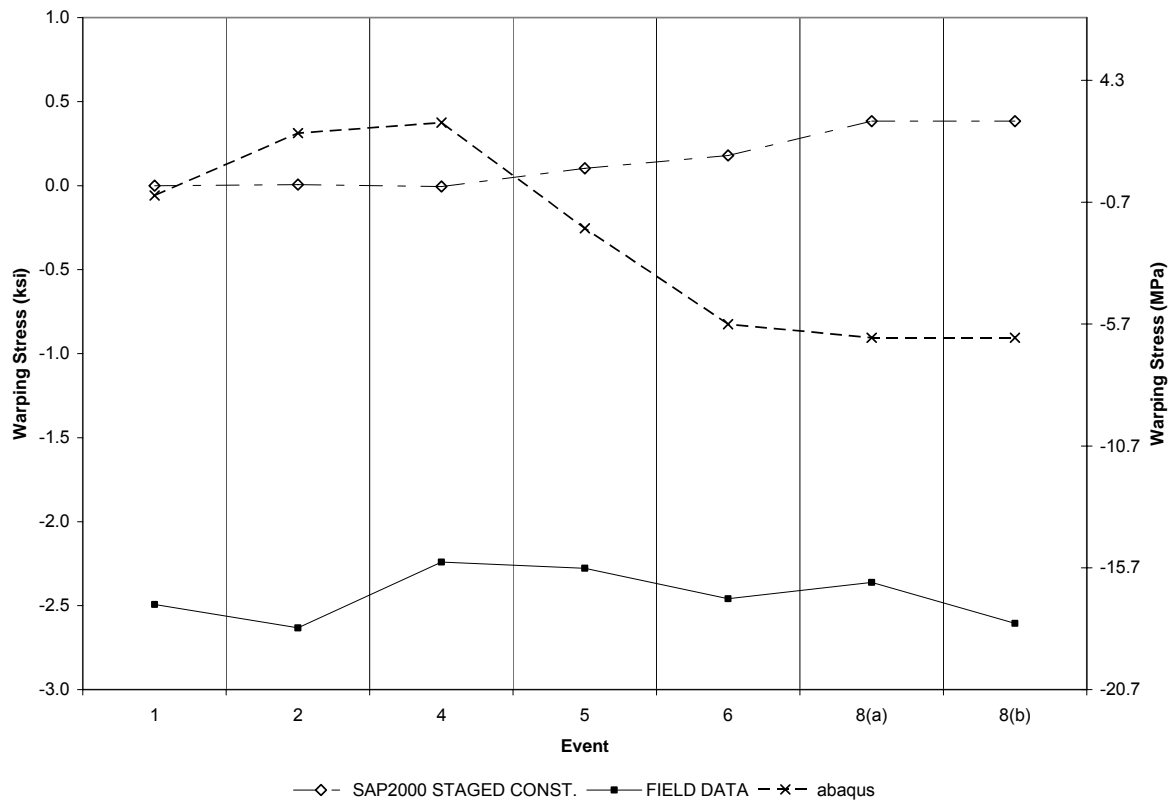**Figure 67. Results Comparison for Girder 5 Top Flange Section B-B (Fig. 7).**

An additional comparison between cross frame forces obtained from the field data and those determined from the ABAQUS shell model can be found in Table 14. Stresses for Stage 8, at the completion of steel erection, are shown and they indicate, in general, small stresses in the cross frame members and reasonable predictions by the ABAQUS model.

Table 14. Results Comparison for Cross Frame Axial Stresses, Stage 8.

Location	Field Stress, ksi	ABAQUS Stress, ksi
G1 B-B Bottom	0.08	0.25
G1 B-B Diagonal	0.50	4.41
G1 B-B Top	1.98	1.02
G5 B-B Bottom	2.23	0.91
G5 B-B Diagonal	0.53	3.91
G5 B-B Top	4.00	1.30
G1 C-C Bottom	3.39	3.19
G1 C-C Diagonal	0.18	1.99
G1 C-C Top	1.31	0.65
G5 C-C Bottom	0.54	2.61
G5 C-C Diagonal	1.71	0.35
G5 C-C Top	0.47	0.84

6.1.1.2   Results for Staged Construction (Slab)

This section compares the finite element model results to the field test results and the grillage model results for the placement of the concrete deck. For all figures Stage 8b is considered the initial point and all stresses are relative to that point.

Figure 68 shows that for Girder 1 bottom flange Section B-B all three models predict the behavior of the bridge well for Stage 10. However, none of the models portrays behavior of the bridge well during Stages 12 and 14. Both the ABAQUS shell and brick models predict similar responses for the bridge for all three portions of the deck pour.
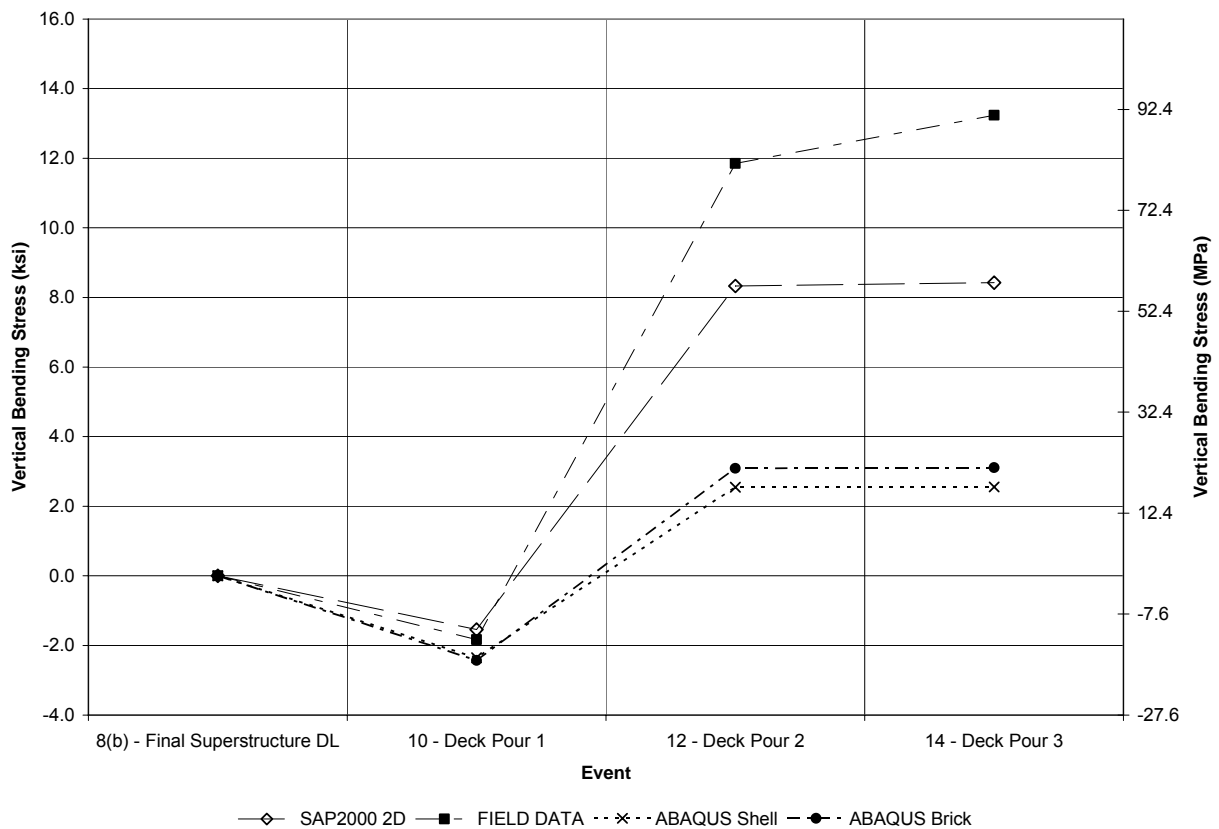

Figure 68. Results Comparison (Slab) for Girder 1 Bottom Flange Section C-C (Fig. 7).

Figure 69 shows the results for Girder 3 Bottom Flange Section C-C. It shows that the ABAQUS brick model predicts the behavior of the bridge and that the ABAQUS shell model behaves similar to the grillage model. The ABAQUS shell model results do not compare well with the ABAQUS brick model results. Figure 70 shows the results for Girder 3 Top Flange Section C-C. It shows that the grillage predicts the behavior observed in the field more accurately than eithier of the ABAQUS models.

Figure 69. Results Comparison (Slab) for Girder 3 Bottom Flange Section B-B (Fig. 7).

Figure 70. Results Comparison (Slab) for Girder 3 Top Flange Section C-C (Fig. 7).

Figure 71 shows the results for Girder 1 Bottom Flange Section B-B. It shows that all three models predict the behavior of the bridge in the field accurately for Stage 10. However, none of the models predicts the behavior of the bridge well for Stage 14.

Figure 71. Results Comparisons (Slab) for Girder 1 Bottom Flange Section B-B (Fig. 7).

Figure 72 shows the results comparison for Girder 3 Bottom Flange Section B-B. It shows that the grillage model and the ABAQUS shell model predict the behavior of the bridge in the field more accurately than the ABAQUS brick model. The ABAQUS brick model predicts smaller stress for Stages 12 and 14 than those observed in the field. Figure 73 shows the results comparison for Girder 3 Top Flange Section C-C. It shows that the grillage model predicts the bridge behavior more accurately than the ABAQUS models.
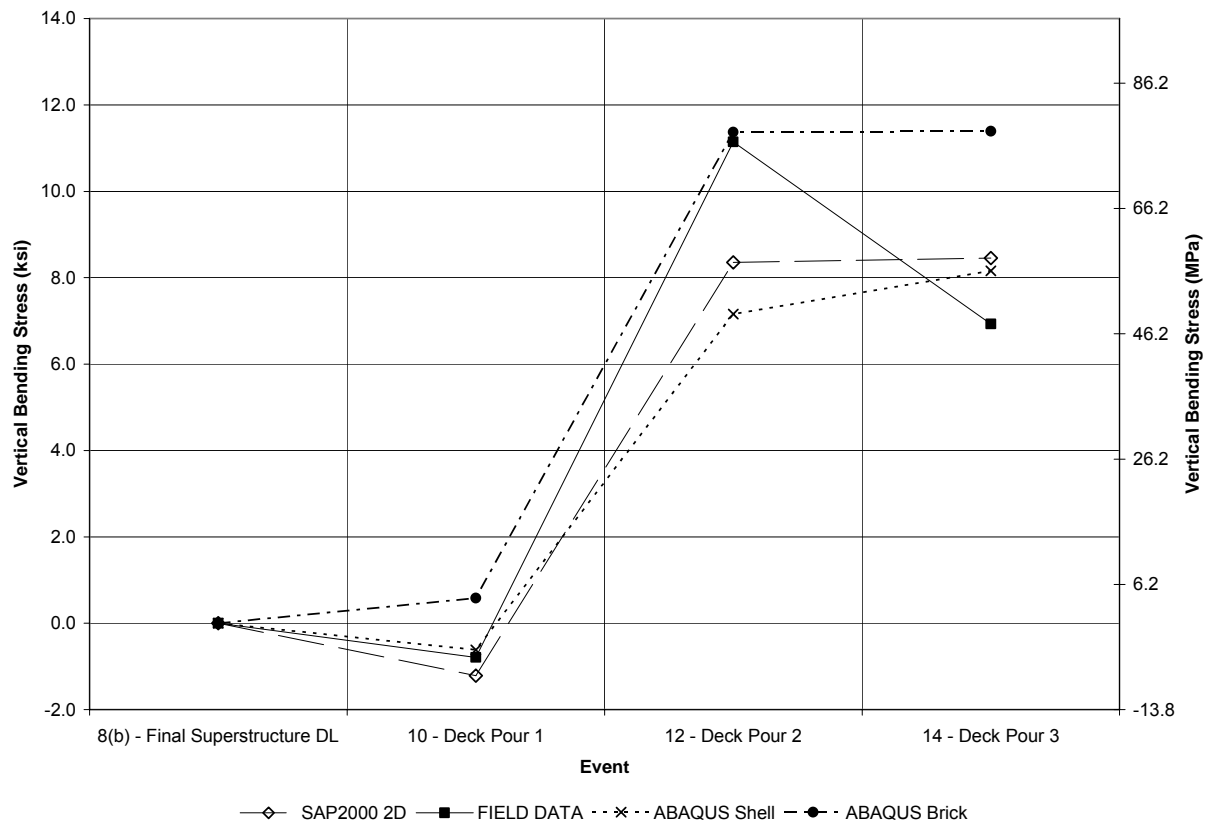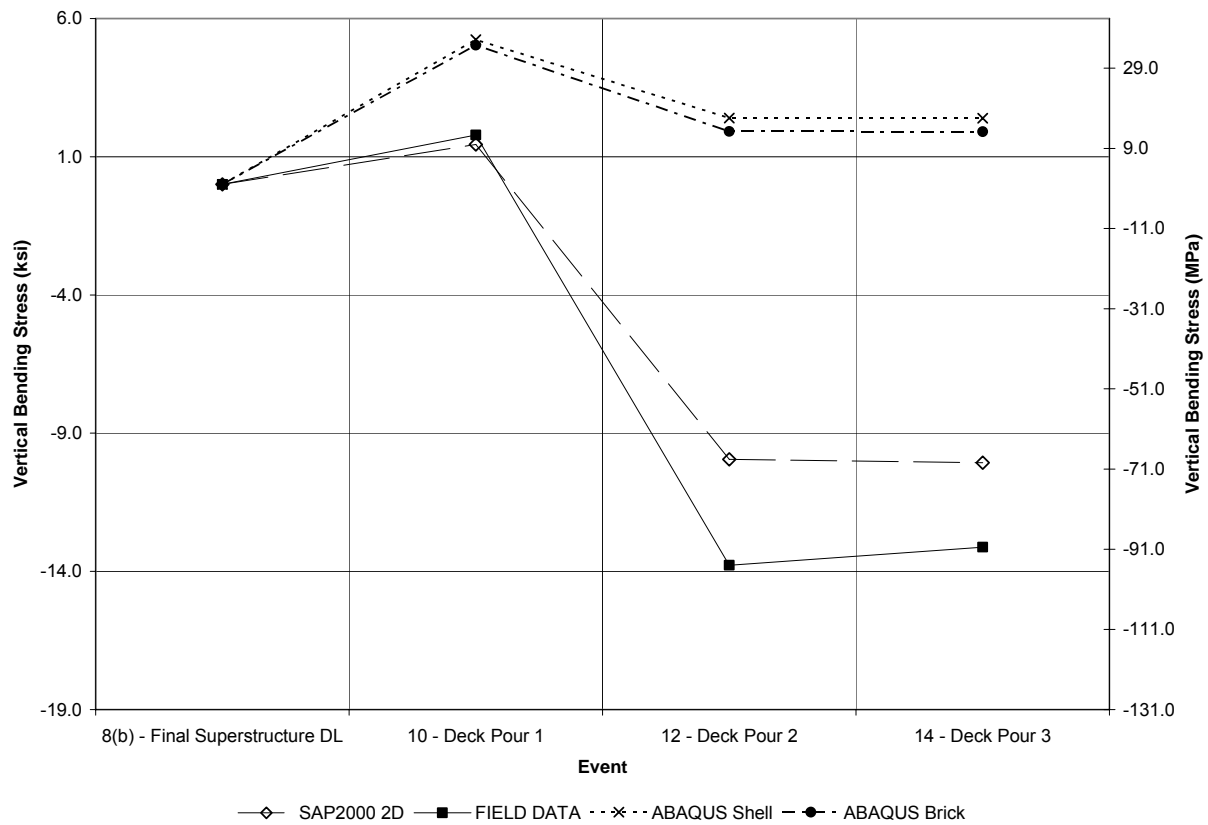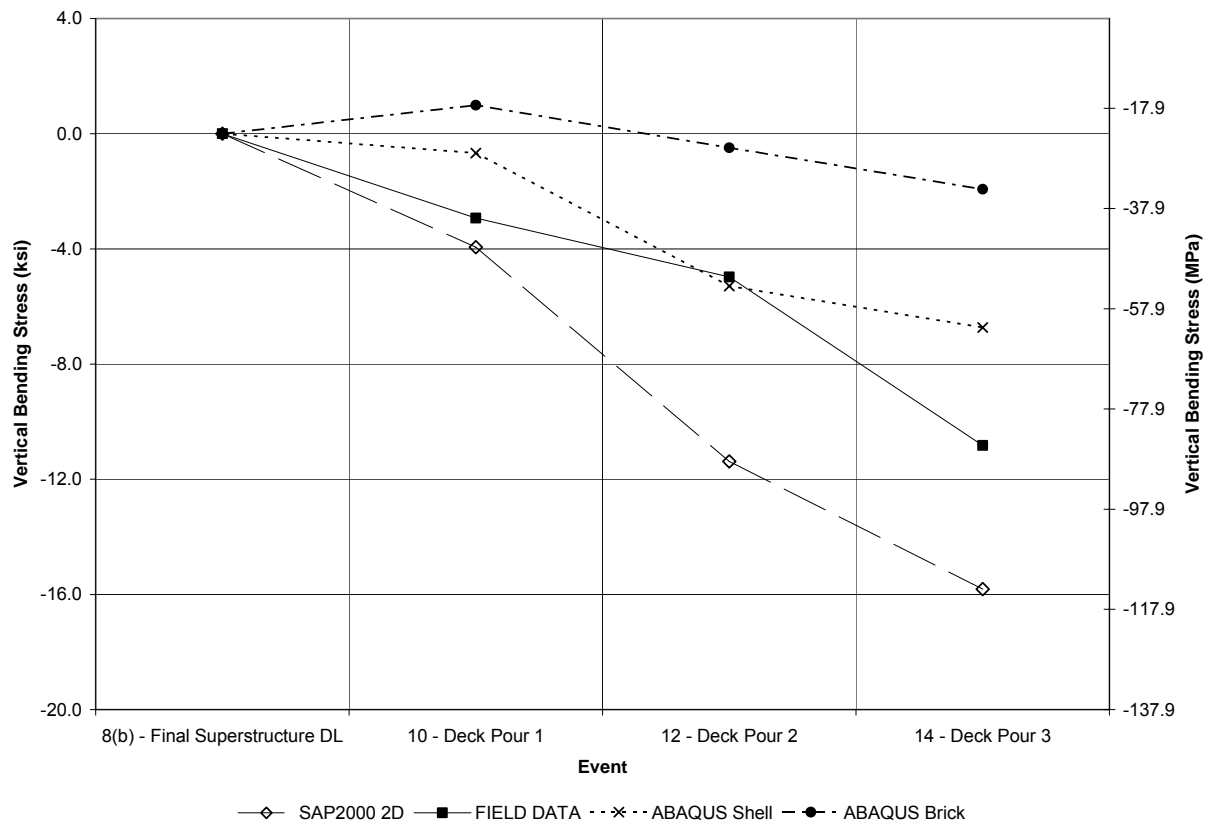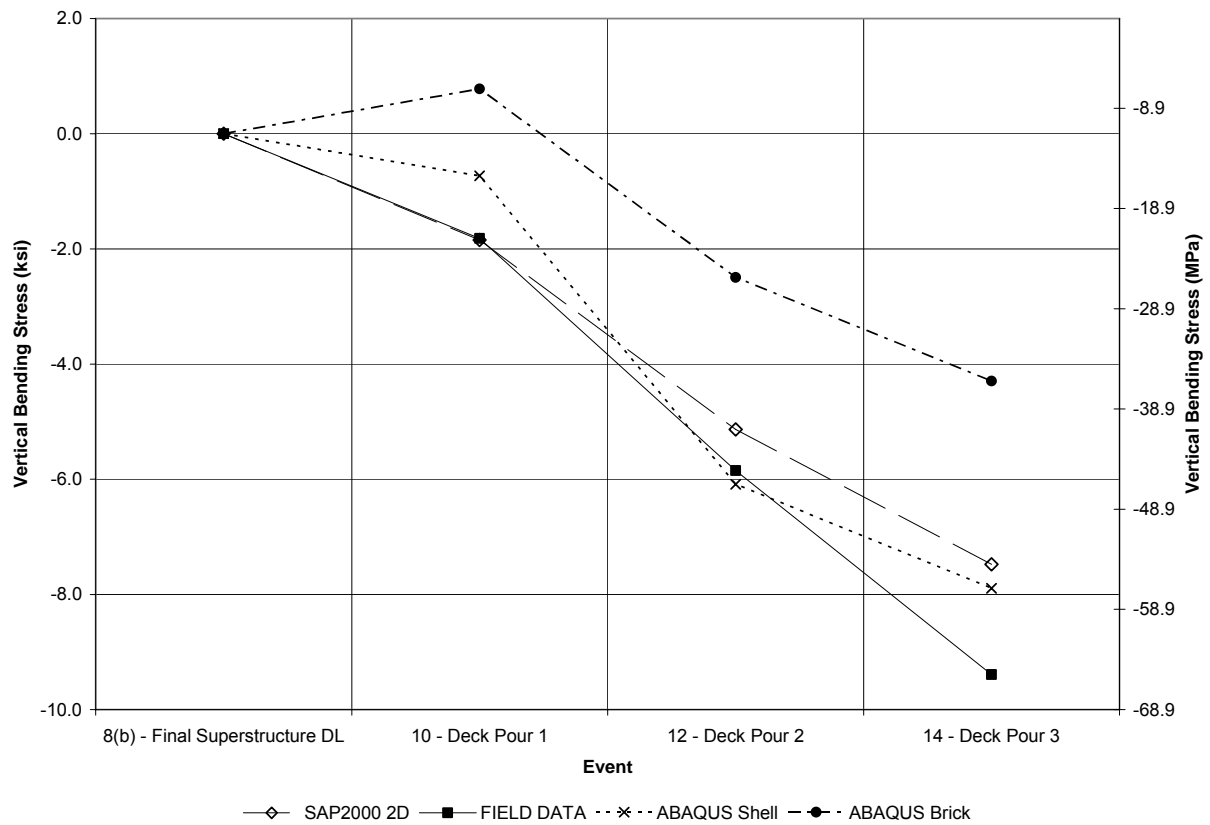
Figure 72. Results Comparison (Slab) for Girder 3 Bottom Flange Section B-B (Fig. 7).

Figure 73. Results Comparison (Slab) for Girder 3 Top Flange Section B-B (Fig. 7).

Table 15 shows the results comparison for the HS20 live load placed on the structure. The HS20 truck was placed to induce maximum moment in Girder 1 at Section C-C. It shows that both models predict similar results for Girder 1 Bottom Flange Section C-C. Both ABAQUS models predict differing stress values at other locations on the structure.

Table 15. Results Comparison for HS20 Live Load.

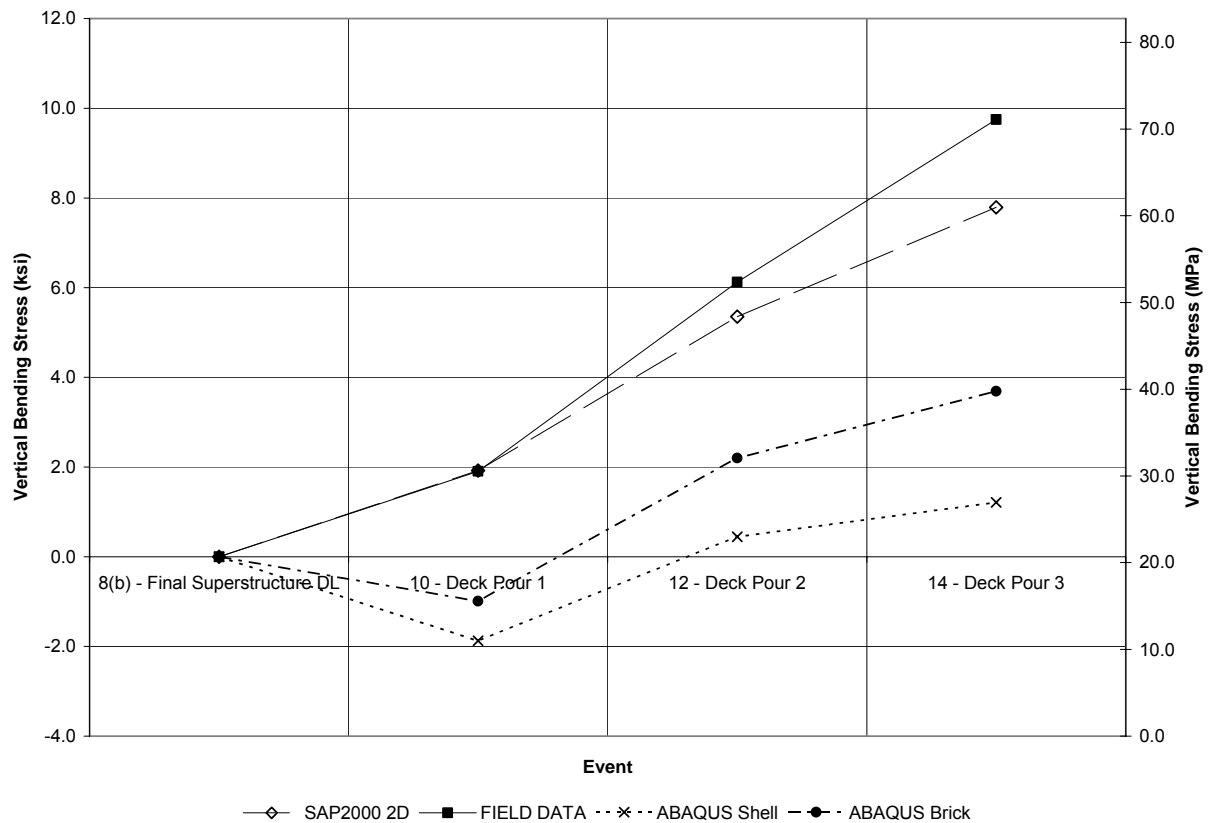| Location	ABAQUS Shell Model Results, MPa (ksi)	ABAQUS Brick Model Results, MPa (ksi)
Girder 1 C-C Bottom Flange	31.84 (4.62)	32.33 (4.69)
Girder 2 C-C Bottom Flange	40.61 (5.89)	78.10 (11.33)
Girder 3 C-C Bottom Flange	58.98 (8.55)	84.31 (12.20)
Girder 3 C-C Top Flange	14.44 (2.10)	10.38 (1.51)
Girder 5 C-C Bottom Flange	-26.27 (-3.81)	-8.33 (-1.21)
Girder 3 B-B Bottom Flange	-57.23 (-8.30)	-30.32 (-4.40)
Girder 3 B-B Top Flange	9.47 (1.37)	26.83 (3.89)
Girder 5 B-B Bottom Flange	-41.21 (-5.98)	-23.76 (-3.45)

6.2 STRUCTURE #314

Comparisons between the collected field data and select results from the grillage, full-shell 3D and 3D finite element model containing a combination of frame members and shell and brick elements are provided herein. Comparisons that are shown are for along the length of Girders 6 and 12.

Figures 74 and 75 show comparisons of vertical deformations for Girders 1 and 6 from the grillage, shell and solid models at the completion of the deck pour for Span 1. These plots indicate a clear differentiation between the predicted deformations for the three model types.
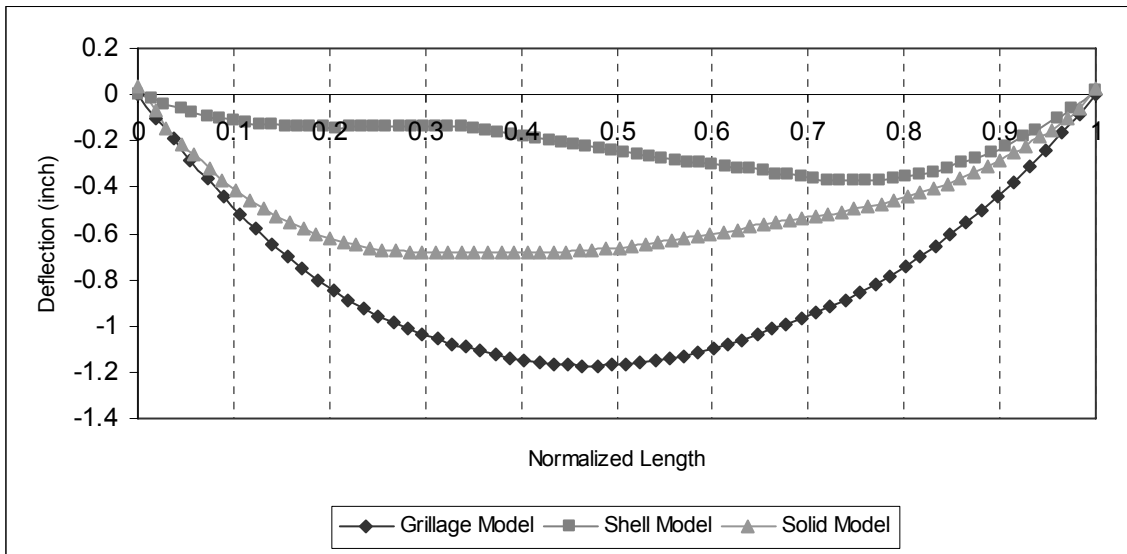
Figure 74. Vertical Deflection Results Comparison for Girder 1 at Completion of Span 1 Deck Pour (Fig. 3).
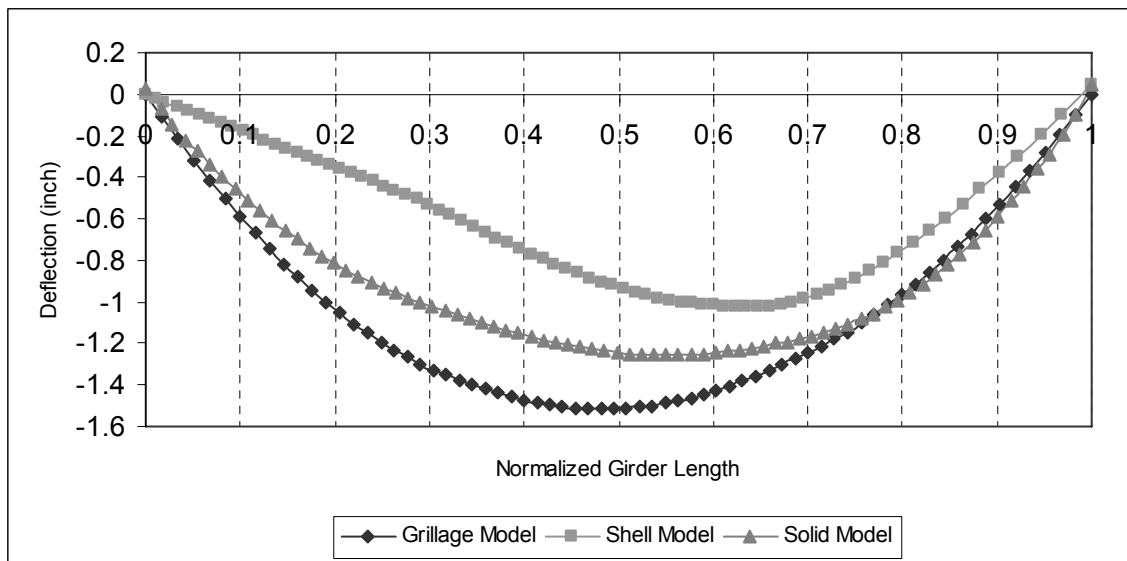
Figure 75. Vertical Deflection Results Comparison for Girder 6 at Completion of Span 1 Deck Pour (Fig. 3).

Figures 76 and 77 show stress comparisons for the three model types to measured field data on the bottom flange at Sections B-B, C-C and D-D for Girders 6 and 12. These figures indicate that, at the completion of the pour, neither the grillage model nor the shell and solid models very accurately predicted stress levels measured in the field.

Figure 76. Normal Stress Results Comparison for Girder 6 at Total Dead Load (Fig. 3).

Figure 77. Normal Stress Results Comparison for Girder 12 at Total Dead Load (Fig. 3).

Figures 78 and 79 compare deflections from the three models and indicate that, at the completion of the pour, the grillage model predicted larger magnitudes than the shell and solid models.

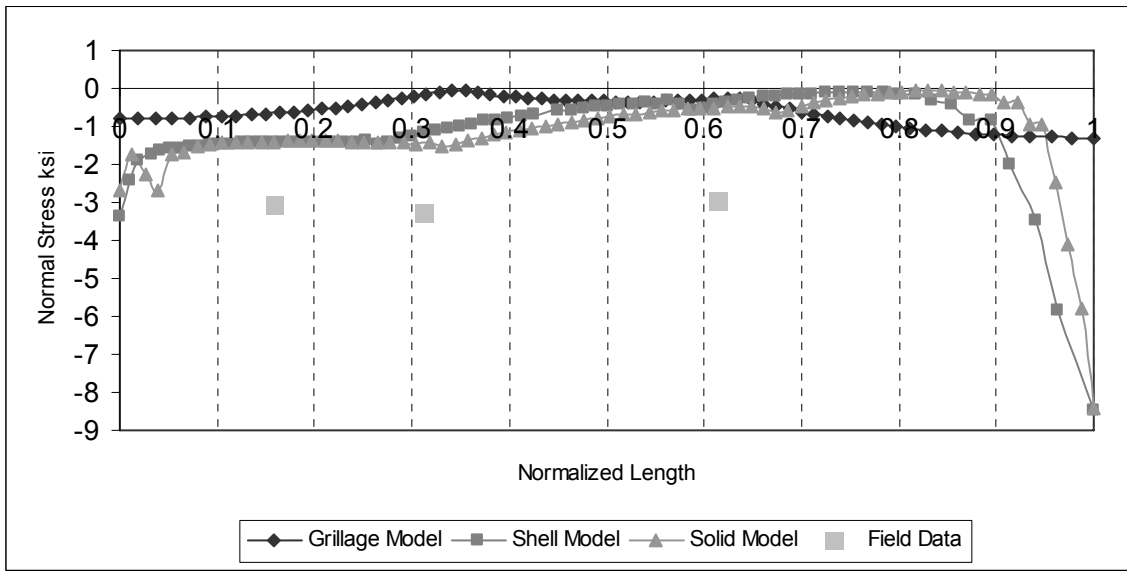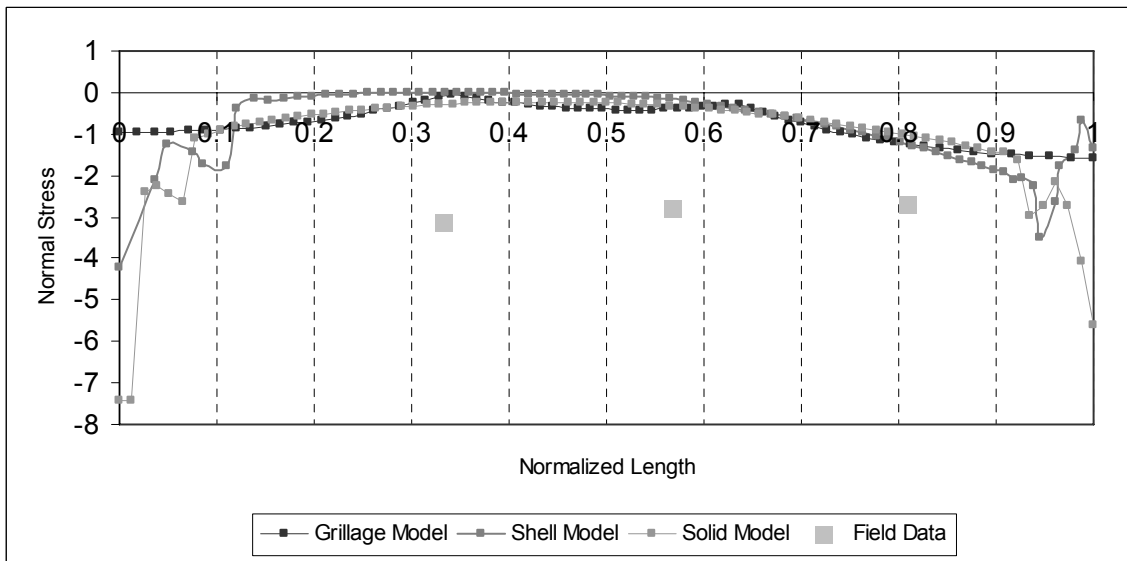**Figure 78. Vertical Deflection Results Comparison for Girder 6 at Total Dead Load (Fig. 3).**
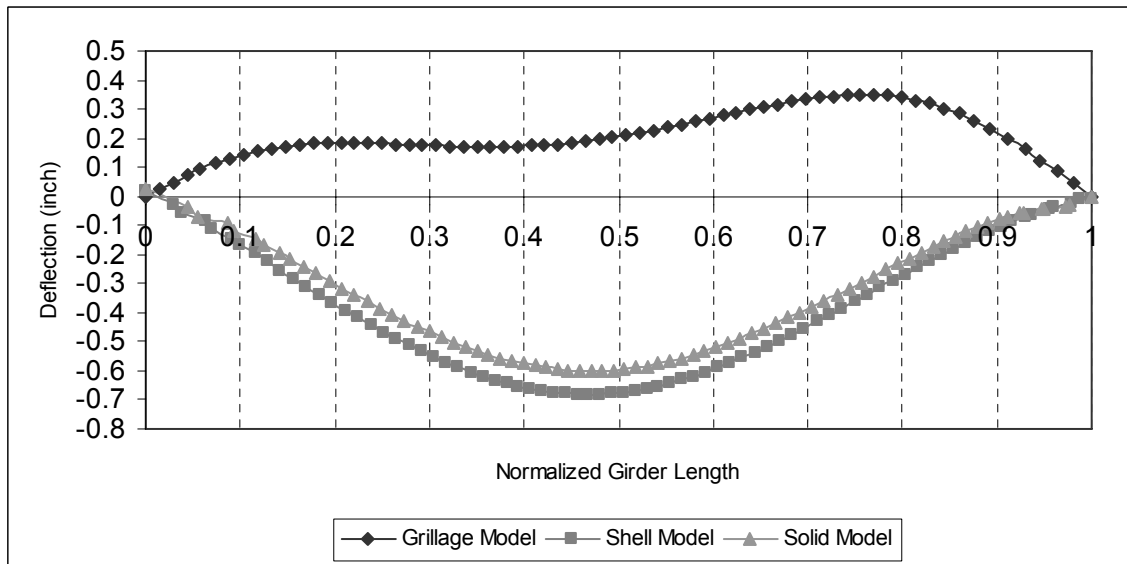
Figure 79. Vertical Deflection Results Comparison for Girder 12 at Total Dead Load (Fig. 3).

Figures 80 and 81 show results comparisons for the three models for placement of an HS20 truck at midspan of the longest girder, Girder 6. As was shown for the results comparisons for the deflections, the grillage model predicted larger stresses than the shell or solid models.
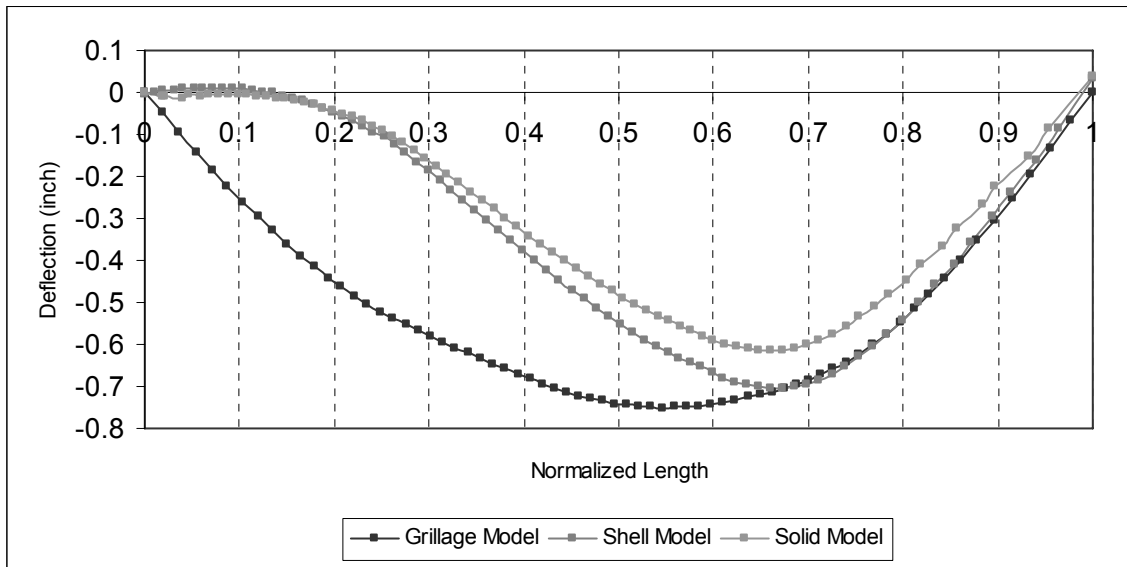
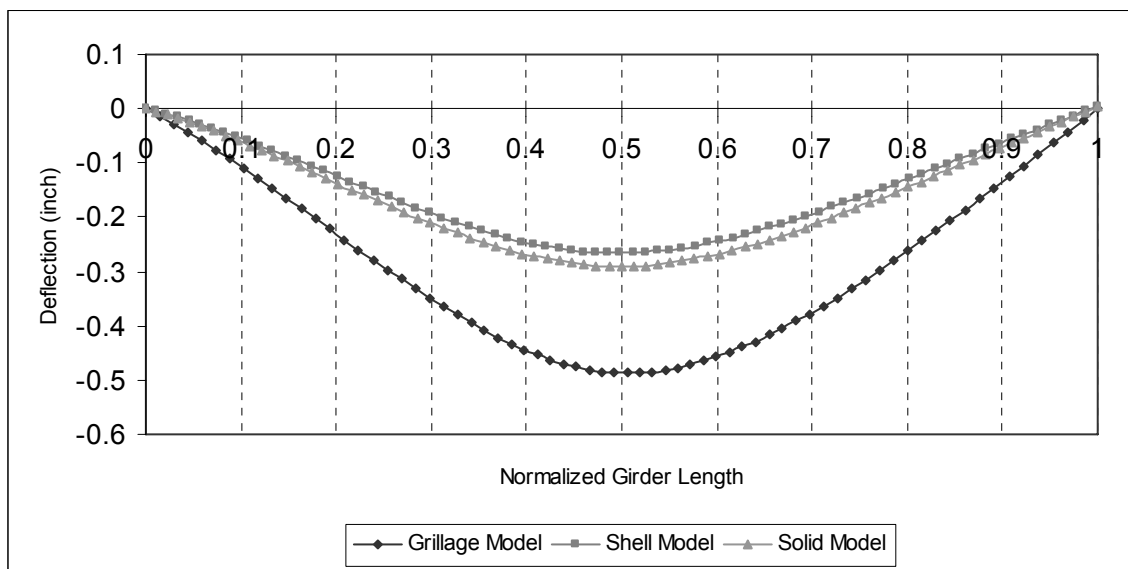**Figure 80. Vertical Deflection Results Comparison for Girder 6, HS20 Truck (Fig. 3).**
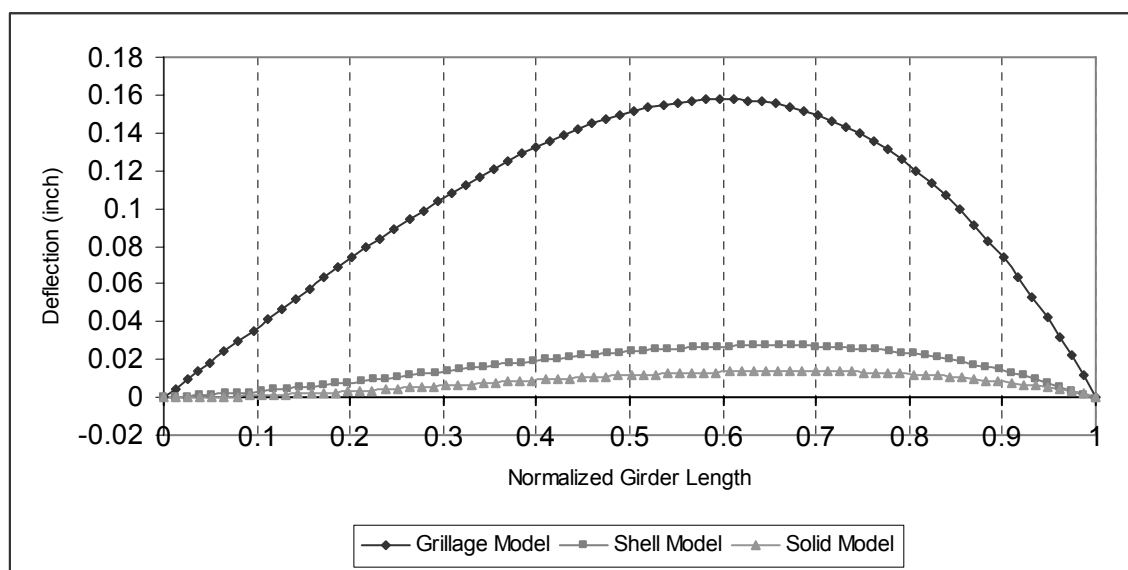

Figure 81. Vertical Deflection Results Comparison for Girder 12, HS20 Truck (Fig. 3).

7   SUMMARY

Summarized herein are activities completed for MAUTC Work Order No. 2. Tasks completed for this project included: replacing damaged/missing instruments on Structure #s 207 and 314; hard-wiring instruments to acquisition systems; collecting, compiling and summarizing recorded data and comparing data to numerical results from a grillage model, a full-shell 3D finite element model and a 3D finite element model containing a combination of frame members and shell and brick elements.

Findings from this study are summarized in the list below. It should be noted that these findings are explicitly for: (1) the structures that were investigated; (2) the models that were created; and (3) the assumptions made while developing those models.

- Structure 207:
    - Field data produced during the project indicated small and somewhat constant changes in stress for the completed structure due to temperature changes;
    - Comparisons between analysis results and field data recorded during staged construction (steel superstructure only) produced no conclusive findings for the modeling approaches (grillage vs. shell) for vertical bending stresses. For the girder cross sections that were investigated, certain instances showed the grillage model more accurately predicting vertical bending stress changes and other instances showed the shell model more accurately predicting stress changes. Radial and tangential cross section location appeared to have no bearing on these findings.
    - Comparisons between analysis results and field data recorded during staged construction (steel superstructure only) produced no conclusive findings for the modeling approaches (grillage vs. shell) for lateral bending stresses. For the girder cross sections that were investigated, certain instances showed the grillage model more accurately predicting lateral bending stress changes and other instances showed the shell model more accurately predicting stress changes. It should be noted that all lateral bending stress changes, be they from the field data or the computer models, were small during staged construction. Radial and tangential cross section location appeared to have no bearing on these findings.
    - Comparisons between analysis results and field data recorded during placement of the concrete deck produced some findings regarding the modeling approaches that were investigated (grillage vs. shell vs. brick). For the girder cross sections that were investigated, results indicated that the shell and brick models produced similar predictions for changes in stress level, especially at the top flanges. This stiffening did not necessarily indicate better prediction of measured field response when compared to the grillage model, however, which appeared to provide more accurate predictions of response for these stages. As was discussed above, radial and tangential cross section location appeared to have no bearing on these findings.
    - Results from the HS20 live load comparison as for the modeling approaches that

84

were investigated (shell vs. brick) also indicated closer agreement between the stress predictions at the top flange than at the bottom flange.
- o Results for cross frame forces predicted by the ABAQUS shell model indicate reasonable prediction of the small axial stress levels measured in the field at the completion of steel superstructure erection.
- Structure 314:
    - o Comparisons between analysis results and field data recorded at completion of construction did not provide conclusive results regarding a preferred modeling technique (grillage vs. shell vs. brick). All three model types, which utilized load-balancing to incorporate pre-stressing forces, appeared to under-predict normal stresses developed at completion of construction.
    - o Comparisons between analysis results for deflections (grillage vs. shell vs. brick) for both the completion of construction and under an HS20 live load indicate that the grillage model that was created was the most flexible, with the shell and brick models producing results that were somewhat similar.

8   REFERENCES

Bennett, A. (2004), "Analysis of Lateral Bending and Torsional Stresses in a Skewed Composite Prestressed Concrete Bridge during Construction," M.S. Thesis, Department of Civil and Environmental Engineering, The Pennsylvania State University: University Park, Pa.

Hiltunen, D.R., Johnson, P.A., Laman, J.A., Linzell, D.G., Miller, A.C., Niezgoda, S.L., Scanlon, A., Schokker, A.J. and Tikalsky, P.J. (2004), *Interstate 99 Research*, Final Report PTI 2005-02, Pennsylvania Transportation Institute, The Pennsylvania State University: University Park, Pa., October, 324 pp.

Linzell, D.G., Laman, J.A., Bell, B., Bennett, A., Colon, J., Lobo, J., Norton, E. and Sabuwala, T. (2003), *Prediction of Movement and Stresses in Curved and Skewed Bridges,* Final Report PTI 2003-06, Pennsylvania Transportation Institute, The Pennsylvania State University: University Park, Pa., March, 192 pp.

Linzell, D.G. and Laman, J.A. (2001), *I-99 Advanced Technology Test Bed, Work Order 79: Prediction of Movement and Stresses in Curved and Skewed Bridges, Work Plan and Literature Review*, Pennsylvania Transportation Institute, The Pennsylvania State University: University Park, Pa., April, 37 pp.

Shura, J. (2005), "The Effects of Horizontal Curvature on Warping during Construction of a Steel Plate Girder Bridge with Large Radii," M.S. Thesis, Department of Civil and Environmental Engineering, The Pennsylvania State University: University Park, Pa.